ABSTRACT

Title of Dissertation:	SYSTEMS-LEVEL MODELING AND VALIDATION OF CARDIOVASCULAR SYSTEM RESPONSES TO FLUID AND VASOPRESSOR INFUSION FOR AUTOMATED CRITICAL CARE SYSTEMS
	Ramin Bighamian, Doctor of Philosophy, 2017
Dissertation directed by:	Assistant Professor Jin-Oh Hahn Department of Mechanical Engineering

Effective treatment of critically ill patients requires adequate administration of drugs to resuscitate and stabilize the patient by maintaining the volume of blood against bleeding and preserving the blood circulation to the body tissues. In today's clinical practice, drug dose is adjusted by human clinicians. Therefore, treatment is often subjective and ad-hoc depending on the style and experience of the clinician. Thus, in theory, it is anticipated that well-designed automated critical care systems can help clinicians make superior adjustments to drug doses while they are always vigilant and never distracted by other obligations. Yet, automated critical care systems developed by researchers are ad-hoc, because they determine the control law, i.e., drug infusion rate, using input-output observations rather than the insights on the patient's physiological states gained from rigorous data-based analysis of mathematical models. Thus, it is worth developing model-based automated systems relating the fluid and

vasopressor dose input to the underlying physiological states. This necessitates dose-response mathematical models capable of reproducing realistic physiological and dose-mediated states with reasonable computational load. However, most of existing models are too simplistic to reflect physiological reality, while others are too complicated with thousands of parameters to tune. To address these challenges, we believe that a hybrid physiologic-phenomenological modeling paradigm is effective in developing mathematical models for automated systems: low-order phenomenological models with adaptive personalization capability are suited to develop control algorithms, while physiological models can provide high-fidelity patterns with physiological transparency suited to interpret the underlying physiological states.

In this study, hybrid physiologic-phenomenological models of blood volume and cardiovascular responses to fluid and vasopressor infusion are successfully developed and validated using experimental data. It is shown that the models can adequately reproduce the underlying physiological states and endpoints to fluid and vasopressor infusion. The main contributions of this research are lined in the following three folds. First, the models are robust against inter-individual variability, in which they can be adapted to each patient with a small number of tunable parameters. Second, they are physiologically transparent where the underlying physiological states not measured in the standard clinical setting can be interpreted and streamlined during an intervention. And eventually the interpreted underlying states can be employed as direct endpoints to monitor the patient and guide the treatment in a closed-loop or decision-support platform.

SYSTEMS-LEVEL MODELING AND VALIDATION OF CARDIOVASCULAR SYSTEM RESPONSES TO FLUID AND VASOPRESSOR INFUSION FOR AUTOMATED CRITICAL CARE

by

Ramin Bighamian

Dissertation submitted to the Faculty of the Graduate School of the
University of Maryland, College Park, in partial fulfillment
of the requirements for the degree of
Doctor of Philosophy
2017

Advisory Committee:
Assistant Professor Jin-Oh Hahn, Chair
Associate Professor Andrew T. Reisner, Co-Advisor
Associate Professor Derek A. Paley, Dean's Representative
Professor Balakumar Balachandran
Associate Professor Sarah Bergbreiter
Associate Professor Miao Yu

Acknowledgements

There are many individuals who made this work possible and deserve thanks. First and foremost is my advisor, Professor Jin-Oh Hahn, whose guidance and inspiration were critical to the success of the work. It has been an honor to be his first Ph.D. student. He continually conveyed a spirit of adventure in regard to research and scholarship, and an excitement in regard to teaching. Without his guidance and persistent help this dissertation would not have been possible. The enthusiasm he has for his research was contagious and motivational for me, even during tough times in the Ph.D.

I would like to equally thank my co-advisor, Professor Andrew T. Reisner, for all his passionate guidance and assistance throughout my Ph.D. He offered me a great deal of physical insight on many different aspect of critical care systems. While being a long distance advisor, he was always available to me for any questions and concerns. Without his help, this research might not have ever come to fruition.

I'm grateful to Professors Balakumar Balachandran, Sarah Bergbreiter, Derek A. Paley and Miao Yu for serving on my dissertation committee. Their time, interest, and insightful feedback on my research were very constructive, and improved the quality of work. Specifically, I would like to extend my gratitude to Professor Balachandran for all his support during my Ph.D.

I would like to thank Professors David A. Kass, Michael Kinsky, George Kramer, and Istvan Seri for sharing invaluable data on human and animal studies. The validation of my algorithms was not possible without their priceless data. I also would like to express my gratitude to Professor Steven T. Shipley for all his help and enormous effort to make possible the animal subject study at the University of North Carolina.

My sincerest thanks go to all my lab mates, including Albert, Azin, Bahram, Bryce, Cal, Ghazal, Jonathan, Junxi, Nima, Siavash, Shiva, Stephanie, Xin, and Zahra for all

their support and friendship. I greatly look forward to having all of them as colleagues in the years ahead. I would like to extend my deepest thank to Dr. Kim for his gracious help in the animal study and being a great lab neighbor for the last four years. I would like to also acknowledge all my co-authors including Dr. Christopher Scully. I am very grateful to my friends, old and new, for keeping in touch and being supportive. In particular, I would like to thank Adel, Masoud and Pejman for being my everlasting friends. Having spent all these years, I may have overlooked thanking you for being terrific friends. I would like to thank Farinaz for your continuous presence, patience and support each and every time I feel frustrated. I look forward to sharing many more of life's lovely moments with you.

I gratefully acknowledge the funding sources that made my Ph.D. work possible. My research was funded by the Office of Naval Research (ONR), under Grant No. N000141410591 and N000141512018, and Craig H. Neilsen Foundation, under Grant No. 297533, and I was honored to be the recipient of the Graduate Dean's Dissertation Fellowship in the last year of my Ph.D, 2016-2017.

Finally, words cannot express how thankful I am to my mother and father who raised me with a love of science and supported me in all my pursuits, and my brothers Dr. Amin and Mohammad, and my sister Afrooz for their continuous love, encouragement and advice.

Table of Contents

List of Tables

Table 18: Identified parameters (mean (SD)) averaged between 4 animal subjects. 149

List of Figures

List of Symbols

Parameter	Unit	Description
$V_B(t)$	l	BV
$\Delta V_B(t)$	l	Change in BV
$\overline{V}_B$	-	Fractional BV
$\Delta V_{ISF}(t)$	l	Change in ISFV
V_{B0}	l	Baseline BV
$V_{ed}(t)$	ml	End-diastolic volume
$V_{es}(t)$	ml	End-Systolic Volume
$\overline{V_{ed}}$	ml	Effective preload
$\Delta V_{RBC}(t)$	l	Change in RBCV
δV	ml	Stroke volume
$\delta \overline{V}$	ml/m^2	SVI
δV_0	ml	Baseline SV
V_{BU}	l	Unstressed BV
$VR(t)$	l/m	Venous return
$CO(t)$	l/m	Cardiac output
$u(t)$	l/min	Rate of fluid infusion
$v(t)$	l/min	Rate of fluid loss
$v_H(t)$	l/min	Loss rate due to hemorrhage
V_0	ml	LV volume at zero LV pressure
P_s	mmHg	SBP
P_d	mmHg	DBP
P_m	mmHg	MAP
$P_{m,0}$	mmHg	Baseline MAP
$P_{ed}(t)$	mmHg	End-diastolic pressure
$P_{MS}(t)$	mmHg	Mean systemic pressure
$P_{CV}(t)$	mmHg	Central venous pressure
$P(t)$	mmHg	Arterial Pressure
$q(t)$	l/min	Transcapillary fluid shift
$r_B(t)$	l	Reference BV
α_u	-	Fluid distribution ratio
α_v	-	Fluid loss distribution ratio
$e_B(t)$	l	Error in BV from its reference
K_p	1/min	Proportional gain in PI controller
K_i	1/min^2	Integral gain in PI controller
$HR(t)$	bpm	Heart rate
HR_0	bpm	Baseline HR
$H(t)$	-	Hematocrit
$H(0)$	-	Baseline hematocrit
$V_{LV}(t)$	ml	Left ventricular volume
E_S	mmHg/ml	Left ventricular elastance
E_A	mmHg/ml	Arterial elastance

$R(t)$	mmHg.min/l	TPR
R_0	mmHg.min/l	Baseline TPR
R_{VR}	mmHg.min/l	Resistance to venous return
C_S	l/mmHg	Systemic capacitance
C	l/mmHg	Arterial compliance
t_{ed}	min	Time instant of end-diastole
t_{es}	min	Time instants of end-systole
T	min	Heart period
t_D	min	Transport delay
T_S	min	Sampling interval
τ	min	Drug infusion time constant
d	m(n)g/kg/min	Vasopressor dose level
$\mathcal{S}_{V_B}(t)$	-	BV parametric sensitivity
$\mathcal{S}_{CO}(t)$	-	CO parametric sensitivity
$\mathcal{S}_{\delta V}(t)$	-	SV parametric sensitivity
$\mathcal{S}_{P_m}(t)$	-	BP parametric sensitivity

Chapter 1: Introduction

1.1.Background

The tasks of medical science fall into three categories. The first is to understand disease biology. The second is to find effective therapies. And the last is to ensure that those therapies are delivered effectively. This third category, which is perhaps the most important for clinical outcomes, has been almost ignored by research funders, government, and academia. For instance, in daily practice, clinicians are confronted by many critically ill patients who require major surgeries to stabilize their hemodynamic state. For the aforementioned reason, however, standard therapeutic methods may lead to suboptimal treatments with the occurrence of one or more intra- and post-operative complications, resulting in significant morbidity and mortality.

The delivery of effective treatment to critically ill patients requires adequate administration of drugs to resuscitate (e.g., by maintaining circulation against blood loss) and stabilize (e.g., by mitigating pain due to injury) a given patient. In today's clinical practice, a medication dose is iteratively and empirically adjusted by human clinicians. A complicating factor is that medications typically have undesired side effects. Therefore, they can be either beneficial or detrimental to the recovery since there is a relatively narrow range for safe drug administration and both an over-dose and under-dose of medication can adversely affect outcomes, i.e., they can lead to a longer length of hospital stay with more treatment costs (Classen et al., 1997). In this regard, the standard practice suffers from two main limitations: (i) caregivers may fail to notice when a medication dose must be adjusted to meet resuscitation goals, and (ii)

caregivers may not always select optimal dose changes in case dose changes are required, leading to patients subjected to suboptimal therapy or pronounced side effects.

Automated therapeutic systems, including closed-loop or decision support systems (Figure 1-1), can ensure the delivery of effective therapy by addressing the abovementioned challenges. It is anticipated that automated systems may be superior to human clinicians particularly when clinicians are in short supply, pressed for time, or overwhelmed by many patients (Michard, 2013). These systems are always vigilant and never distracted by other obligations. Furthermore, they employ careful and exacting computations, whereas a clinician often resorts to subjective ad hoc estimations to make clinical decisions. Studies have shown that the human brain has difficulties processing more than 5 to 7 variables simultaneously (Michard, 2013). Unfortunately, this is what a clinician's brain is supposed to do when closely monitoring and treating patients, since most therapeutic decisions cannot be based on a limited number of clinical variables. Thus, in theory, a well-designed automated medication control system could help clinicians make superior adjustments to medication doses, avoiding dangerous delays in noticing the need for adjustments, and avoiding dose adjustments that are far from being optimal.

Automated control of medication administration has received attention during recent decades. As such, a multitude of algorithms have been reported on insulin control in diabetes, control of anesthetics and opioids, and fluid treatment against blood loss, e.g., B. P. Kovatchev et al. 2009; S. Bibian, Dumont, and Black 2015. Despite this level of evidence, a survey published in 2011 showed that the footprint of

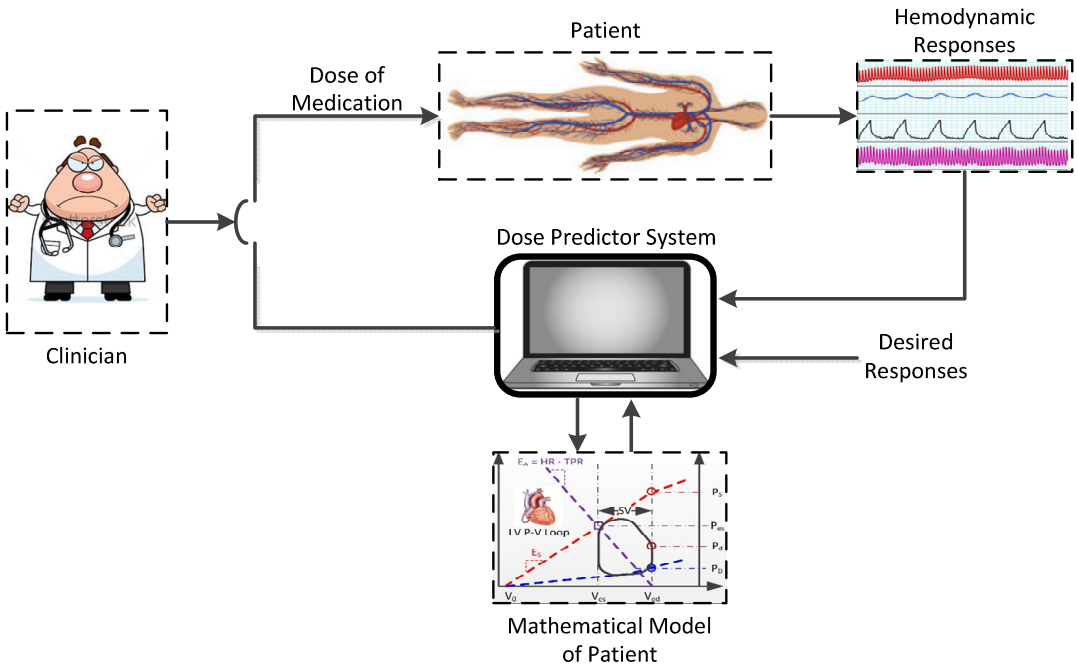

Figure 1-1: Schematic of automated drug administration. A clinician can close the loop to deliver the treatment in a closed-loop manner or take machine calculated dose of medication as a background to support his/her decisions.

goal-directed automated therapy in the realm of critical patient care is negligible. For example, goal-directed closed-loop therapy is used by only 5.4% of US anesthesiologists (Michard, 2013). This indicates that there should be still a number of challenges that must be addressed by today's technology. It is anticipated that investigating key technical challenges and finding successful solutions to them may be a vital step towards the development and widespread deployment of automated therapeutic systems. These technologies can ultimately be a benefit to patients, care providers, health systems, and researchers (Rinehart and Canales, 2015) by reducing medication errors and eventually morbidity and mortality in critical care, reducing provider's workload and the number of manual interventions needed during treatment, delivering cost-effective treatments and portable expertise, and providing

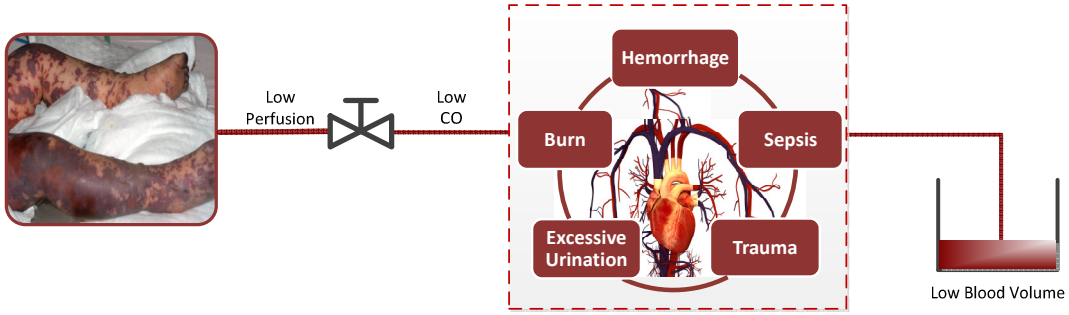

Figure 1-2: Examples of pathophysiologic conditions leading to hypovolemia.

new research studies to improve the efficacy of automated systems, respectively.

Among the critical care disease, hypovolemia is recognized as the one may most benefit from automated critical care systems (ACCS). Hypovolemia can be attributable to many injuries and pathophysiologic conditions, such as hemorrhage, burns, trauma and infections (e.g., sepsis) (Barrow et al., 2000; Bortolani et al., 1996; Chien, 1971; Guillamet et al., 2012; Hollenberg et al., 1999; Hunter and Doddi, 2010; Pruitt, 1978; Vatner, 1974) (Figure 1-2), either alone or in combination, and requires fluid resuscitation to restore venous return, cardiac output (CO), and ultimately blood pressure (BP) by optimizing the intravascular blood volume (BV). In many hypovolemic scenarios, early and closely monitored resuscitation is crucial for survival. Previous investigations indicate that delayed and inadequate fluid resuscitation was shown to be responsible for increased mortality and morbidity (Michard, 2013; Varadhan and Lobo, 2010; Wolf et al., 1997). Considering the lack of expert physicians and intensivists for fluid resuscitation, technologies for automated control of fluid resuscitation may reduce clinical workload by a large amount. The technology may especially find meaningful applications in low-resource settings, such as the treatment and management of BV in the care of combat and mass casualties.

To serve the needs of the body tissues, i.e., to transport nutrients to and waste products away of the body tissues, apart the adequate BV explained above, adequate perfusion pressure is required to force blood into the capillaries of all organs. In particular, in patients with decreased cardiovascular (CV) reserve, fluid resuscitation alone is not sufficient to augment CV performance. Therefore, vasoactive agents are utilized to supplement fluid infusion. Vasoactive drugs are medications that act to elevate arterial BP in critically ill patients suffering from a body-wide reduction in blood circulation. Vasoactive agents can act through one or more physiological mechanisms, including increasing resistance to blood exiting the arteries (total peripheral resistance, TPR) and increasing CO through increased heart rate (HR), cardiac contractility, and decreased venous capacitance. The ultimate medical benefit of vasopressors is not increased BP per se, but increased blood flow to peripheral tissues driven by the increase in BP. From here on in this research, the act of regulating BV and its perfusion pressure via fluid resuscitation and vasopressor infusion will be called hemodynamic management.

1.2.Research Motivation

Current ACCS capabilities to deliver adequate BV and perfusion pressure pose four unique, significant challenges in developing and validating the technology towards its maturation, which are explained below:

First, the ACCS must be robust against individual variability in dose-response behaviors. In many of the control systems reported in the literature, the robustness aspect is not considered rigorously, or even if it is considered, a simple approach of

sacrificing the system's performance to achieve reasonable level of robustness is taken. The efforts to personalize control algorithm is relatively rare, which is due, at least in part, to the prevalent use of traditional pharmacological models as control design models, which do not offer an ideal platform for real-time adaptive personalization. Second, almost all available decision support systems are not physiologically transparent, at which they simply try to conjecture their endpoint of interest without even considering the underlying physiological mechanisms. Despite this superficial conjecture might work in the favor of tuning the system using as little as possible data, two evident shortcomings of this approach are: (i) hemodynamic alerts are only produced based on the forecasted endpoint, while the real underlying factors responsible for a true alert are still dismissed. For example, a normal BP, which is the most common endpoint for alerting critical care systems, can be reproduced by low blood flow but high vasculature resistance, that can hypo-perfuse and eventually damage peripheral tissues; and (ii) even if a true alert is produced by a superficial endpoint, this may not assist a clinician in maintaining the patient within the therapeutic target with complying the best treatment protocol since the fundamental cause of hemodynamic failure remains ambiguous. Third, sensor technologies are not fully mature yet, which limits the control system performance. For example, subcutaneous glucose monitors exhibit significant time delay with respect to the blood glucose level; sensors applicable to analgesia control do not exist; all the endpoints currently used in automated fluid treatment suffer from critical drawbacks; that is, there is no sensor providing a measure of CV preload change due to fluid perturbation. Even for the sensors used in current clinical care, the credibility of the measurement quality is still

an open challenge. For instance, BP waveform measurements are commonly corrupted and distorted by signal artifacts and noises. Using the measurements with unknown creditability can make a drastic impact on the performance of automated systems. And fourth, the validation of technology is not trivial, if not impossible. The closed-loop medication control systems are intended for human use. However, the validation in humans is not practical due to ethical reasons. It's anticipated that a high-fidelity model-based simulation that can reproduce physiological responses to critical care medications may provide a viable platform to streamline translation and deployment of emerging ACCS capabilities.

1.3.Objectives and Scientific Approach

Within the scope of this research, we seek an answer to the question of how to construct a new modeling paradigm for ACCS, which relies on readily available data, and can be used in personalized closed-loop therapy. As mentioned in Section 1.2, current available methods suffer from practical challenges they may have in employing hemodynamic measurements from low-resource setting to interpret the status of patient's health condition and guide closed-loop therapies. To address these practical challenges, this research develops hybrid physiologic-phenomenological mathematical models that can appropriately reproduce dose-response behaviors to critical care medications, including fluid resuscitation and vasopressor infusion. The physiological models are built upon physical principles of underlying dose-mediated responses, and thus provide transparency and predictive accuracy, but are typically complex. The phenomenological models, on the other hand, are based upon empiric observations (i.e.

data), so they are typically simple and amenable to adaptation but lack physical implication. Therefore, in this novel modeling paradigm, the desired balance between a model's transparency and complexity is achieved by concurrent exploitation and integrations of physiological and phenomenological models.

This research shows that the hybrid physiologic-phenomenological modeling paradigm is effective in developing mathematical models for ACCS, in which the objectives of modeling can be met in two fields. First, this paradigm can provide low-order models with adaptive personalization capability suited to develop ACCS control algorithms. Second, this paradigm can provide high-fidelity models with physiological relevance and transparency suited to interpret the underlying physiological principals. In other words, the model's transparency can make it possible to streamline the interpretation of the model during a closed-loop ACCS event. In summary, the above mentioned challenges can be addressed by a hybrid modeling paradigm as below:

Personalized closed-loop therapy (challenge 1) can be achieved via a desired balance between a model's accuracy and complexity by concurrent exploitation and integrations of physiological and phenomenological models while the underlying physiological mechanisms in a treatment that may not be available due to sensor limitations or only having access to non-invasive measurements (challenges 2, 3) can be estimated and monitored via reasonably complex physiological models. Furthermore, pre-clinical validation of control algorithms can be done using dose-response models capable of reproducing realistic physiological and dose-mediated responses with reasonable computational load. It is noted that models currently available for use in validating ACCS and closed-loop control algorithms fail to achieve

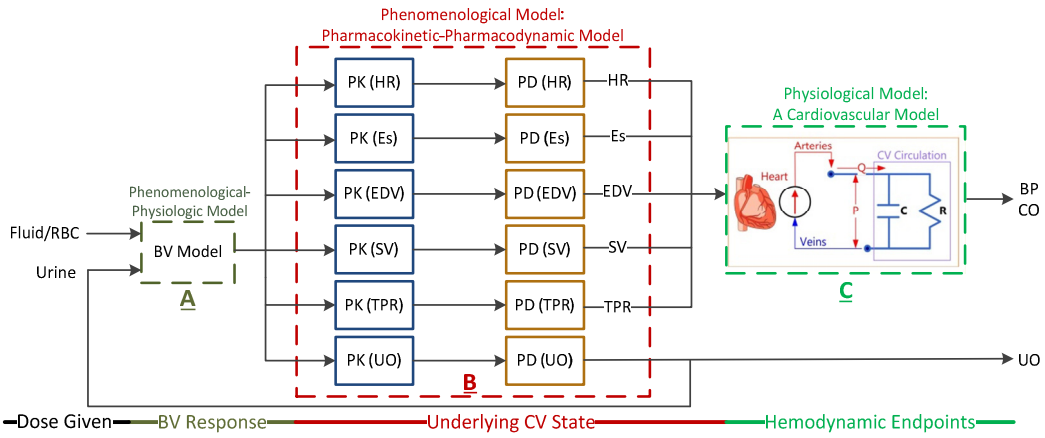

(a)

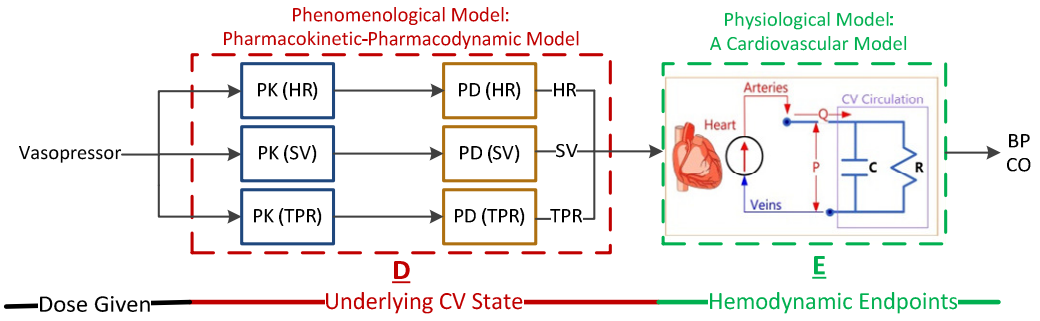

(b)

Figure 1-3: Model of hemodynamic responses to (a) fluid and (b) vasopressor infusion. RBC: red blood cell, PK: pharmacokinetics, PD: pharmacodynamics, HR: heart rate, Es: ventricular elastance, EDV: end-diastolic volume, SV: stroke volume, TPR: total peripheral resistance, UO: urinary output, BP: blood pressure, CO: cardiac output.

the balance between fidelity and complexity: some models are too simplistic to reflect physiological reality (Westerhof et al., 2009), while others are too complicated with thousands of parameters to tune (which is impossible to do systematically with limited observations) (Guyton et al., 1972).

1.4.Dissertation Contributions

This section illustrates the statement of the main contributions of this study.

Need for ACCS:

- A comprehensive retrospective analysis was performed on critical care patients receiving vasopressor infusion by human clinicians. Hemodynamic data associated with 224 ICU patients were collected from a database and investigated for effectiveness of treatment. It was shown that treatment by human clinicians is not optimum and ACCS may lead us to better treatment scenarios (see Chapter 2).

Model of BV and hemodynamic endpoints to fluid perturbation:

- A control-oriented model of BV to fluid infusion was developed. The model was validated in three different situations via data collected from human subjects: (i) fluid resuscitation in different BV states, (ii) fluid resuscitation via different types of fluids, and (iii) fluid resuscitation in different CV states. It was shown that the model is accurate despite its simplicity. More importantly, the model is transparent so that the interpretation of the model can be streamlined during an intervention. Since the model was intended for use in case of only fluid infusion and could not be translated to hemorrhage, the model was also refined to be adapted to both hemorrhage and fluid infusion. The refined model was validated via data from animal subjects and it was shown that the model remained accurate and transparent (see Chapters 3 and 4). Then, the model of BV was expanded to the hemodynamic endpoints, including CO and BP, to fluid infusion and hemorrhage. The low-order hybrid physiologic-phenomenological models of CO and BP were validated via data from animal subjects. The models of BV, CO, and BP were integrated as a single model with as few as 10 parameters to fluid perturbation. A parametric sensitivity analysis showed that among all the parameters, 2 of the parameters are low sensitive and may be fixed at their nominal values. Akaike information

criterion showed a better trade-off between accuracy and complexity when the low sensitive parameters were fixed at their nominal values. This model was proposed to be employed for future ACCS design and evaluation when *in vivo* assessment is unlikely (see Chapter 4).

Model of cardinal parameters and hemodynamic endpoints to vasopressor infusion:

- A dose-dependent model of vasopressor infusion was developed to predict hemodynamic endpoints to new upcoming dosages using only existing non-invasive BP measurements. The model includes two steps: (i) model personalization, where a model of a patient conceived by a physiological model of CV system and phenomenological models of underlying parameters were patient specifically trained to existing vasopressor dose and non-invasive BP data, and (ii) response prediction, where the trained model was interpolated or extrapolated to a new upcoming dose to predict hemodynamic endpoints to new vasopressor dosages. In this regard, first, low-order Phenomenological models of underlying parameters (or cardinal parameters) were developed. The two advantages of the developed models are: (i) they can be tuned using as few as two vasopressor dosage observations, and (ii) they can be trained via trend of cardinal parameters, and in fact non-invasive BP measurements. The models were validated using sparse steady-state data collected from human subjects as well as high resolution dynamic transient data collected from animal subjects (see Chapter 5). However, cardinal parameters often times are not available in standard clinical setting. Therefore, a mathematical tool was developed to (i) estimate the trend of cardinal parameters, and (ii) predict hemodynamic endpoints, and in particular BP, to upcoming

vasopressor doses using existing BP measurements to previous vasopressor dose levels. To this end, the well-received model of CV system, i.e., Windkessel model, was employed. The model was examined to predict hemodynamic endpoints in response to epinephrine, a common vasopressor agent for patients with heart failure, and it was shown that the model can capture the bi-phasic behavior of epinephrine pretty well, even if we only employ two existing vasopressor dosages. Using a mathematical analysis, it was shown that Windkessel model may fail when there is a wide variation of pulse pressure (PP) during fluid infusion (See Chapter 6).

Universal model of hemodynamic endpoints to combined BV perturbation and vasopressor infusion:

- Although the models developed above could adequately reproduce the hemodynamic responses in separate scenarios of BV perturbation and vasopressor infusion, the feasibility of a systematic way to merge them as a single model to combined BV perturbation and vasopressor infusion is dubious, but not impractical. Therefore, for the first time, a universal model of hemodynamic endpoints to combined BV perturbation and vasopressor infusion was developed. This new model necessitates adding new complexities and parameters, including left ventricular preload, and its validation requires a unique set of data. A unique set of data including left ventricular pressure and volume measurement were collected from animal subjects. It was shown that the model could adequately reproduce the hemodynamic responses. The identifiability and parametric sensitivity analysis

indicated that there are two low sensitive parameters that may be fixed at their nominal values.

1.5.Dissertation Organization

This dissertation is arranged into the following chapters. Chapter 2 will review the existing works on closed-loop hemodynamic management as well as analytic models for BV and vasopressor agents. The need for ACCS will also be shown by illustrating the statistics for critical care patients receiving treatment by human clinicians. Chapter 3 will present a low-order physiological model of BV to estimate change in BV in response to fluid infusion (block A in Figure 1-3(a)). The BV model will be validated against different BV states, different types of fluids, and different CV states via experimental data from human subjects. In Chapter 4, a physiological model relating the change in BV to the hemodynamic endpoints will be proposed (block B and C in Figure 1-3(a)). This model will estimate the underlying CV states and hemodynamic endpoints in response to BV perturbation. The model validation will be performed via experimental data from sheep subjects under hemorrhage and fluid infusion. Chapter 5 will develop dose-response relationships for the underlying CV state and employ dose relationship to predict the hemodynamic endpoints to vasopressor infusion (block D in Figure 1-3(b)). The relationships will be validated using both human and animal subjects under vasopressor infusion. Chapter 6 will present a method based on the Windkessel model that relates the BP measurements to the underlying CV state in response to vasopressor infusion (block E in Figure 1-3(b)). In the later part of this chapter, it will be illustrated that this method cannot adequately

work for the fluid infusion. In order to define a universal framework to reproduce the underlying CV state and hemodynamic endpoints to consecutive (and perhaps concurrent) fluid and vasopressor infusion, Chapter 7 will propose a new paradigm built upon the left-ventricular (LV) pressure-volume (P-V) loop context. The model will be validated by the animal data collected by our group on the hemodynamic responses to BV perturbation and vasopressor infusion. Chapter 8 will summarize the contributions of this dissertation and propose directions for future research.

Chapter 2: Literature Review

2.1.Need for Automated Critical Care Systems

Hypovolemia is the state of decreased BV and can be due to either blood loss or loss of body fluids. Hypovolemia can be attributable to many injuries and pathophysiologic conditions, such as hemorrhage, burns, trauma and infections (e.g., sepsis) (Barrow et al., 2000; Bortolani et al., 1996; Chien, 1971; Guillamet et al., 2012; Hollenberg et al., 1999; Hunter and Doddi, 2010; Pruitt, 1978; Vatner, 1974). Initially, after a severe hypovolemia occurrence, the body compensates for the volume loss by increasing the HR, increasing the strength of heart contractions, and constricting blood vessels in the periphery while preserving blood flow to the brain, heart and kidneys. With continuing volume loss, the body loses its ability to compensate and CO and BP drops. At this point, the heart is unable to pump enough blood to vital organs to meet their needs, cells start to malfunction, and waste products build up, leading to further cell death and eventually tissue damage.

Given that severe blood loss causes an impairment of the ability to self-regulate CO and BP, BV regulation and circulatory system must then be restored by means of carefully calculated external fluid and vasopressor infusion. The ultimate goal of fluid resuscitation and vasopressor infusion is to restore venous return, CO, and essentially BP, by optimizing the intravascular BV perfusion. In many hypovolemic scenarios, early and closely hemodynamic management is crucial for survival. Previous investigations indicate that delayed and inappropriate doses of fluid and vasopressor were shown to be responsible for increased mortality and morbidity (Barrow et al.,

2000; Michard, 2013; Varadhan and Lobo, 2010; Wolf et al., 1997). Fluid and vasopressor overdose can lead to rebleeding, pulmonary edema, congestive heart failure, hypertension and its consequences of heart attack and stroke, while inadequate fluid and vasopressor infusion results in acute renal failure, suboptimal perfusion to burned and vital organs and, eventually, death. Therefore, the level of fluid and vasopressor dose administration during hemodynamic management needs to be tightly controlled.

However, the complexity and pressure of the clinical environment and the large degree of individual patient variability can limit the clinicians' ability to provide strict standards of care and as a result, the performance of the human clinicians in hemodynamic management is suboptimal. There is increasing evidence that suboptimal hemodynamic management by the clinicians can significantly influence longer-term outcomes (Komajda et al., 2009; Parmer et al., 2015). A decrease in variation in clinical practice to improve the consistency and adequacy of individual treatment is a key factor in critical care quality improvement. Therefore, development of ACCS is considered as a vital step that needs to be taken to achieve optimal treatment, specifically when human clinicians are in short supply, pressed for time and overwhelmed by many patients (Michard, 2013).

In a retrospective analysis (Bighamian et al., 2014b), we investigated the degree to which today's intensive care unit (ICU) patients receive appropriate vasopressor therapy, in terms of how often the mean arterial pressure (MAP) was kept within a

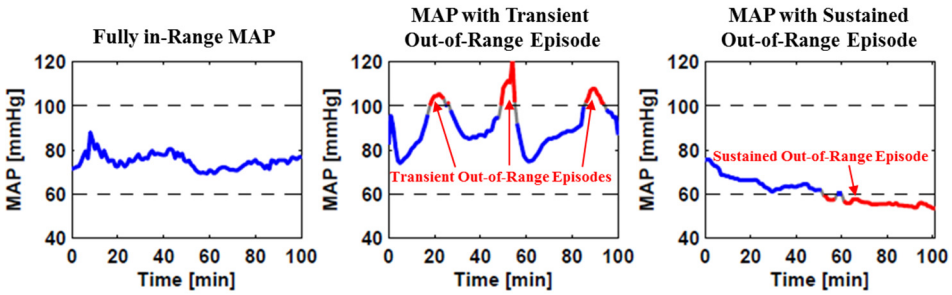

Figure 2-1: Example of in-range MAP vs. transient/sustained out-of-range MAP episodes.

normative range. Using a publically available database of ICU clinical data, the MIMIC II (Multi-Parameter Intelligent Monitoring in Intensive Care) database (Saeed et al., 2011), we studied patients with minute-by-minute MAP data, sourced from the bedside monitor, who were receiving vasopressor therapy. For each record, we identified MAP samples that were out-of-range, i.e., MAP < 60 mmHg or MAP > 100 mmHg, and grouped these into out-of-range episodes. Each out-of-range episode was categorized as either transient (< 15 min) or sustained (≥ 15 min) (e.g., see Figure 2-1). Out of the 224 ICU stays, we identified 152 ICU stays (68% of ICU stays) (see Table 1) with at least one sustained MAP out-of-range episode. In that subset, MAP was frequently out-of-range (out-of-range 18.4% of the time) due to a combination of sustained episodes of hypotension and hypertension (additional statistics are shown in Table 2).

There was no evidence that these episodes tended to cluster in time. Indeed, there was significant time between each episode (see Table 2; time between episodes = 87 min). The median episode lasted over 27 min, and episodes longer than that were commonplace. Compared with all ICU stays, those stays with sustained out-of-range events did not demonstrate an increased MAP variability per hour. It is possible that the out-of-range events resulted from insufficient dose-adjustment. We anticipated that

technologies like ACCS that might continuously optimize vasopressor dosing throughout the patient's stay and thereby minimize these abnormal CV states may be worthy of further study (Bighamian et al., 2014b).

ACCS, including closed-loop or decision support systems, are medical systems capable of autonomous decision making based on feedback from physiological sensors. These medical devices have the potential to reduce the workload of clinicians and autonomously deliver accurate, consistent, and timely therapy (Dumont, 2014; Dumont and Ansermino, 2013; Michard, 2013). The nature of these devices can facilitate knowledge transfer from clinical research to patient bedside to improve consistency of use and speed adoption of clinical best practice; an automated system can be more powerful and accurate when compensating for dynamic interactions in a multivariable setting. One of the key advantages of these medical devices is that they are not distractible. This can reduce the incidence of human error and inattention by allowing the clinician to focus on higher level tasks (Dumont, 2014).

Table 1: Statistics for patients with sustained out-of-range episodes

Statistics for Patients with Sustained Out-of-Range Episodes	
Expression	Number
Total number of distinct subjects, n	127
Total number of ICU stays, n	152
Length on pressors per ICU stay, [min]	Median = 1276 IQR = 569 - 2980
% of in-range MAP, [%]	Median = 81.6 IQR = 66.9 - 91.7
% of MAP out-of-range during transient episodes, [%]	Median = 3.7 IQR = 1.9 - 6.2
% of MAP sustained < 60 mmHg, [%]	Median = 8.5 IQR = 1.6 - 20.1
% of MAP sustained > 100 mmHg, [%]	Median = 0.0 IQR = 0.0 - 3.9
Variation of MAP per hour, [%]	Median = 4.1 IQR = 2.9 - 6.2
Number of vasopressor dose changes per hour, (average for ICU stays ± std. dev., n)	0.5 ± 0.4

Table 2: Statistics for sustained out-of-range episodes

Statistics for Sustained Out-of-Range Episodes	
Expression	Number
Number of episodes per ICU stay, n (among ICU stays with at least one episode)	Median = 3 IQR = 1 - 9
Time between episodes, [min]	Median = 86.5 IQR = 60.8 - 487
Duration of episodes, [min]	Median = 27.0 IQR = 22.0 - 37.5
Longest episode per stay, [min] (among ICU stays with at least one episode)	Median = 51.5 IQR = 30.0 - 98.0

In ACCS, a key factor that needs to be controlled in a hypovolemic patient is the patient's level of fluid perfusion to tissues and in this regard, the knowledge of the BV and CO is required. However, due to immature sensor technology, e.g., there is no sensor to measure the amount of BV during fluid resuscitation, or the absence of invasive hemodynamic measurements, e.g., stroke volume (SV) and CO; a tight control of hemodynamic management using standard practice is not fully achievable. Due to these limitations, clinicians augment the fluid and vasopressor dose until a physiological endpoint reaches its target value specified by the clinician. The underlying assumption is that regulating that physiological endpoint to target is equivalent to optimizing the blood perfusion to tissues, i.e., minimizing the sensitivity of the blood perfusion to additional fluid and vasopressor dose augmentation. Unfortunately, the success of the above-mentioned efforts has been modest due to the limited quality of the endpoints used. For example, central venous pressure (CVP) is invasive and is also a poor predictor of fluid responsiveness (Bendjelid and Romand, 2003; Marik, 2009; Marik et al., 2008; Michard, 2005). The monitoring technologies for gold-standard CO are highly invasive. Urinary Output (UO) is a late detector of hypovolemia. The use of pulse pressure (PP) variability (PPV) is limited to

mechanically ventilated subjects (Rinehart et al., 2011). HR and MAP are non-specific and affected by many common pharmacologic agents and compensatory mechanisms (Kramer et al., 2008). Moreover, hypotension should not serve as an automatic trigger for fluid administration since not all hypotensive events are due to hypovolemia (Navarro et al., 2015). Moreover, recent reports indicate that PP, a well-known and widely accepted surrogate of SV, underestimates SV (Convertino et al., 2006; Leonetti et al., 2004). It is, therefore, obvious that a major leap toward better control of hemodynamic management is required and must accompany a significant advancement in the monitoring technologies for fluid perfusion-responsive endpoints.

2.2.Closed-Loop Systems

Patients suffering from hypovolemia require carefully calculated external fluid resuscitation followed by vasopressor infusion, i.e., BV management, to restore their volume state. The goal of a closed-loop control system is thus to mimic the functionality of the BV circulatory system in providing automatic regulation of BV and CO level in patients. Several researches have been conducted to design closed-loop systems that can determine how much fluid or vasopressor dose has to be given to patients over time until a physiological endpoint achieves its target value specified by the clinician. In the reminder of this section, closed-loop algorithms of fluid and vasopressor administration proposed in the literature and their pros and cons will be introduced. It is noted again that regardless of the employed control algorithms, a major drawback of many of these previous studies is that they still try to control the endpoints that are not good surrogates of BV perfusion in hypovolemic patients.

2.2.1. Empirical Closed-Loop Algorithms

In practice, it's difficult to completely understand how a body responds to severe hypovolemia since many underlying mechanisms get involved in this situation. Hence, the simplest way to design a controller would be to observe fluid and vasopressor dose and their corresponding target endpoints in real-time, and formulate a control rule based on the observed relationship between the variables of interest. The majority of available closed-loop algorithms to treat hypovolemic patients relate the target endpoint to dose of fluid and vasopressor based on experimental data and not on a theory. Although an empirical closed-loop algorithm is an easy approach to relate fluid and vasopressor dose to target endpoint in real-time with no need to tune the patient's parameters in advance, this method suffers from few serious drawbacks. It's a black-box approach, offering no insight into the underlying physiological mechanism in a hypovolemic patient (an appropriate BP can be harmful without monitoring underlying mechanisms, i.e., SV and TPR). Furthermore, its predictive capability is very limited; they may extrapolate the dose-response relationship to a huge dose of fluid or vasopressor in absence of enough dose-response samples that may risk a patient's safety. In other words, the success of the algorithm relies on the human clinician's experience in adjusting the level of perturbation in dose.

In this respect, many existing works on closed-loop fluid resuscitation and vasoactive agent administration are designed based on empirical closed-loop algorithms. These works employ simple PID and/or rule-based controllers to mostly control superficial endpoints, e.g., UO, MAP, systolic BP (SBP), mean systemic pressure (MSP), in fluid resuscitation (see Table 3; Bowman and Westenskow 1981;

Table 3: Existing closed-loop systems for fluid resuscitation

First author	Year	Controlled Parameter	Control Approach	Intervention
Bowman	1981	UO	Empiric (PID Control)	Fluid Resuscitation
Debey	1987	UO	Empiric (P Control)	Fluid Resuscitation
Blankenship	1990	Left Atrial Pressure (Measured)	Empiric (P Control)	Auto-Transfusion
Parkin	1994	Mean Systemic Pressure	Empiric (P Control)	Fluid Resuscitation
Ying	2002	MAP	Empiric (Fuzzy-PID Control)	Fluid Resuscitation
Chaisson	2003	CO, O_2 Saturation (Measured)	Empiric (Nonlinear P Control)	Fluid Resuscitation
Hoskins	2006	UO	Empiric (PID Control)	Fluid Resuscitation
Vaid	2006	MAP	Empiric (Nonlinear P Control)	Fluid Resuscitation
Salinas	2008	UO	Empiric (PID Control)	Fluid Resuscitation
Rinehart	2011-3	SV (Measured)	Empiric (Population-Based Model + Fuzzy Control)	Fluid Resuscitation

Table 4: Existing closed-loop systems for vasoactive infusion

First author	Year	Controlled Parameter	Control Approach	Intervention
Ying	1990	MAP	Empiric (Fuzzy Control)	Vasoactive Infusion
Mackenzie	1993	SBP	Empiric (PID Control)	Vasoactive Infusion
Uemura	2006	BP, CO, Left Atrial Pressure	Empiric (PI/Nonlinear Control)	Vasoactive Infusion
Kee	2007	SBP	Empiric (Rule-Based Control)	Vasoactive Infusion
Merouani	2008	MAP	Empiric (Fuzzy Control)	Vasoactive Weaning
Karar	2011	MAP and CO	Empiric (Fuzzy Neural Network Control)	Vasoactive Infusion
Sng	2014	BP	Empiric (Rule-Based Control)	Vasoactive Infusion
Wassar	2014	MAP	Empiric (PD Control)	Vasoactive Infusion

DeBey et al. 1987; Blankenship, Wallace, and Pacifico 1990; G. Parkin et al. 1994; Ying et al. 2002; Hoskins et al. 2006; Vaid et al. 2006; Salinas et al. 2008) and vasoactive infusion (see Table 4; Ying and Sheppard 1990; Mackenzie et al. 1993; Ngan Kee et al. 2007; Merouani et al. 2008; Sng, Tan, and Sia 2014; Wassar et al. 2014). Besides, there are some works employing measured CO and SV to control fluid resuscitation (Chaisson et al., 2003; Rinehart et al., 2011, 2012, 2013) and vasoactive infusion (Karar and El-Brawany, 2011; Uemura et al., 2006), which are not yet optimal since measurement technologies for CO and SV are highly invasive.

2.2.2. Model-Based Closed-Loop Algorithms

Against empirical models, a model-based approach relates a target endpoint to the fluid and vasopressor dose input via a mathematical model. Once the mathematical solution is obtained, depending on the extent of derivation of the model and its adequacy, the model can offer different helpful information that was not achievable using an empirical model. The model can offer useful insight into the underlying physiological mechanism during a hemodynamic management scenario, e.g., trends of SV and TPR can be monitored when BP is chosen as the target endpoint. The model has great potential to do prediction, e.g., one step ahead and pure prediction, under a wide variety of dose perturbation, where the model's prediction performance is limited by the extent to which the model is valid or accurate. It also allows testing of a control algorithm without involving real patients, in which a patient's safety won't be taken under risk. Furthermore, mathematical models can be employed to derive virtual sensors; those hemodynamic variables that cannot be measured due to immature sensor technology in a standard clinical practice are estimated using derivation of mathematical-based virtual sensors. These virtual sensors can help clinicians have access to those physiological variables that are direct and true surrogates of hemodynamic management.

2.3.Mathematical Models for Hemodynamic Management

As discussed in the previous section, a model-based algorithm is more helpful than empirical methods to control hemodynamic management and is of interest in this research. In this section, we then examine the available models in the literature that

can be employed in a model-based control algorithm. We first briefly study the models developed for BV and then we investigate those of vasopressor.

2.3.1. Blood Volume Models

Fluid resuscitation is an essential component of treatment for critically ill patients. By virtue of its capability to deliver BV states via the analysis of fluid infusion-hemodynamic response data, judicious use of a mathematical model may offer a unique opportunity in providing objective guidance to fluid resuscitation. Ideally, such a model must be simple enough for real-time use while at the same time transparent enough to elucidate volume distribution in the body by revealing how the infused fluid is distributed in the blood and interstisium. In this respect, many existing models are not best suited for the purpose of guiding fluid resuscitation for a few reasons. Existing mechanistic models of BV dynamics can reproduce the volume changes in blood and interstitial fluid (ISF) volume (ISFV) (Arturson et al., 1989; Carlson et al., 1996; Cervera and Moss, 1974; Gyenge et al., 2003; Hedlund et al., 1988; Mazzoni et al., 1988; Pirkle and Gann, 1976; Tatara et al., 2007) and even intracellular fluid (Arturson et al., 1989; Carlson et al., 1996; Gyenge et al., 2003; Hedlund et al., 1988; Mazzoni et al., 1988). However, these models are prohibitively complex for real-time use. On the other hand, existing simple models are governed by empiric equations (Champion et al., 1975; Hirshberg et al., 2006; Lewis, 1986; Mardel et al., 1995; Simpson et al., 1996; Wears and Winton, 1990). In some of these models, the blood flow from the interstitium to blood is not even considered (Champion et al., 1975; Lewis, 1986), while in some others this blood flow is crudely approximated via the population-averaged knowledge (Hirshberg et al., 2006; Mardel et al., 1995; Simpson

et al., 1996; Wears and Winton, 1990). Thus, these simple models may have limited efficacy in transparently revealing volume states. More recently developed volume kinetic models (Svensén and Hahn, 1997; Drobin and Hahn, 1999, 2002) may be superior in compromising simplicity and transparency. However, these models determine the volume changes in blood versus ISF by their respective baseline volumes, which is not consistent with the real-world physiology and may thus hamper their physiological interpretation. This is proved below:

For illustration purposes, a two-compartment volume kinetic model is considered. However, the finding applies to general volume kinetic models. The governing equation is given by (Hahn, 2010):

$$\begin{aligned}\dot{v}_c &= R_0 - CL_0 - CL\frac{v_c - v_{c0}}{v_{c0}} - CL_d\left(\frac{v_c - v_{c0}}{v_{c0}} - \frac{v_t - v_{t0}}{v_{t0}}\right)\\ \dot{v}_t &= CL_d\left(\frac{v_c - v_{c0}}{v_{c0}} - \frac{v_t - v_{t0}}{v_{t0}}\right)\end{aligned} \tag{2-1}$$

where v_c and v_{c0} are the BV and its baseline value, v_t and v_{t0} are the ISFV and its baseline value, R_0 is fluid infusion rate, CL_0, CL and CL_d are the clearances associated with the baseline fluid loss, dilution-dependent elimination and inter-compartmental distribution, respectively. Denoting the changes in BV and ISFV as state variables x_1 and x_2, (2-1) is reformulated into the following:

$$\begin{bmatrix}\dot{x}_1\\ \dot{x}_2\end{bmatrix} = \begin{bmatrix}-(K_1 + K_2) & K_3\\ K_2 & -K_3\end{bmatrix}\begin{bmatrix}x_1\\ x_2\end{bmatrix} + \begin{bmatrix}1\\ 0\end{bmatrix}u \tag{2-2}$$

where $K_1 = \frac{CL}{v_{c0}}$, $K_2 = \frac{CL_d}{v_{c0}}$, $K_3 = \frac{CL_d}{v_{t0}}$ and $u = R_0 - CL_0$. So, taking the Laplace transform and solving for x_1 and x_2 yields:

$$x_1(s) = \frac{s + K_3}{s^2 + (K_1 + K_2 + K_3)s + K_1K_3}u(s),$$
$$x_2(s) = \frac{K_2}{s^2 + (K_1 + K_2 + K_3)s + K_1K_3}u(s) \quad (2\text{-}3)$$

This results in the following:

$$\frac{x_2(s)}{x_1(s)} = \frac{K_2}{s + K_3} \quad (2\text{-}4)$$

Thus, the steady-state ratio between x_1 and x_2 reduces to $\lim_{s\to 0}\frac{x_2(s)}{x_1(s)} = \frac{K_2}{K_3} = \frac{v_{t0}}{v_{c0}}$, meaning that the ratio between the change in BV and the change in ISFV is determined by the ratio of their baseline values, which is not consistent with the known physiological principles (Guyton et al., 1975).

2.3.2. Vasopressor Models

The ultimate goal of vasopressor therapy is superior blood circulation and tissue perfusion, i.e., volumetric blood flow. Therefore, it is reasonable to presume that there would be additional benefit to analytic tools identifying dose-response relationships in terms of both circulatory flow as well as BP: CO would indicate the level of overall blood delivery to the body, while BP would indicate when perfusion pressures are so low that even the heart and brain are likely hypo-perfused or conversely, when excessive BP raises the risk of undue physiological stress on the heart. Such a tool could help clinicians to select an optimized vasopressor dose. In practice, such analytic tools for adjusting vasopressor dosages have not been widely adopted, and we theorize that this is, at least partially, related to their ongoing limitations. In the ideal, a tool

would infer the complete circulatory state of an individual patient on the basis of limited hemodynamic data, rather than the input of a multitude of parameters and a multitude of serial measurements (Chase et al., 2010; Gingrich and Roy, 1991).

In this section, existing technologies for hemodynamic responses to vasopressors are summarized. In essence, we found that none of the existing technologies is capable of the following (see Table 5):

1- Existing technologies cannot predict patient-specific cardiac and vascular responses only based on non-invasive BP (NIBP).

2- Existing technologies cannot predict patient-specific dose-response only with as few as two NIBP measurements observed at two infusion rates.

3- Existing technologies cannot predict patient-specific dose-response by combining population-based parameters for one class of cell receptor effects while fitting a patient-specific dose-response for another class of cell receptor effects.

For example, Chase et al. (Chase et al., 2010) reported a patient-specific response model to epinephrine. Prediction was done by a linear curve fitting of identified epinephrine-specific parameters defined in the paper. It does not involve a phenomenological model; instead, it depends on simple linear regression. These parameters accommodate both cardiac and vascular effects. Since the curves are linear, a prediction based on two observations is possible. This method is not a NIBP based approach (depending on measurements of LV end-systolic volume (ESV) and end-diastolic volumes (EDV)). This method doesn't work based on the receptor effects. Woodruff et al. (Woodruff et al., 1997) reported a pharmacokinetic-pharmacodynamic

Table 5: Capabilities and limitations of existing vasopressor models; Y: Yes, N: No

Markers	Gingrich, 1991	Woodruff, 1997	Johnston, 2004	Chase, 2010	Görges, 2010
Ability to predict patient-specific cardiac vs vascular response?	Y	Y	Y	Y	N
Ability to predict phenomenological dose responses?	N	Y	Y	N	N
Ability to predict patient-specific cardiac vs vascular response only with NIBP?	N	N	N	N	N
Ability to use as few as two observations from two infusion rates?	N	N	N	Y	N
Ability to use only NIBP observations?	N	N	N	N	N
Ability to accommodate alpha vs beta effects?	N	N	N	N	N

(PK-PD) patient-specific response model to vasopressor drugs, including sodium nitroprusside, nitroglycerin, dobutamine and dopamine. Some of the phenomenological PD models include more than two parameters; therefore, the prediction cannot be done by using two measurements. These parameters accommodate both cardiac and vascular effects. This method is not a NIBP based approach (depending on measurements of TPR, venous unstressed volume and LV contractility). This method can accommodate the effects of alpha and beta receptors for case of dopamine, but the number of parameters has increased rather than using the population-wide parameters. Görges et al. (Görges et al., 2010) reported a patient-specific response model to epinephrine. The MAP prediction was done using empiric models and drug sensitivity identification. Prediction based on two observations is not possible since more than 2 parameters should be individualized. This method is a NIBP based approach and doesn't work based on receptor effects. Gingrich et al. (Gingrich and Roy, 1991) reported a patient-specific response model to dopamine. Prediction based on two observations is not

possible since CO model involves more than 2 parameters to be individualized. This method is a NIBP based approach and doesn't work based on the receptor effects. Johnston et al. (Johnston et al., 2004) did a regression analysis to show a quadratic relationship between the infusion rate of dopamine and the CO and TPR. They showed that the break-point in quadratic fitting is consistent with predominantly beta-adrenergic stimulation at lower doses of dopamine and alpha-adrenergic stimulation at higher doses. Note that other BP control approaches determine the drug dose level by directly analyzing the relationship between drug and BP (MAP) (e.g., (Görges et al., 2010)), where the underlying physiology of the drug infusion is ignored, making it difficult to predict the interactions of multiple drug infusions and pathophysiology responses.

2.4.Need for Physiological Models

As discussed above, most of closed-loop efforts proposed for hemodynamic management are empiric (model-less) and use superficial endpoints that are not direct surrogates of BV and tissue perfusion. Lack of low-order, precise and physiological models that can be adapted for each individual patient using routinely available measured endpoints and be employed in a closed-loop manner with low computational time and cost is one substantial reason that researches still try to design empiric control systems. Therefore, it's time to develop low-order and physiologic models with outstanding merits of prediction for ACCS. The remaining chapters of this proposal will focus on developing such models that can be optimally employed for automated hemodynamic management.

Chapter 3: Development and Validation of a Model of Blood Volume Response to Fluid Administration

This chapter presents a macroscopic mathematical model that reproduces the BV response to fluid infusion. The model represents the fluid shift between the intravascular and ISF compartments as a feedback control system that regulates the ratio between the volume changes in the intravascular and ISF at a target value. The resulting model is characterized by three summary parameters: target volume change ratio between the intravascular and ISF, feedback gain specifying the dynamics of fluid shift, and initial BV. The novelty of this model is that it can obviate the need to incorporate complicated mechanisms involved in the fluid shift in reproducing the BV response to fluid infusion. The validity of the model was examined by fitting it to a series of data on fractional BV responses to fluid infusion.

3.1.Fluid Shift between Intravascular and Interstitial Compartments

The fluid shift between the intravascular and ISF compartments is an essential mechanism of homeostasis, and a key determinant of the physiological response to circulatory pathology and medical therapy. The net fluid shift is determined by the summary action occurring across the body's massive network of microvasculature, and the determinants of flow for each microscopic segment are complex, including the permeability of the vessels and the local Starling forces (i.e., hydrostatic pressure and oncotic pressure gradients). Each of these determinants can be, in turn, altered by a wide range of other factors, including the vasomotion of upstream and downstream

vessels, lymphatic flow, and a myriad of endocrine and exocrine signals that affect the preceding determinants.

Given the undeniable complexity that underlies fluid shift between the intravascular and ISF compartments, it can be challenging to mathematically model an individual subject or patient. Existing models of fluid shift dynamics can reproduce the volume changes in blood and ISF and even intracellular fluid. However, there are so many disparate factors that, without exhaustive and impractical measurements, it is really not possible to characterize the fluid shift dynamics associated with an individual comprehensively. A reasonable alternative is to use "typical" values for certain parameter values (i.e., values that represent average values in a population) but this is no longer an individualized model (e.g., (Mardel et al., 1995; Simpson et al., 1996; Wears and Winton, 1990)) (for more details see Section 2.3.1). To overcome these challenges, a mathematical model that could reproduce the dynamic fluid shift between the intravascular and ISF compartments is developed in this chapter. Specifically, the model is designed to be simple enough to be fitted to individual subjects with only a rudimentary set of measurements, and accurate enough to characterize that subject's dynamic response to fluid infusion.

3.2.Development of Blood Volume Model

The proposed macroscopic model involves only three summary parameters to dynamically describe an individual's fluid shift after fluid infusion: target volume change ratio between the intravascular and ISF, α_u; feedback gain specifying the dynamics of fluid shift, K_p; and initial BV, V_{B0}.

The first summary parameter of the proposed model is the target volume change ratio between the intravascular and ISF, α_u. By way of background, the volume of fluid stored in the intravascular, ISF and intracellular compartments is determined by the hydraulic and osmotic pressure gradients at the capillary walls and cell membranes. From microscopic standpoint, the kinetics of a number of ions and proteins as well as the P-V relationships of the fluid compartments determine the hydraulic and osmotic pressure gradients, and therefore, the fluid volume stored in each compartment. However, from macroscopic standpoint, the interaction among these complex mechanisms is that the ratio between the volume changes associated with the intravascular and ISF may be summarized by a constant parameter value, denoted as α_u (Guyton et al., 1975). This physiologic summary parameter α_u varies depending on the overall state of the subject. Typically, ISF volume changes 2-3 times as much as intravascular volume changes (i.e., α_u =2-3) up to a critical BV level. Beyond this level, however, majority of the fluid infused to the body is not stored in the intravascular compartment but is transferred to the ISF compartment (i.e., $\alpha_u \gg$2-3), which is a mechanism that prevents pathophysiologic conditions such as pulmonary edema (Bajwa and Kulshrestha, 2012). In sum, the way BV responds to an infusion of fluid may be summarized as that of a hypothetical feedback control system that regulates the volume changes associated with the intravascular and ISF at a target ratio $1:\alpha_u$, via the body's physiologic processes to produce the fluid shift between the intravascular and ISF compartments.

The second summary parameter of the model is the phenomenological feedback gain, K_p, which specifies the dynamics of fluid shift, i.e., the rate of fluid shift

between the intravascular and ISF compartments. This summary parameter is predicated on a feedback control system analogy, in which the intravascular and ISF compartments can be represented as two connected buckets (Figure 3-1(a)). The left and right buckets represent the intravascular and ISF compartments, respectively, while the valve represents a summary of all the physiologic processes that produce the fluid shift between the two compartments. In this analogy, it is both fluid infusion (u) and loss (v; e.g., hemorrhage and UO) that act on the intravascular compartment to alter the BV (V_B). The valve opening is a function of the discrepancy between the target versus actual BV: there is an increased rate of fluid shift between the intravascular and ISF compartments (q) when the discrepancy between target versus actual BV grows larger.

The third summary parameter of the model is the physiologic initial BV, V_{B0}. Its purpose is to normalize the change in BV to yield its fractional change from the initial value. In this way, the proposed macroscopic model becomes compatible with the state-of-the-art techniques to measure BV (Drobin and Hahn, 1999, 2002).

The representation in Figure 3-1(a) can be formalized into the mathematical model shown in Figure 3-1(b). The fluid infusion (u) and loss (v; e.g., hemorrhage and UO) are the inputs to the model, while the change in BV (V_B) is the output. The objective of the control system is to retain the $\frac{1}{1+\alpha_u}$ fraction of the inputted fluid volume in the intravascular compartment while shifting the remaining $\frac{\alpha_u}{1+\alpha_u}$ fraction to the ISF compartment in the steady-state. The fluid shift from the intravascular to ISF compartment (q) acts as feedback control to steer V_B to the target value (r_B). In this

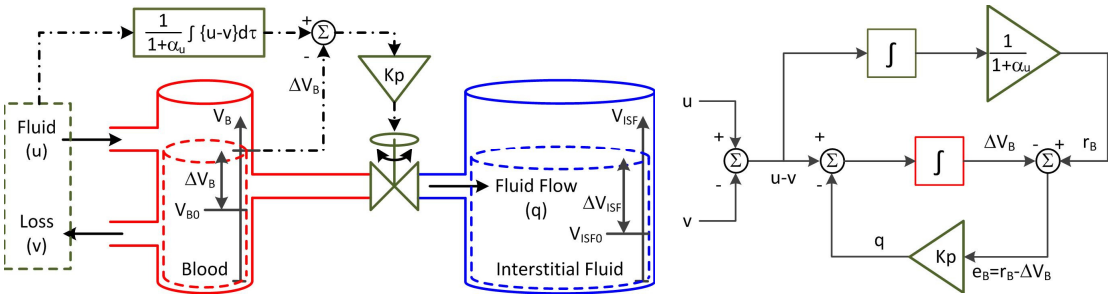

Figure 3-1: Macroscopic BV dynamics model.

way, the steady-state volume changes in intravascular and ISF achieves the $1{:}\alpha_u$ ratio.

The governing equation associated with this mathematical model is derived as follows. The rate of change in BV is given by the following ordinary differential equation:

$$\Delta\dot{V}_B(t) = u(t) - v(t) - q(t) \tag{3-1}$$

where $\Delta V_B(t)$ is change in BV from its initial state. The fluid shift q from the intravascular to ISF compartment is formulated so that the discrepancy between the target versus actual changes in BV converges to zero. As described above, the target change in BV (r_B) in response to the inputs u and v is the $\frac{1}{1+\alpha_u}$ fraction of the accumulated resultant fluid intake $u - v$:

$$r_B(t) = \frac{1}{1+\alpha_u}\int_0^t [u(\tau) - v(\tau)]d\tau \tag{3-2}$$

To capture the macroscopic behavior of q with the simplest possible mathematical expression, q is modeled to be proportional to $e_B = r_B - \Delta V_B(t)$:

$$q(t) = -K_p e_B(t) \tag{3-3}$$

where K_p is the proportionality gain. This expression physically means that 1) fluid shifts from the intravascular to ISF compartment if the BV is larger than its target ($r_B < \Delta V_B(t)$) while from ISF to intravascular compartment if the BV is smaller than its target ($r_B > \Delta V_B(t)$), and that 2) the rate of fluid shift increases as the discrepancy between r_B and $\Delta V_B(t)$ increases. Combining (3-1)-(3-3) yields the following ordinary differential equation as the macroscopic BV dynamics model that relates $u - v$ to V_B:

$$\Delta\ddot{V}_B(t) + K_p\Delta\dot{V}_B(t) = [\dot{u}(t) - \dot{v}(t)] + \frac{K_p[u(t) - v(t)]}{(1 + \alpha_u)} \tag{3-4}$$

To rewrite (3-4) in terms of the fractional BV response, ΔV_B must be normalized by its initial value (V_{B0}). Dividing both sides of (3-4) by V_{B0} yields:

$$\overline{\ddot{\Delta V}}_B(t) + K_p\overline{\dot{\Delta V}}_B(t) = \frac{[\dot{u}(t) - \dot{v}(t)]}{V_{B0}} + \frac{K_p[u(t) - v(t)]}{V_{B0}(1 + \alpha_u)} \tag{3-5}$$

3.3. Validation of Blood Volume Model for Different Blood Volume States and Fluids

The macroscopic model detailed above in Section 3.2 is intended to summarize the BV response to fluid infusion of an individual subject or patient using just three fixed summary parameter values. However, it is possible that the underlying physiology is too complex to be adequately reproduced by such a simple model. Thus, we sought to evaluate this macroscopic model, by fitting it to a multitude of different experimental datasets, to assess whether or not such a simple model is capable of accurately summarizing experimental data.

A series of datasets available in the literature were used to analyze the model. All reported the fractional BV response through time, which was measured as

hemoglobin as tracer (Svensen et al., 2009). Specifically, the datasets included 1) fractional BV response to fluid infusion under different BV states (Set 1) (Drobin and Hahn, 1999); 2) fractional BV response to the infusion of crystalloid fluids (Set 2) (Drobin and Hahn, 2002); and 3) fractional BV response to the infusion of colloid fluids (Set 3) (Hedin and Hahn, 2005).

From the aforementioned reports, the quantity of fluid infused and the fractional BV response were extracted at 10 min intervals as the average of the maximum and minimum responses across all subjects. The UO rate was estimated by dividing the total urine volume by the study duration (infusion time + post-infusion observation time) based on the simplifying assumption that it remained constant, because only the total urine volumes were reported.

Overall, we studied a total of seven distinct protocols summarized in Table 6: in Set 1, there were three protocols (with 0 ml, 450 ml and 900 ml pre-infusion hemorrhage); in Set 2, there were two protocols (with infusions of 0.9 % saline and

Table 6: Data sets used for model validation

	Set 1 (Drobin & Hahn 1999)	Set 2 (Drobin & Hahn 2002)	Set 3 (Hedin and Hahn 2005)
Number of Subjects	10	10	15
Age (min-max)	23-33 year	24-44 year	18-36 year
Weight (min-max)	65-85 kg	72-95 kg	70-94 kg
Fluid Infused	Crystalloid (Ringer's Acetate)	Crystalloid (Saline & Ringer's Lactate)	Colloid (Albumin & Autologous Plasma)
Infused Volume	25 ml/kg	25 ml/kg	10 ml/kg
Infusion Time	30 min	30 min	30 min
Observation Time (Post-Infusion)	150 min	210 min	450 min
Hemorrhage Volume (Pre-Infusion)	0 ml / 450 ml / 900 ml	0 ml	0 ml

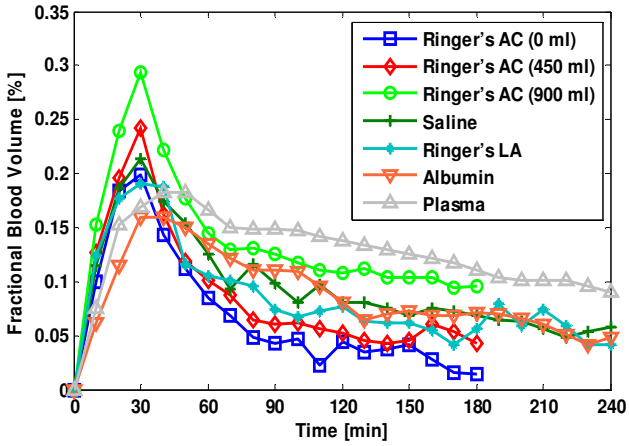

Figure 3-2: Fractional BV responses to fluids. Ringer's AC: ringer's acetate (Set 1 Drobin & Hahn 1999); Saline: 0.9 % saline (Set 2 Drobin & Hahn 2002); Ringer's LA: ringer's lactate (Set 2 Drobin & Hahn 2002); Albumin: 5 % albumin (Set 3 Hedin and Hahn 2005); Autologous Plasma: autologous plasma (Set 3 Hedin and Hahn 2005).

with ringer's lactate); and in Set 3, there were two protocols (with infusions of 5 % albumin and with autologous plasma). The fractional BV responses associated with all the datasets are shown in Figure 3-2.

Now that the model (3-5) is developed, we fitted the model to each dataset, i.e., the values of the three summary parameters α_u, K_p and V_{B0} associated with each dataset were identified. In order to do this, three steps were required to be taken. First, (3-5) was discretized into a difference equation using the Euler's method ($\frac{d}{dt} \approx \frac{z-1}{T_S}$, where z is forward shift operator and T_S is sampling interval) (Nise, 2010):

$$\overline{\Delta V_B}(k) = 2\overline{\Delta V_B}(k-1) - \overline{\Delta V_B}(k-2) - K_p T_S[\overline{\Delta V_B}(k-1) - \overline{\Delta V_B}(k-2)] + \frac{T_S}{V_{B0}}\{[u(k-1) - u(k-2)] - [v(k-1) - v(k-2)]\} + \frac{K_p T_S^2}{V_{B0}(1+\alpha_u)}[u(k-2) - v(k-2)] \quad (3\text{-}6)$$

Second, an optimization problem was formulated to derive the set of summary parameters minimizing the error between the fractional BV data ($\overline{\Delta V_B}$) and their model-reproduced counterparts ($\widehat{\overline{\Delta V_B}}$):

$$\begin{aligned}\Theta^* = \{\alpha_u^*, K_P^*, V_{B0}^*\} &= \arg\min_{\Theta} \sum_{i=1}^{M} J_i(\Theta) \\ &= \arg\min_{\Theta} \sum_{i=1}^{M} \sum_{k=1}^{N} \left[\overline{\Delta V}_{B,i}(k) - \widehat{\overline{\Delta V}}_{B,i}(k)\right]^2\end{aligned} \tag{3-7}$$

where Θ is a vector of (unknown) summary parameters, Θ^* is the optimal Θ, $\widehat{\overline{\Delta V}}_{B,i}(k)$ is model-reproduced $\overline{\Delta V}_{B,i}(k)$ at a discrete time instant k ($k = 1 \cdots N$) for the i-th pre-infusion hemorrhage state, and M is the number of pre-infusion hemorrhage states ($M = 3$ for Set 1 and $M = 1$ for Sets 2 and 3). For a given set of Θ, $\widehat{\overline{\Delta V}}_{B,i}$ was computed by inputting the fluid infusion (u) and urine excretion rate (v) data to (3-6). The optimization problem (3-7) was solved using MATLAB's Optimization Toolbox (MathWorks, MA, USA).

Eventually, the validity of the macroscopic BV dynamics model (3-5) derived from the model fitting (3-7) was tested by analyzing 1) its ability to reproduce the fractional BV data, 2) the model-reproduced changes in the intravascular and ISF volumes associated with different protocols, and 3) the behaviors of the summary parameters across different fluids and pre-infusion hemorrhage states.

First, the ability of the model to reproduce the fractional BV data was assessed by analyzing the goodness of fit associated with each protocol, in terms of sample-by-sample error and root-mean-squared error (RMSE) normalized by the average fractional BV:

$$e(k) = \frac{\overline{\Delta V_B}(k) - \widehat{\overline{\Delta V_B}}(k, \Theta^*)}{\overline{\overline{\Delta V_B}(k)}}, \qquad k = 1, \cdots, N$$

$$\text{RMSE} = \frac{1}{\overline{\overline{\Delta V_B}(k)}} \sqrt{\frac{\sum_{k=1}^{N} \left[\overline{\Delta V_B}(k) - \widehat{\overline{\Delta V_B}}(k, \Theta^*)\right]^2}{N}} \tag{3-8}$$

where $\overline{\overline{\Delta V_B}(k)}$ is the average fractional BV response over the study duration, and $\widehat{\overline{\Delta V_B}}(k, \Theta^*)$ is the fractional BV reproduced by inputting the fluid infusion and UO rate data to (3-6) characterized by Θ^*. Second, the change in BV $\widehat{\Delta V_B}(k, \Theta^*)$ associated with each protocol was estimated by $\widehat{\Delta V_B}(k, \Theta^*) = V_{B0}^* \cdot \widehat{\overline{\Delta V_B}}(k, \Theta^*)$, while the change in ISF volume $\widehat{\Delta V_{ISF}}(k, \Theta^*)$ was estimated by computing the numerical integration of the fluid shift q:

$$\begin{aligned} \widehat{\Delta V_{ISF}}(k, \Theta^*) &= \sum_{n=1}^{k} q(n, \Theta^*) = \sum_{n=1}^{k} K_P^* e_B(n, \Theta^*) \\ &= \sum_{n=1}^{k} K_P^* \left[r_B(n) - \widehat{\Delta V_B}(n, \Theta^*)\right] \end{aligned} \tag{3-9}$$

Third, the following hypotheses on the summary parameters were generated to gauge if they were meaningfully derived by the model fitting: 1) V_{B0}^* decreases as pre-infusion hemorrhage increases; 2) α_u decreases as pre-infusion hemorrhage increases; and 3) α_u is larger in crystalloids than in colloids. These hypotheses were tested by examining the values of α_u^* and V_{B0}^* with respect to accepted typical values as well as their behaviors across different fluids and pre-infusion hemorrhage states.

3.4. Fitting Results

Table 7 summarizes the results of data analysis, including the estimated summary parameters for each dataset and the associated error metrics. Figure 3-3 - Figure 3-5 show the fractional BV responses reproduced by the model, together with the actual data, associated with Sets 1, 2 and 3, respectively, where the upper and lower panels present the actual versus model-reproduced fractional BV responses and the model-derived changes in the blood and ISF volumes, respectively. Each column in Figure 3-3 shows the results associated with different pre-infusion hemorrhage states (1^{st}: 0 ml; 2^{nd}: 450 ml; 3^{rd}: 900 ml). Each column in Figure 3-4 - Figure 3-5 presents the results associated with crystalloids and colloids.

Table 7, at the first glance, indicates that the macroscopic mathematical model can reproduce the BV response to fluid infusion. To better understand the model effectiveness, the validity of the model and its strengths and limitations are further discussed in terms of the model's parsimony, accuracy and physiologic transparency.

1) Parsimony: The macroscopic BV dynamics model presented in this chapter is essentially a minimal model (3-5) characterized by only three summary parameters: α_u specifying the steady-state changes in the intravascular and ISF volumes due to fluid infusion, K_p dictating the dynamics associated with the fluid shift between the intravascular and ISF compartments, and V_{B0} reflecting the initial BV. That this model can be fully characterized just by these summary parameters to reproduce BV response in a subject is its key benefit compared with the existing physiology-based BV dynamics models (e.g., (Hedlund et al., 1988; Mazzoni et al., 1988; Pirkle and Gann, 1976)) whose complexity makes it very challenging to reproduce subject-specific BV responses to fluid infusion without exhaustive and impractical measurements.

Table 7: Data analysis results: estimated summary parameters and error metrics.

		K_P^*	V_{B0}^* [l]	α_u^*	Error [%]	RMSE [%]
Set 1	Ringer's AC (0 ml)	0.052	4.86	4.45	0.49+/-14.1	13.3
	Ringer's AC (450 ml)	0.065	3.88	4.00	0.57+/-7.93	7.52
	Ringer's AC (900 ml)	0.076	3.27	2.57	0.38+/-4.04	3.84
Set 2	Saline	0.047	5.56	2.35	0.46±10.0	9.62
	Ringer's LA	0.069	5.03	2.39	1.81±17.6	16.9
Set 3	Albumin	0.028	3.94	0.45	0.05±9.09	8.73
	Autologous Plasma	0.147	3.11	0.34	0.62±6.49	6.25

2) Accuracy: The results of data analysis (Table 7 and Figure 3-3 - Figure 3-5) support the ability of the model to accurately reproduce BV responses to fluid infusion. The goodness of fit between the actual versus model-reproduced fractional BV responses in Figure 3-3 - Figure 3-5 is encouraging. These results, derived from five different fluids one of which was also associated with three different pre-infusion hemorrhage states (Set 1), suggest that the model may be suitable for summarizing BV responses to a wide range of fluids over diverse volume states.

3) Transparency: The proposed macroscopic model is a highly simple and structured model constrained by the physiologic principle that the ratio between the changes in the intravascular and ISF volumes is regulated at a target value (Guyton et al., 1975). Thus, it is not obvious if the summary parameters estimated from the model fitting (3-7) would retain the intended physiologic meanings. The physiologic transparency of the proposed model is supported by a few observations from the data analysis (Table 7), as detailed below.

First, the optimal values of V_{B0} and α_u were comparable, at least in terms of the orders of magnitude, to the known nominal plasma volume (~3.3 l for an 80 kg male) and the

ratio between the changes in blood and ISF volumes due to a perturbation in the body fluid (~2.3; (Hirshberg et al., 2006; Mardel et al., 1995; Simpson et al., 1996; Wears and Winton, 1990)): the values of V_{B0} derived for the models (Sets 1-3) ranged between 3.1 l and 5.6 l, while the values of α_u derived for the models associated with isotonic crystalloids (Sets 1-2) ranged between 2.4 and 4.5.

Second, the hypothesis made for V_{B0} was validated: it exhibited a decreasing trend with an increase in the pre-infusion hemorrhage (Set 1), which accords with the expectation that pre-infusion hemorrhage would decrease the initial BV.

Third, the hypotheses made for α_u were also validated. Specifically, the value of α_u decreased with an increase in the pre-infusion hemorrhage volume (Set 1). This is in fact consistent with the physiologic principle that more fluid is retained in blood as its volume decreases (Guyton et al., 1975). In particular, a fluid infusion dose of ~2.0 l (according to Table 6, assuming an 80 kg male subject) to a normovolemic subject is likely to result in a state of volume overload, under which α_u would assume a large value. However, the same infusion dose is may not yield serious volume overload in a hypovolemic subject due to relatively small initial BV, under which α_u is close to the nominal value. The systems-level BV dynamics model associated with the data in Set 1 could capture all these anticipated behaviors via model fitting: comparing the lower panels in Figure 3-3, the model estimated that the fluid flow from blood to ISF decreases as pre-infusion hemorrhage increases, which is due to a decrease in α_u. Furthermore, the values of α_u associated with colloids (Set 3) were largely smaller than those associated with crystalloids (Sets 1-2). This accords with widely known knowledge on colloids: colloid molecules are too large to pass through the capillary

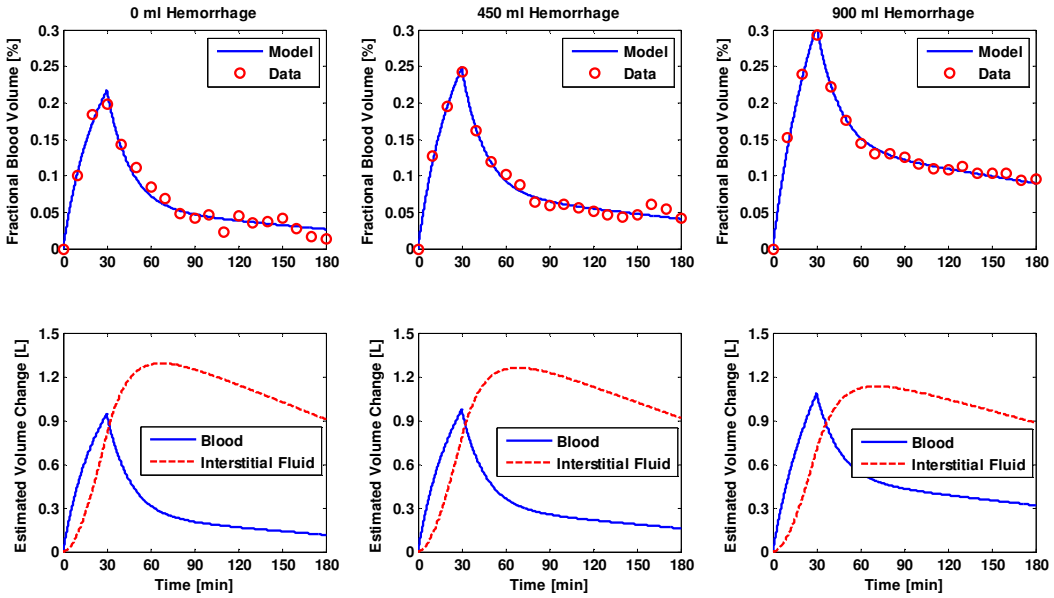

Figure 3-3: Fractional BV responses to 0.9 % saline (1st column) and ringer's lactate (2nd column) reproduced by the macroscopic BV dynamics model.

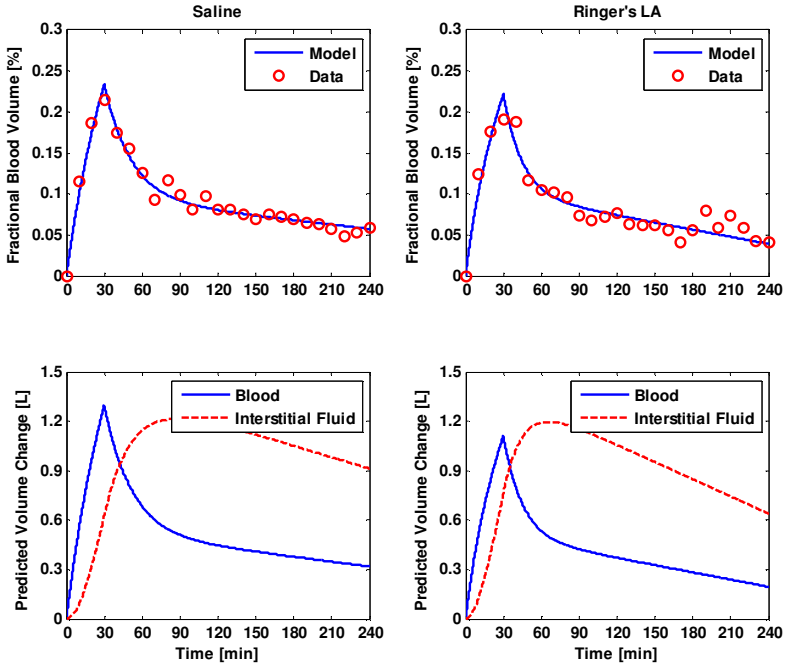

Figure 3-4: Fractional BV responses to 5 % albumin (1st column) and autologous plasma (2nd column) reproduced by the macroscopic BV dynamics model

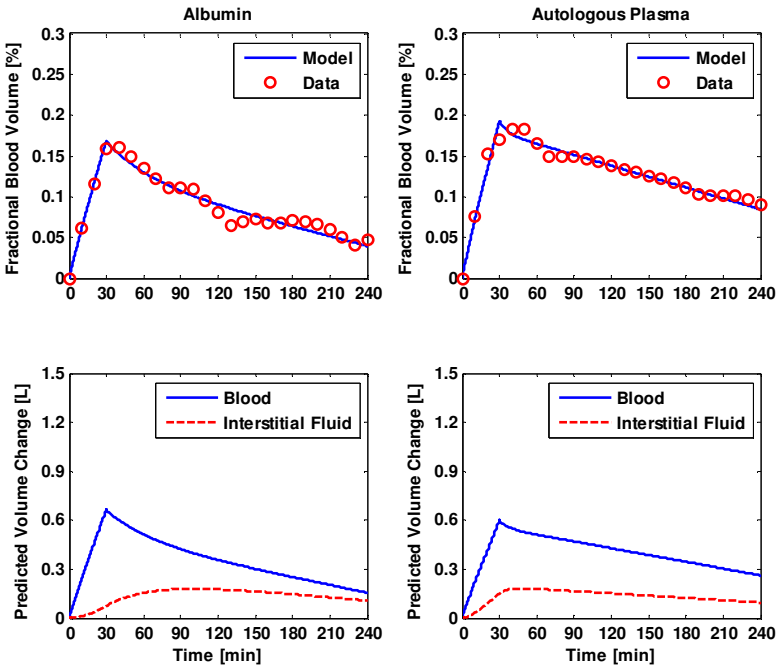

Figure 3-5: Fractional BV responses to 5 % albumin (1st column) and autologous plasma (2nd column) reproduced by the macroscopic BV dynamics model.

membranes, thus slowing down the distribution of colloid from blood to ISF (Hahn, 2013). This in turn decreases α_u associated with colloids, since more fluid tends to be retained in the blood than is distributed to the interstitium. The systems-level BV dynamics model associated with the data in Sets 1-3 captured this behavior via model fitting: comparing the lower panels in Figure 3-3 - Figure 3-5, the model estimated that the fluid volume distributed from blood to interstitium relative to the change in BV is largely smaller for colloids than crystalloids, which originates from relatively small α_u in colloids than crystalloids (note that the colloid infusion dose is only 40 % of the crystalloid infusion dose; Table 6).

In summary, the systems-level model presented in this chapter is 1) simple in that it can be characterized by only three parameters; 2) able to reproduce real-world

BV responses to fluid infusion; and 3) physiologically transparent in that the parameters behave as physiologically anticipated.

3.5.Mechanism of Underlying Model Fitting

The parametric sensitivity analysis was performed in the frequency domain. The sensitivity functions associated with the model (3-5) to V_{B0} and α_u were derived as the normalized partial derivatives of $G(j\omega)$, the frequency response function associated with (3-5), with respect to V_{B0} and α_u:

$$S_{V_{B0}}(j\omega) = \frac{V_{B0}}{G(j\omega)} \frac{\partial G(j\omega)}{\partial V_{B0}}\bigg|_{\Theta=\Theta^*} = -1$$
$$S_{\alpha_u}(j\omega) = \frac{\alpha_u}{G(j\omega)} \frac{\partial G(j\omega)}{\partial \alpha_u}\bigg|_{\Theta=\Theta^*} = \frac{-\alpha_u^*}{(1+\alpha_u^*)^3} \frac{K_P^*}{(1+\alpha_u^*)(j\omega)+K_P^*} \quad (3\text{-}10)$$

Then, the frequency responses of these sensitivity functions were examined to elucidate how V_{B0} and α_u are tuned to fit the model to the fluid infusion-plasma dilution response data. The optimal values of V_{B0} and α_u were comparable to the known nominal values (Section 3.4). However, V_{B0} was in general larger than what is regarded as nominal. The reason for this observation may be found by elucidating the mechanism underlying the model fitting via the parametric sensitivity analysis as detailed below.

The value of α_u was assumed to be constant in the data analysis. However, α_u may continuously vary in reality as BV varies (Guyton et al., 1975). This discrepancy between the model and the reality may have modestly affected the way V_{B0} was derived from the optimization (3-7) as follows. First, the Bode magnitude plots of the sensitivity functions (3-10) to V_{B0} and α_u suggest that the model's response is primarily

affected by V_{B0} in the high frequency regime while comparably affected by V_{B0} and α_u in the low frequency regime (Figure 3-6(a)). Physically, this implies that the model's transient response is largely affected by V_{B0} while its steady-state response is affected comparably by both V_{B0} and α_u. Thus, in solving (3-7), the model tends to fit the transient portion of the response by primarily adjusting V_{B0}, while it tends to fit the steady-state portion of the response by primarily adjusting α_u once a value of V_{B0} that best fits the transient response is determined (Figure 3-6(b)). Second, in response to a fluid infusion, BV first peaks and then decreases as the infused fluid is distributed to the interstitium (Figure 3-3 - Figure 3-5). Thus, the real α_u may first peak and then decrease to a steady-state value as well. However, the model assumes that the

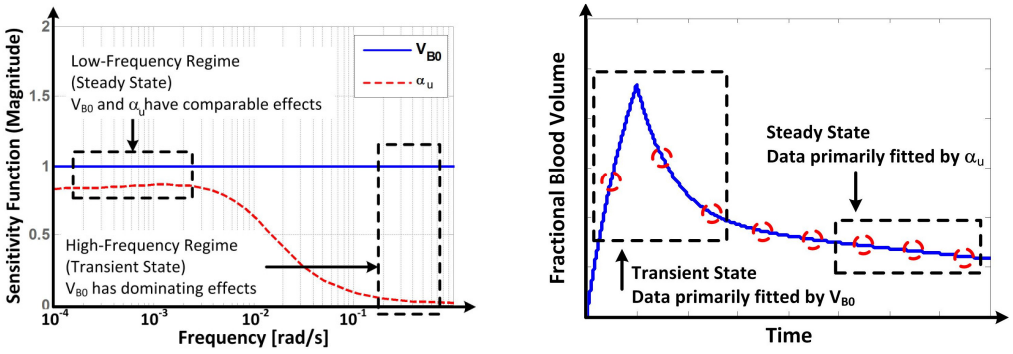

(a) (b)

Figure 3-6: (a) The frequency responses of the model's sensitivity functions (9) to V_{B0} and α_u. (b) The mechanism of how V_{B0} and α_u are tuned to fitting the model to fractional BV response data.

value of α_u is fixed at its steady-state (i.e., the lowest) value. The model (3-6) dictates that this α_u, together with actual V_{B0}, yields an increase in the model-reproduced fractional BV response. To compensate for this discrepancy, V_{B0} is adjusted to be larger than the actual initial volume to decrease the transient fractional BV response. This is presumably the mechanism underlying the large values of V_{B0} derived for the

data in Sets 1-2 (except for the data associated with for 900 ml hemorrhage in Set 1, in which the increase in α_u during the transient response period may have been small).

Compared with crystalloid (Sets 1-2), the initial volumes derived for colloid (Set 3) were closer to physiologic values because the infusion dose of colloid was small (Table 6), resulting in less likelihood of volume overload. It is noted that the assumption of constant α_u was made primarily for the sake of parsimony in modeling and fitting, and drifted initial volume estimation was an artifact due to this assumption. Thus the constant α_u assumption may easily be relaxed. For example, a monotonically increasing parametric function of BV as a model of α_u may allow the model to incorporate transient changes in α_u.

Despite promising initial results obtained for the proposed macroscopic BV dynamics model, there are a few limitations that are mentioned in below.

First, the response of the model only to constant rates of fluid infusion and UO was considered. The model fitting (3-7) was conducted for a UO rate proportional to the fractional BV response (Drobin and Hahn, 1999) to examine the effect of time-varying UO. The results showed no significant deviation from those shown in Table 7. Therefore, the assumption of constant UO rate was deemed quite adequate at least for the datasets examined in this chapter. In any case, the model may readily be extended to reproduce BV responses to time-varying rates of fluid infusion and urine excretion, perhaps by employing more sophisticated expressions for the fluid shift q between the intravascular and ISF compartments.

Second, the amount of data employed to validate the model was rather small (seven datasets). This study successfully demonstrated the initial validity of the model. However, more rigorous assessment of the model, using datasets associated with diverse group of subjects, is desired. Further validation of the model for different CV states using individual subject's BV data is performed in Section 3.6.

3.6.Validation of Blood Volume Model for Different Cardiovascular States

In Section 3.3, the BV model was validated for data collected from subjects with different BV states and different types of fluid. In this section, we validated the model for subjects with different CV states (i.e., CV under control and intervention). To do this, we employed BV data published in the literature (Asmussen et al., 2014). Data were collected from nine human subjects (aged 21-50 years) underwent two randomly assigned protocols that were separated by at least 7 days. Subjects received either a continuous isoproterenol infusion (ISO: 0.05 μg/kg/min) or 0.9% saline (control) 30 min prior to a 25 ml/kg 0.9% saline fluid bolus, which was administered over 20 min. The resulting change in BV and UO were measured at the start of fluid bolus and every 2 min during the fluid bolus, every 5 min for the next 40 min, and then every 30 min for a period of 60 min.

Inspecting the inter-individual variability in BV responses, in particular the data associated with ISO showed an oscillatory behavior that could not be well fitted using a proportional fluid transition mechanism between intravascular and ISF compartments (see K_p in (3-3)). Therefore, we replaced the proportional gain K_p in (3-3) with a proportional-integral (PI) gain as follows:

$$q(t) = \left(-K_p e_B(t) - K_i \int e_B(t)dt\right) \tag{3-11}$$

It was speculated that the source of oscillatory response in ISO was due to the fact that ISO is a significant stimulator of aldosterone production. When aldosterone hormone is released, sodium is reabsorbed from urine to blood, leading to increase the osmolarity of extracellular fluid (i.e., BV and ISF). This increase in the extracellular osmolarity results in a fluid transfer from intracellular to extracellular, and a consequent oscillatory behavior in both BV and ISF. It is noted that (3-11) changes (3-5) as follows:

$$\begin{aligned}\dddot{\overline{\Delta V}}_B(t) + K_p\ddot{\overline{\Delta V}}_B(t) + K_i\dot{\overline{\Delta V}}_B \\ = \frac{[\ddot{u}(t) - \ddot{v}(t)]}{V_{B0}} + \frac{K_p[\dot{u}(t) - \dot{v}(t)]}{V_{B0}(1+\alpha_u)} + \frac{K_i[u(t) - v(t)]}{V_{B0}(1+\alpha_u)}\end{aligned} \tag{3-12}$$

To validate the model in response to two different CV states, the fluid infusion and UO were inputted to the model and the model-reproduced BV responses via (3-6) and (3-11) were fitted to the true BV measurement in both ISO and control protocols. It is noted that since the absolute BV changes was measured in addition to the fractional BV response, two sets of data fitting were executed; first, as Section 3.3, the model of BV (3-6) with 4 tunable parameters including K_p, K_i, α_u and V_{B0} were fitted to the fractional data, while in another attempt the same model was fitted to absolute change in BV assuming $V_{B0} = 1$.

Eventually, the validity of the BV dynamics model derived from the model fitting (3-7) was tested by analyzing 1) its ability to reproduce the absolute and fractional BV data, 2) the behaviors of the summary parameters across different CV

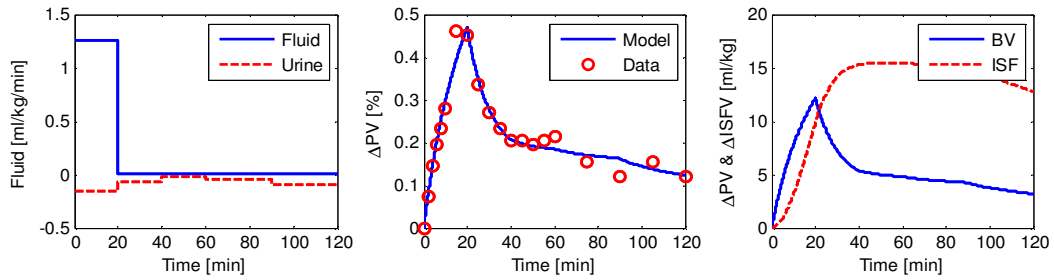

(a)

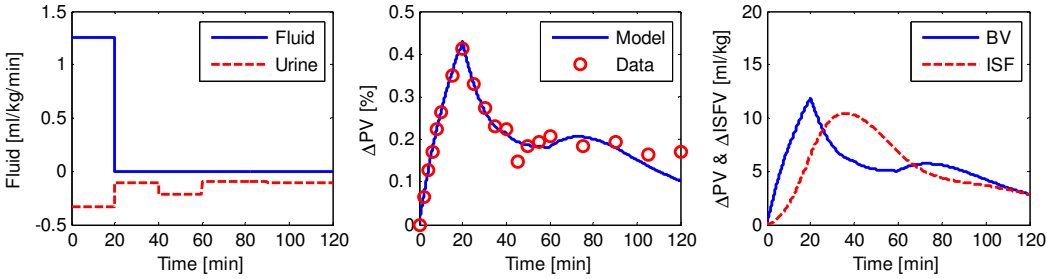

(b)

Figure 3-7: A representative fitting result from one subject, (a) Control (b) ISO.

states. To gauge if the summary parameters were meaningfully derived by the model fitting, the following hypotheses on the summary parameters were generated: 1) α_u is less in ISO than in control and 2) a larger K_i for ISO is expected. The assumption of less α_u for ISO is based on the fact that isoproterenol, as a beta-adrenergic agonist, would enhance the intravascular volume expansion during and after fluid infusion so

Table 8: Estimated summary parameters for absolute BV response data.

Absolute	K_P^*	K_I^*	V_{B0}^* [l]	α_u^*	Error [%]	RMSE [%]
Control	0.077+/-0.025	6e-4+/-8e-4	N/A	3.45+/-2.71	4.60+/-2.91	16.01+/-7.84
Isoproterenol	0.068+/-0.013	3e-3+/-2e-3	N/A	1.40+/-0.68	3.73+/-2.83	13.5+/-6.29

Table 9: Estimated summary parameters for fractional BV response data.

Fractional	K_P^*	K_I^*	V_{B0}^* [ml/kg]	α_u^*	Error [%]	RMSE [%]
Control	0.087+/-0.045	6e-4+/-9e-4	36.2+/-10.9	3.45+/-2.38	1.35+/-1.55	11.9+/-7.21
Isoproterenol	0.099+/-0.033	3e-3+/-3e-3	36.7+/-9.91	1.89+/-0.52	1.15+/-0.34	10.2+/-3.12

that more fluid retains in the blood rather than moving to ISF (Asmussen et al., 2014; Stephens et al., 2011; Vane et al., 2004).

Figure 3-7 shows a representative BV fitting result from one subject. Figure 3-7(a) and Figure 3-7(b) show the results for control and ISO protocols, respectively, where at each one, left, center and right panels show the fluid infusion protocol with UO, measured and model-reproduced BV response, and model-estimated volume changes in the intravascular and interstitial fluid.

The goodness of fit between measured and model-reproduced BV responses was encouraging: the overall root-mean-squared errors associated with control and ISO scenarios were 16.0% and 13.5%; and 11.9% and 10.2% of the mean values of the underlying responses for absolute and fractional BV data, respectively. In addition, the model could represent the enhanced BV expansion observed in the ISO scenario via its parameter α_u, when averaged over the nine subjects, α_u^* was significantly smaller in the data associated with ISO (1.89+/-0.52) than those in control (3.45+/-2.38; mean+/-SD), where SD stands for standard deviation. It is also obvious that K_i in ISO is larger that that of control, which is consistent with oscilatory behaviour of BV response in ISO.

3.7.Mathematical Analysis of the Blood Volume Model

In this section, the developed model of BV was mathematically studied. We first transformed the model to the state space form. In doing this, we defined the variables considered as the system's states. Then, the controllability and observability of the system were investigated. Next, we looked in to the transfer function between

BV response and fluid infusion and studied the stability of the system. Finally, the steady-state and transient responses of the BV model were elaborated.

3.7.1. State Space Model of Blood Volume

To further study the model of BV and employ this model for future design of closed-loop control of fluid resuscitation, the state space model of BV is desired. In this section the state space model of BV is developed. First, we define the variables we considered as the states of the system. Figure 3-8 shows the block diagram of model of BV. To achieve a minimal model, three states corresponding to the three integrators in the model have been considered and labeled as x_1 to x_3, which refer to the BV response, accumulated error in the controller, and accumulated net fluid infusion, respectively.

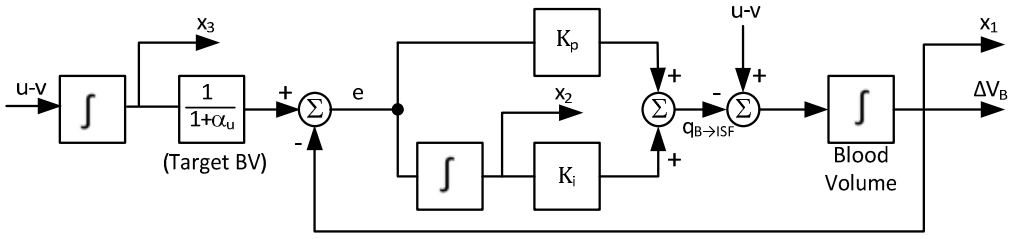

Figure 3-8: The block diagram of model of blood volume

The three differential equations associated with the three state variables are shown in (3-13).

$$\dot{x}_1 = u - v - K_p e - K_i x_2 = u - v - K_i x_2 - K_p\left(\frac{x_3}{1+\alpha_u} - x_1\right)$$

$$\dot{x}_2 = \frac{1}{1+\alpha_u} x_3 - x_1 \qquad (3\text{-}13)$$

$$\dot{x}_3 = u - v$$

By combining the above differential equations, and assuming $x = [x_1 \quad x_2 \quad x_3]^T$ and $\mathcal{u}$ is net fluid infusion, i.e., $\mathcal{u} = u - v$, the following state space model is derived:

$$\dot{x} = Ax + B\mathcal{u}$$

$$y = Cx + D\mathcal{u}$$

$$A=\begin{bmatrix} K_p & -K_i & \frac{-K_p}{1+\alpha_u} \\ -1 & 0 & \frac{1}{1+\alpha_u} \\ 0 & 0 & 0 \end{bmatrix},\ B = \begin{bmatrix} 1 \\ 0 \\ 1 \end{bmatrix},\ C = \begin{bmatrix} 1 & 0 & 0 \\ 0 & 0 & 1 \end{bmatrix},\ D = \begin{bmatrix} 0 \\ 0 \end{bmatrix} \tag{3-14}$$

where the input to the system ($\mathcal{u}$) is net infusion and the model outputs (y) are rate of change in BV and rate of net infusion.

3.7.2. Controllability and Observability of the Blood Volume Model

Based on the model of state space model obtained above, the controllability and observability matrices of the model of BV were derived. By definition, the controllability matrix of the system is as follows:

$$\mathcal{C} \equiv [B \quad AB \quad A^2B] = \begin{bmatrix} 1 & K_p & {K_p}^2 + K_i \\ 0 & -1 & -K_p \\ 1 & 0 & 0 \end{bmatrix} \tag{3-15}$$

while, after removing the dependent rows, the observability matrix is derived as below:

$$\mathcal{O} \equiv \begin{bmatrix} C \\ CA \\ CA^2 \end{bmatrix} = \begin{bmatrix} 1 & 0 & 0 \\ 0 & 0 & 1 \\ K_p & -K_i & -K_p/(1+\alpha_u) \\ {K_p}^2 + K_i & -K_pK_i & -{K_p}^2 - K_i/(1+\alpha_u) \end{bmatrix} \tag{3-16}$$

From (3-14) and (3-15), it is evident that for $K_i = 0$ the rank of controllability and observability matrices drops to two, making the system uncontrollable and unobservable. It is noted that since identified K_p is large enough, having small values of K_p is not of concern. In case of $K_i \approx 0$, we propose to employ a proportional controller rather than proportional-integral controller, in which the order of the state space model becomes two, making the system fully controllable and observable.

3.7.3. Transfer Function of Blood Volume Response and Stability Analysis

By computing the state transition matrix for (3-14) and using equation (3-11), the relationship between input u and BV response in frequency domain can be derived as below:

$$\Delta V_B(s) = G(s)u(s) = \frac{1}{s}\frac{s^2 + \frac{K_p}{1+\alpha_u}s + \frac{K_i}{1+\alpha_u}}{s^2 + K_p s + K_i}u(s) \tag{3-17}$$

where $G(s)$ is the transfer function between the net infusion and BV response. If we divide (3-17) by initial BV, the fractional BV response can be represented as (3-18):

$$\overline{\Delta V_B}(s) = \overline{G}(s)u(s) = \frac{1}{V_{B0}}\frac{1}{s}\frac{s^2 + \frac{K_p}{1+\alpha_u}s + \frac{K_i}{1+\alpha_u}}{s^2 + K_p s + K_i}u(s) \tag{3-18}$$

In regard to the stability of the system, it is essential to verify that the eigenvalues of the system have negative real parts, i.e., real part of the roots of the polynomial $s^2 + K_p s + K_i$ are in the left half plane. In other words, to ensure the system is asymptotically stable it necessitates that both controller coefficients satisfy $K_p, K_i > 0$. In addition, to avoid singularity $\alpha_u > -1$.

3.7.4. Transient and Steady-State Response of Blood Volume

In this section, the steady-state and transient responses of BV are evaluated by employing the final and initial value theorems. For simplicity, it is assumed that the urine excretion is zero. Administering an initial step fluid infusion with rate U to a subject followed by a washout period, the BV response at steady-state during washout can be computed via final value theorem, as below:

$$\lim_{t\to\infty}\overline{\Delta V_B}(t)=\lim_{s\to 0}\frac{1}{V_{B0}}\frac{s^2+\frac{K_p}{1+\alpha_u}s+\frac{K_i}{1+\alpha_u}}{s^2+K_p s+K_i}\left[\frac{1}{s}U(s)\right]$$
$$=\frac{1}{V_{B0}}\frac{1}{1+\alpha_u}\left[\frac{1}{s}U(s)\right] \tag{3-19}$$

where $\left[\frac{1}{s}U(s)\right]$ is accumulated fluid infusion. It's obvious that the results are consistent with Figure 3-6, where steady-state response is impacted by both initial BV and α_u. On the other hand, the transient response of BV during a step fluid infusion with rate U right after fluid resuscitation starts can be derived using initial value theorem. In the frequency domain, (3-18) can be shown as below:

$$s\overline{\Delta V_B}(s)=\frac{1}{V_{B0}}\frac{s^2+\frac{K_p}{1+\alpha_u}s+\frac{K_i}{1+\alpha_u}}{s^2+K_p s+K_i}u(s) \tag{3-20}$$

By applying initial value theorem on (3-20), the following relationship is achieved:

$$\lim_{t\to 0}\overline{\dot{\Delta V}_B}(t)=\lim_{s\to\infty}\frac{s}{V_{B0}}\frac{s^2+\frac{K_p}{1+\alpha_u}s+\frac{K_i}{1+\alpha_u}}{s^2+K_p s+K_i}\frac{U(s)}{s}=\frac{U(s)}{V_{B0}} \tag{3-21}$$

which indicates the rate of change in fractional BV response once step infusion is initiated is impacted by the rate of infusion and initial BV. This is also consistent with Figure 3-6, where the transient response is mainly regulated by initial BV.

4. Modeling of Cardiovascular Endpoint Responses to Blood Volume Perturbation

This chapter presents a systems-level lumped parameter model to reproduce hemodynamic responses to hemorrhage and fluid infusion. The model consists of three sub-models. The first sub-model relates BV response to hemorrhage and fluid infusion. The BV model developed in Chapter 3 is employed and expanded to be adapted to the hemorrhage scenario in addition to the fluid infusion. The second sub-model relates BV to SV and CO; and the third sub-model relates CO to BP. The validity of the model is examined using experimental data collected from 11 animals. To this end, first, a fully individualized model (a model obtained for each animal by estimating all the parameters from the data) is studied. Then, a parametric sensitivity analysis is performed to obtain a well-conditioned model by identifying low-sensitivity model parameters and fixing them at nominal values. Finally, a partially individualized model (a model obtained by estimating only the parameters to be individualized from the data) is studied. It is anticipated that this systems-level model may serve as a viable basis for the design and evaluation of closed-loop decision-assist and control algorithms for fluid resuscitation in critically ill patients.

4.1.Systems-Level Mathematical Model of Hemodynamic Cardiovascular Endpoints

The model consists of three sub-models: (a) a control-theoretic model to relate hemorrhage and fluid infusion to BV; (b) a lumped-parameter physics-based model to relate BV to SV and CO; and (c) a phenomenological model to relate CO to BP

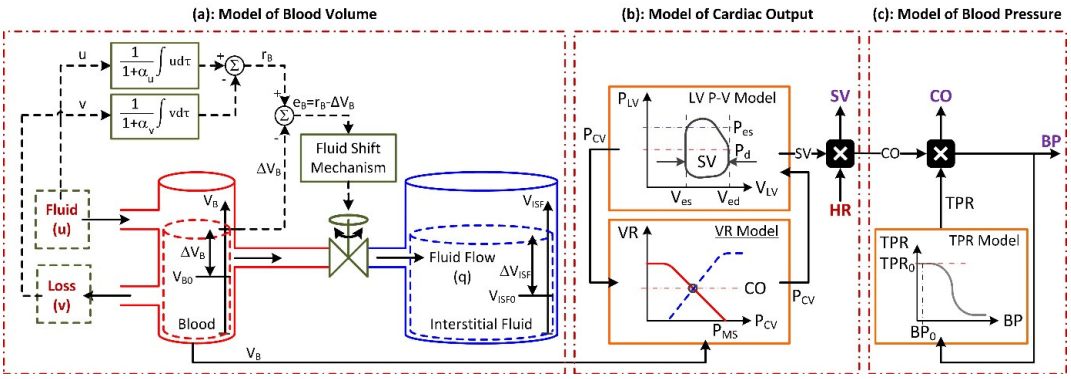

Figure 4-1: A systems-level mathematical model of hemodynamic responses to hemorrhage and fluid infusion.

(Figure 4-1). Compared to existing models available in the literature, a unique characteristic of this model is its balance for simplicity (via abstraction of microscopic physiological mechanisms into a systems-level model) and physiological transparency (via maximal use of established physiological knowledge).

4.1.1. Modeling of Blood Volume Response to Hemorrhage and Fluid Infusion

In previous chapter, a lumped parameter model of BV response to fluid infusion is developed. Given that the ratio between the intravascular and extravascular volumetric changes is in general different for hemorrhage and fluid infusion due to the compositional differences in the fluids involved in each process (blood lost consists of plasma and red blood cells (RBCs) while infused fluid may consist of electrolyte (crystalloid such as Lactated Ringer's solution (LR)) and starch (colloid such as Hextend (Hex)), the original model of BV in Chapter 3 is not applicable to the scenarios in which a patient undergoes both hemorrhage and fluid infusion. In this chapter, we extended the original model as follows to address this limitation. By denoting the ratio between the intravascular and extravascular volumetric changes in the steady-state in

response to fluid gain (fluid infusion) and loss (hemorrhage and urine) as α_u and α_v, respectively, the desired steady-state change in BV, $r_B(t)$, can be written as follows:

$$r_B(t) = \frac{1}{1+\alpha_u}\int_0^t u(\tau)\,d\tau - \frac{1}{1+\alpha_v}\int_0^t v(\tau)\,d\tau \tag{4-1}$$

where $u(t)$ and $v(t)$ denote the rates of fluid gain (infusion) and loss (hemorrhage and UO) at time t. Similar to previous chapter, at each time t, the inter-compartmental fluid shift is dictated by the discrepancy between the desired ($r_B(t)$) versus actual ($\Delta V_B(t)$) changes in BV as follows:

$$q(t) = q\big(e_B(t)\big) = q\big(r_B(t) - \Delta V_B(t)\big) \tag{4-2}$$

Hence, the rate of change in BV can be written as follows:

$$\Delta\dot{V}_B(t) = u(t) - v(t) - q(t) \tag{4-3}$$

If the inter-compartmental fluid shift is abstracted into the action of a simple PI controller to drive $e_B(t)$ to zero in the steady-state:

$$q(t) = -K_p e_B(t) - K_i\int_0^t e_B(\tau)d\tau \tag{4-4}$$

Where, the same as before, K_p and K_i are proportional and integral gains, the dynamics dictating the rate of change in BV can be written as follows by combining (4-1)-(4-4):

$$\begin{aligned}\Delta\dddot{V}_B(t) + K_p\Delta\ddot{V}_B(t) + K_i\Delta\dot{V}_B(t) \\ = [\ddot{u}(t) - \ddot{v}(t)] + \frac{K_p}{1+\alpha_u}\dot{u}(t) - \frac{K_p}{1+\alpha_v}\dot{v}(t) + \frac{K_i}{1+\alpha_u}u(t) \\ - \frac{K_i}{1+\alpha_v}v(t)\end{aligned} \tag{4-5}$$

This model is visualized in Figure 4-1(a) as a two-bucket system connected by a bi-directional flow valve, where the buckets represent the intravascular and extravascular

compartments while the valve represents the collection of all the inter-compartmental fluid shift mechanisms.

4.1.2. Modeling of Stroke Volume and Cardiac Output Responses to Blood Volume Changes

A perturbation in BV entails the corresponding perturbations in SV and CO. The influence of BV on SV and CO can be viewed from 2 complementary standpoints: vascular and ventricular. On one hand, Guyton's CO-venous return (VR) theory dictates that a perturbation in BV results in perturbations in CO and VR by altering MSP (Beard and Feigl, 2011) (Figure 4-1(b)):

$$\mathrm{VR}(t) = \mathrm{CO}(t) = \frac{P_{MS}(t) - P_{CV}(t)}{R_{VR}} \tag{4-6}$$

where $P_{CV}(t)$ is CVP, R_{VR} is the resistance to VR, $P_{MS} = \frac{(V_B - V_{BU})}{C_S}$ is MSP, V_{BU} is the unstressed BV, and C_S is the systemic capacitance (Beard and Feigl, 2011; Young, 2010). Expanding P_{MS} in (4-6) yields the following relationship between BV, SV δV, and CO:

$$\begin{aligned} \mathrm{CO}(t) = \mathrm{HR}(t) \cdot \delta V(t) &= \frac{1}{R_{VR}}\left[\frac{V_B(t) - V_{BU}}{C_S} - P_{CV}(t)\right] \\ &= \frac{1}{C_S R_{VR}} V_B(t) - \frac{1}{R_{VR}} P_{CV}(t) - \frac{V_{BU}}{C_S R_{VR}} \end{aligned} \tag{4-7}$$

Note that $V_B(t) = V_{B0} + \Delta V_B(t)$ is the sum of baseline BV V_{B0} and its change $\Delta V_B(t)$ at time t given by (4-5). On the other hand, the Frank-Starling mechanism together with the left ventricular (LV) pressure-volume loop theory dictates that a perturbation in BV results in perturbations in SV and CO by altering the LV preload: LV EDV

(Sagawa et al., 1988) (Figure 4-1(b)). First, SV and CO are related to EDV $V_{ed}(t)$ as follows:

$$\delta V(t) = \frac{CO(t)}{HR(t)} = \frac{E_S}{E_S + E_A}(V_{ed}(t) - V_0) \tag{4-8}$$

where E_S is the LV elastance, E_A is the arterial elastance (defined as the product of HR and TPR), and V_0 is a constant parameter. Using the LV end-diastolic P-V relationship (Morley et al., 2007; Santamore and Burkhoff, 1991) evaluated at the end of diastole ($V_{LV}(t) = V_{ed}(t)$ and $P_D(V_{LV}(t)) = P_{ed}(t)$, where $P_{ed}(t)$ is LV end-diastolic pressure (EDP)):

$$\begin{aligned} P_D(V_{LV}(t)) &= B\left[e^{A(V_{LV}(t)-V_0)} - 1\right] \xrightarrow{V_{LV}(t)=V_{ed}(t)} V_{ed}(t) - V_0 \\ &= \frac{1}{A}\log\left(\frac{1}{B}P_{ed}(t) + 1\right) \end{aligned} \tag{4-9}$$

where A and B are constant parameters specifying the end-diastolic LV P-V relationship. By assuming that $P_{ed}(t)$ is proportional to $P_{CV}(t)$, $P_{ed}(t) \approx \gamma P_{CV}(t)$ (Uemura et al., 2005), (4-8) reduces to the following:

$$\delta V(t) = \frac{CO(t)}{HR(t)} = \frac{E_S}{E_S + E_A}\frac{1}{A}\log\left(\frac{\gamma}{B}P_{CV}(t) + 1\right) \tag{4-10}$$

To obtain a direct relationship between BV and SV, (4-7) and (4-10) can be combined to yield the following by canceling CVP:

$$\delta V(t) = \frac{E_S}{E_S+E_A}(V_{ed}(t) - V_0) = \theta_1 \log(\theta_2 \cdot HR(t) \cdot SV(t) + \theta_3 V_B(t) + \theta_4) \tag{4-11}$$

where $\theta_1 = \frac{E_S}{A(E_S+E_A)}$, $\theta_2 = -\frac{\gamma R_{VR}}{B}$, $\theta_3 = \frac{\gamma}{BC_S}$, and $\theta_4 = -\frac{\gamma}{B}\frac{V_{BU}}{C_S} + 1$ are the parameters that must be tuned to each individual based on the experimental data. A direct relationship between BV and CO can then be obtained by multiplying HR to (4-11):

$$\mathrm{CO}(t) = \mathrm{HR}(t) \cdot \delta V(t) = \mathrm{HR}(t) \cdot \theta_1 \log(\theta_2 \cdot \mathrm{CO}(t) + \theta_3 V_B(t) + \theta_4) \quad (4\text{-}12)$$

In this way, SV and CO responses to hemorrhage and fluid infusion can be reproduced. In addition, CVP response may also be reproduced from SV or CO either by (4-7) or (4-10). This model is visualized in Figure 4-1(b).

4.1.3. Modeling of Blood Pressure Response to Cardiac Output Changes

A perturbation in CO entails the corresponding perturbations in BP and TPR. Specifically, a perturbation in CO first results in a proportional change in BP, which is compensated by a decrease in TPR via the arterial autonomic-cardiac regulation (Coleman and Guyton, 1969; Montani and Van Vliet, 2009). Despite its complex first principles nature, it has been suggested that autonomic-cardiac regulation is approximated by a sigmoidal relationship reasonably well (Cheng et al., 2010; Kawada et al., 2001, 2004; Magosso et al., 2001; Pruett et al., 2013; Ursino et al., 1994). Hence, we used the following phenomenological model to relate the influence of BP on TPR, i.e., R:

$$R(t) = R_0 - \frac{\Delta R}{2} \frac{\mathrm{sgn}\left(P_m(t) - P_{m,0}\right) \sqrt[3]{\left|P_m(t) - P_{m,0}\right|}}{1 + \sqrt[3]{\left|P_m(t) - P_{m,0}\right|}} \quad (4\text{-}13)$$

where R_0 and $P_{m,0}$ are TPR and MAP at nominal state, respectively, and ΔR is the maximal possible change in TPR. Then, the relationship between CO and MAP can be given by multiplying (4-13) to CO:

$$P_m(t) = \mathrm{CO}(t) \times R(t) = \mathrm{CO}(t) \times \left(R_0 - \frac{\Delta R}{2} \frac{\mathrm{sgn}\left(P_m(t) - P_{m,0}\right) \sqrt[3]{\left|P_m(t) - P_{m,0}\right|}}{1 + \sqrt[3]{\left|P_m(t) - P_{m,0}\right|}} \right) \quad (4\text{-}14)$$

This model is visualized in Figure 4-1(c). In sum, the mathematical model relating hemorrhage and fluid infusion to hemodynamic responses (including BV, SV, CO, and BP) consists of (4-5), (4-12), and (4-14).

4.2.Experimental Data for Model Validation

The experimental data used in this chapter were collected from 11 conscious sheep undergoing intravenous blood loss and fluid infusion. The measurements included the rates of hemorrhage, infusion, and UO, as well as BV, CO, BP, and HR. The data collection protocol was approved by the Institutional Animal Care and Use Committee (IACUC) at the University of Texas Medical Branch and is described in detail elsewhere (Rafie et al., 2004).

All 11 animals received LR. 5 of these animals also received Hex. For the 5 animals which received both fluids, LR and Hex experiments were performed separately in a randomized order, with the experiments at least 5 days apart from each other. The duration of study for each fluid in each animal was 180 min. After the baseline data were recorded, an initial hemorrhage (25 mL/kg) was performed over 15 min. Fluid infusion was started 30 min after the start of the hemorrhage and continued for 150 min. Second and third hemorrhage (5 mL/kg) were performed 50 and 70 min after the start of the initial hemorrhage, and each lasted for 5 min. Fluid infusion was performed automatically with a closed-loop controller. Baseline BV was measured via indocyanine green dye (ICG) (Henschen et al., 1993). Hematocrit, the ratio between the red blood cell volume (RBCV) and BV, was measured before and throughout the experiment at 5 to 10 min intervals and was used to measure the fractional change in

BV (Henschen et al., 1993). Other hemodynamic responses were measured at similar time instants.

4.3.Individualized Model Evaluation Method

We evaluated the ability of the proposed model to reproduce hemodynamic responses to hemorrhage and fluid infusion. Our primary focus was to investigate if the model could be tuned to each individual animal and reproduce subject-specific hemodynamic responses. First, we performed the fitting of the model to the experimental data of each animal (called fully individualized model identification). Second, we performed parametric sensitivity analysis of the fully individualized model in order to obtain a well-conditioned model by identifying low-sensitivity model parameters and fixing them at nominal values. Third, we performed the fitting of the model to the experimental data of each animal while fixing low-sensitivity model parameters to their nominal values (called partially individualized model identification). Fourth, we compared the performance of the fully and partially individualized models in terms of accuracy and accuracy-complexity trade-off.

4.3.1. Individualized Model Identification and Analysis

We performed fully individualized model identification via numerical optimization. All sub-models combined, the model involves 10 tunable parameters: 4 in (4-5) (α_u, α_v, K_p, K_i); 4 in (4-12) (θ_i, $i = 1 \cdots 4$); and 2 in (4-14) (R_0 and MAP_0) after fixing ΔR to cover experimentally observed maximal change in TPR in all animals (30 [mmHg·min/l]). Given a set of initial parameter estimates, the model computed BV, CO, and BP responses from the inputted experimental hemorrhage, fluid infusion

UO, and HR data as follows. First, the change in BV was computed from (4-5). On the other hand, the change in RBCV was computed as follows:

$$\Delta V_{RBC}(t) = -\int_0^t H(\tau) v_H(\tau) d\tau \tag{4-15}$$

where $\Delta V_{RBC}(t)$ is RBCV at time t, while $H(t)$ is hematocrit at time t, related to BV and RBCV as follows:

$$H(t) = \frac{V_{B0} H(0) + \Delta V_{RBC}(t)}{V_{B0} + \Delta V(t)} \tag{4-16}$$

where V_{B0} is initial BV (measured). Second, CO response was computed by inputting the computed BV and HR to (4-12) and employing a root finding algorithm to solve for CO that best satisfies (4-12) at each time t. Third, MAP was computed by inputting the computed CO to (4-14). The computed BV, CO, and MAP responses were compared with the respective experimental data, and the discrepancy between them was minimized by solving the following optimization problem to estimate the optimal set of model parameters:

$$\begin{aligned} \Omega^* &= \left\{\alpha_u^*, \alpha_v^*, K_p^*, K_i^*, \theta_1^*, \theta_2^*, \theta_3^*, \theta_4^*, R_0^*, P_{m,0}^*\right\} \\ &= \arg\min_{\Omega} \left\| \left[\left(\frac{\widetilde{\Delta V_B}(t) - \Delta V_B(t|\Omega)}{\overline{\widetilde{\Delta V_B}(t)}} \right) \left(\frac{\widetilde{CO}(t) - CO(t|\Omega)}{\overline{\widetilde{CO}(t)}} \right) \left(\frac{\widetilde{P_m}(t) - P_m(t|\Omega)}{\overline{\widetilde{P_m}(t)}} \right) \right] \right\|_2 \end{aligned} \tag{4-17}$$

where $\widetilde{\Delta V_B}(t)$, $\widetilde{CO}(t)$, and $\widetilde{P_m}(t)$ are measured BV, CO, and MAP responses, while $\Delta V_B(t|\Omega)$, $CO(t|\Omega)$, and $P_m(t|\Omega)$ are the same hemodynamic variables predicted by the model. $\overline{\widetilde{\Delta V_B}(t)}$, $\overline{\widetilde{CO}(t)}$, and $\overline{\widetilde{P_m}(t)}$ are the same hemodynamic variables averaged over the entire study duration and were used to normalize the error magnitudes associated with each hemodynamic variables. The optimization problem (4-17) was solved using the differential evolution (DE) algorithm (Storn and Price, 1997), a derivative-free

method suited to solve problems with multimodal and continuous-valued cost functions.

We analyzed the identified fully individualized model for (i) its ability to reproduce hemodynamic responses in each animal, (ii) accuracy-complexity trade-off via Akaike Information Criterion (AIC) (Burnham and Anderson, 2003), and (iii) the relevance of its parameter estimates. First, we assessed the models' ability to reproduce experimental hemodynamic responses by computing the RMSEs between measured versus model-reproduced BV, hematocrit, SV, CO, and BP responses. Second, we computed the AIC value associated with the model identified for each animal. Third, we assessed the physiological relevance of the estimated model parameters in terms of the following: (i) α_u^* identified for crystalloid (LR) infusion versus colloid (Hex) infusion (colloid contains large molecules which allows it to be retained better than crystalloid, resulting in smaller α_u^* compared with crystalloid (Bighamian et al., 2016; Hedin and Hahn, 2005)); (ii) measured V_{B0} versus V_{BU} derived from the identified CO model parameters ($V_{BU}^* = (1 - \theta_4^*)/\theta_3^*$); (iii) correlation between measured V_{B0} and R_{VR} derived from the identified CO model parameters ($C_S^* R_{VR}^* = -\theta_2^*/\theta_3^*$; noting that inter-individual variability in systemic compliance C_S^* is not large (Oren et al., 1996) and that V_{B0} and R_{VR} are known to exhibit positive correlation (Chirinos et al., 2009), model-derived $C_S^* R_{VR}^*$ may be positively correlated to V_{B0}); and (iv) discrepancy between measured MAP and TPR in the steady-state versus $P_{m,0}^*$ and R_0^* (noting from (4-13) that $P_{m,0}^*$ and R_0^* indicate nominal MAP and TPR, they may be close to steady-state experimental values).

4.3.2. Post-Hoc Parametric Sensitivity Analysis

We conducted post-hoc parametric sensitivity analysis using the identified mathematical models in order to determine high-sensitivity parameters (those having a large influence on the model outputs) and low-sensitivity parameters (those having a small influence on the model outputs), and thereby to (a) understand the identifiability properties of the model as well as to (b) obtain a well-conditioned model (a model with low parametric variance) by fixing low-sensitivity parameters to their nominal values. Noting that BV, CO, and MAP were all used in identifying the model, we performed the parametric sensitivity analysis at the sub-model level. That is, we examined the sensitivity of the BV model (4-5) to $\{\alpha_u^*, \alpha_v^*, K_p^*, K_i^*\}$; sensitivity of the CO model (4-12) to $\{\theta_1^*, \theta_2^*, \theta_3^*, \theta_4^*\}$; and sensitivity of the MAP model (4-14) to $\{R_0^*, P_{m,0}^*\}$, respectively. Details follow.

We constructed two nominal models: one nominal model to simulate crystalloid response, equipped with parameters averaged over all subjects and α_u^* averaged over 11 crystalloid subjects, and another model to simulate colloid response, equipped with parameters averaged over all subjects and α_u^* averaged over 5 colloid subjects. To elucidate the parametric sensitivity of the models to both fluid gain and loss, we simulated the model with a hemodynamic perturbation scenario consisting of (i) 30 min of 0.05 ml/kg/min hemorrhage and (ii) 30 min of 0.05 ml/kg/min LR infusion or 0.05/3 ml/kg/min Hex, which were separated by 150 min zero-input period. We used the data thus acquired to compute parametric sensitivity as follows. First, we formulated the control-theoretic BV model (4-5) into the following state space model:

$$\dot{\mathbf{x}}(t) = \mathbf{f}\left(\mathbf{x}(t), u(t), v(t), \Omega_{V_B}\right) = \boldsymbol{\mathcal{A}}\mathbf{x}(t) + \boldsymbol{\mathcal{B}}\begin{bmatrix} u(t) \\ v(t) \end{bmatrix}$$

$$= \begin{bmatrix} -K_p & K_i & \frac{K_p}{(1+\alpha_u)} & \frac{-K_p}{(1+\alpha_v)} \\ -1 & 0 & \frac{1}{(1+\alpha_u)} & \frac{-1}{(1+\alpha_v)} \\ 0 & 0 & 0 & 0 \\ 0 & 0 & 0 & 0 \end{bmatrix}\mathbf{x}(t) + \begin{bmatrix} 1 & -1 \\ 0 & 0 \\ 1 & 0 \\ 0 & 1 \end{bmatrix}\begin{bmatrix} u(t) \\ v(t) \end{bmatrix}, \qquad (4\text{-}18)$$

$$\mathbf{x}(t_0) = \mathbf{x}_0$$

$$\Delta V_B(t) = \boldsymbol{\mathcal{C}}\mathbf{x}(t) = [1 \quad 0 \quad 0 \quad 0]\mathbf{x}(t)$$

Where

$$\mathbf{x}(t) = [\Delta V_B(t) \quad \int e_B(\tau)d\tau \quad \int u(\tau)d\tau \quad \int v(\tau)d\tau]^T,$$

$\Omega_{V_B} = [\alpha_u \quad \alpha_v \quad K_p \quad K_i]^T$, and $\boldsymbol{\mathcal{A}}$ and $\boldsymbol{\mathcal{B}}$ are the system and input matrices. Form (4-18), we constructed the following sensitivity function (Khalil, 2001):

$$\begin{aligned} \dot{\mathcal{S}}_{\mathbf{x}}(t) &= \boldsymbol{\mathcal{A}}\mathcal{S}_{\mathbf{x}}(t) + \boldsymbol{\mathcal{H}}(t), \qquad \mathcal{S}_{\mathbf{x}}(t_0) = \mathbf{0}_{4\times 4} \\ \mathcal{S}_{V_B}(t) &= \boldsymbol{\mathcal{C}}\mathcal{S}_{\mathbf{x}}(t) \end{aligned} \qquad (4\text{-}19)$$

where $\mathcal{S}_{\mathbf{x}}(t)$ is the parametric sensitivity matrix associated with $\mathbf{x}(t)$, $\mathcal{S}_{V_B}(t)$ is the parametric sensitivity function associated with BV, and $\boldsymbol{\mathcal{H}}(t)$ is given by:

$$\boldsymbol{\mathcal{H}}(t) = \frac{\partial \mathbf{f}\left(\mathbf{x}(t), u(t), v(t), \Omega_{V_B}\right)}{\partial \Omega_{V_B}}$$

$$= \begin{bmatrix} \frac{-K_p \int u(\tau)d\tau}{(1+\alpha_u)^2} & \frac{K_p \int v(\tau)d\tau}{(1+\alpha_v)^2} & \frac{\int u(\tau)d\tau}{1+\alpha_u} - \frac{\int v(\tau)d\tau}{1+\alpha_v} - \Delta V_B(t) & \int e_B(\tau)d\tau \\ \frac{-\int u(\tau)d\tau}{(1+\alpha_u)^2} & \frac{\int v(\tau)d\tau}{(1+\alpha_v)^2} & 0 & 0 \\ 0 & 0 & 0 & 0 \\ 0 & 0 & 0 & 0 \end{bmatrix} \qquad (4\text{-}20)$$

Second, we constructed the sensitivity functions associated with the lumped-parameter SV-CO model (4-12) and phenomenological MAP model (4-14) by computing their partial derivatives with respect to the respective model parameters:

$$\mathcal{S}_{\mathrm{CO}}(\mathrm{t}) = \begin{bmatrix} \dfrac{\partial \mathrm{CO}(\mathrm{t})}{\partial \theta_1} \\ \dfrac{\partial \mathrm{CO}(\mathrm{t})}{\partial \theta_2} \\ \dfrac{\partial \mathrm{CO}(\mathrm{t})}{\partial \theta_3} \\ \dfrac{\partial \mathrm{CO}(\mathrm{t})}{\partial \theta_4} \end{bmatrix}$$

$$= \begin{bmatrix} \dfrac{\mathrm{HR}(\mathrm{t})(\theta_2 \mathrm{CO}(\mathrm{t}) + \theta_3 \mathrm{V_B}(\mathrm{t}) + \theta_4)\log(\theta_2 \mathrm{CO}(\mathrm{t}) + \theta_3 \mathrm{V_B}(\mathrm{t}) + \theta_4)}{(\theta_2 \mathrm{CO}(\mathrm{t}) + \theta_3 \mathrm{V_B}(\mathrm{t}) + \theta_4) - \theta_1 \theta_2 \mathrm{HR}(\mathrm{t})} \\ \dfrac{\theta_1 \mathrm{HR}(\mathrm{t})\mathrm{CO}(\mathrm{t})}{(\theta_2 \mathrm{CO}(\mathrm{t}) + \theta_3 \mathrm{V_B}(\mathrm{t}) + \theta_4) - \theta_1 \theta_2 \mathrm{HR}(\mathrm{t})} \\ \dfrac{\theta_1 \mathrm{HR}(\mathrm{t})\mathrm{V_B}(\mathrm{t})}{(\theta_2 \mathrm{CO}(\mathrm{t}) + \theta_3 \mathrm{V_B}(\mathrm{t}) + \theta_4) - \theta_1 \theta_2 \mathrm{HR}(\mathrm{t})} \\ \dfrac{\theta_1 \mathrm{HR}(\mathrm{t})}{(\theta_2 \mathrm{CO}(\mathrm{t}) + \theta_3 \mathrm{V_B}(\mathrm{t}) + \theta_4) - \theta_1 \theta_2 \mathrm{HR}(\mathrm{t})} \end{bmatrix} \tag{4-21}$$

$$\mathcal{S}_{\mathrm{P_m}}(\mathrm{t}) = \begin{bmatrix} \dfrac{\partial \mathrm{P_m}(\mathrm{t})}{\partial \mathrm{R}_0} \\ \dfrac{\partial \mathrm{P_m}(\mathrm{t})}{\partial \mathrm{P_{m,0}}} \end{bmatrix}$$

$$= \begin{bmatrix} \dfrac{\mathrm{CO}(\mathrm{t})\left(1 + \sqrt[3]{\left|\mathrm{P_m}(\mathrm{t}) - \mathrm{P_{m,0}}\right|}\right)^2}{\left(1 + \sqrt[3]{\left|\mathrm{P_m}(\mathrm{t}) - \mathrm{P_{m,0}}\right|}\right)^2 + 5\mathrm{CO}(\mathrm{t})\left(\left|\mathrm{P_m}(\mathrm{t}) - \mathrm{P_{m,0}}\right|\right)^{-2/3}} \\ \dfrac{5\mathrm{CO}(\mathrm{t})\left(\left|\mathrm{P_m}(\mathrm{t}) - \mathrm{P_{m,0}}\right|\right)^{-2/3}}{\left(1 + \sqrt[3]{\left|\mathrm{P_m}(\mathrm{t}) - \mathrm{P_{m,0}}\right|}\right)^2 + 5\mathrm{CO}(\mathrm{t})\left(\left|\mathrm{P_m}(\mathrm{t}) - \mathrm{P_{m,0}}\right|\right)^{-2/3}} \end{bmatrix} \tag{4-22}$$

We then numerically computed $\mathcal{S}_{\mathrm{V_B}}(\mathrm{t})$, $\mathcal{S}_{\mathrm{CO}}(\mathrm{t})$, and $\mathcal{S}_{\mathrm{P_m}}(\mathrm{t})$ by solving (4-19), (4-21), and (4-22) simultaneously with (4-5), (4-12), and (4-14) subject to the hemodynamic

perturbation scenario described above. Since the model parameter values exhibited diversity in terms of magnitude, we normalized the computed $\mathcal{S}_{V_B}(t)$, $\mathcal{S}_{CO}(t)$, and $\mathcal{S}_{P_m}(t)$ using the respective nominal parameter values and time series sequence of $\Delta V_B(t)$, $CO(t)$, and $P_m(t)$. For each sub-model, we compared the magnitudes of the normalized parametric sensitivity functions and identified low-sensitivity parameter(s) as those whose sensitivity magnitudes are considerably small relative to the sensitivity functions associated with the remaining parameters. Since these parameters do not exert a large influence on the model's response compared with the remaining parameters, they may not be identified accurately, and therefore, may be fixed at nominal value(s) without making a large influence on the model's ability to reproduce the experimental hemodynamic responses.

4.3.3. Partially Individualized Model Identification and Analysis

We performed partially individualized model identification via numerical optimization. The parametric sensitivity analysis showed that K_i and θ_1 could be classified as low-sensitivity parameters (see Section 4.4). All sub-models combined, the model involves 8 tunable parameters: 3 in (4-5) (α_u, α_v, K_p); 3 in (4-12) (θ_i, $i = 2 \cdots 4$); and 2 in (4-14) (R_0 and $P_{m,0}$) after fixing K_i and θ_1 to their respective average values in all animals. We solved the same optimization problem as previously described to estimate the optimal set of model parameters for the partially individualized model. Then, we analyzed the identified partially individualized model in comparison with its fully individualized counterpart for (i) its ability to reproduce hemodynamic responses in each animal, (ii) accuracy-complexity trade-off via AIC, and (iii) the relevance of its parameter estimates.

4.4.Fitting Results and Model's Performance

Table 1 shows the RMSEs associated with the fully and partially individualized models in reproducing BV, hematocrit, SV, CO, and MAP (mean (SD)). In terms of AIC, partially individualized model outperformed its fully individualized counterpart in 6 (out of 11) animals for LR and in 4 (out of 5) animals for Hex. In sum, the former was superior to the latter, for either LR or Hex or both, in 8 animals. Figure 4-2 shows a representative example of measured hemodynamic responses to (a) LR and (b) Hex, and the same responses reproduced by the partially individualized model (the results for fully individualized model were highly comparable and thus are not shown). Table 11 summarizes the model parameter values associated with the fully and partially individualized models. Figure 4-3 shows the time evolution of normalized parametric sensitivity functions in response to hemorrhage and crystalloid infusion (the results for colloid infusion exhibited the same trend and thus are not shown).

4.5.Model's Interpretation, Sensitivity and Usability

We developed a systems-level mathematical model that can reproduce hemodynamic responses to hemorrhage and fluid infusion, equipped with simplicity to facilitate the design of closed-loop algorithms and transparency to allow credible validation and interpretation. Here we elaborate on the accuracy and physiological relevance properties of the proposed model.

4.5.1. Fully versus Partially Individualized Models

Once tuned to the data associated with individual animals, both fully and partially individualized models could reproduce hemodynamic responses to

hemorrhage as well as infusion of crystalloid (LR) and colloid (Hex) fluids accurately, including BV, hematocrit, SV, CO, and BP (Table 10). When root-mean-squared, the RMSEs associated with BV, SV, CO, and BP were 1.9 ml/kg and 2.2 ml/kg, 0.12 ml/kg and 0.13 ml/kg, 0.42 lpm and 0.44 lpm, and 7.2 mmHg and 7.3 mmHg, respectively, which, when normalized by the respective average response, was consistently smaller than 14.4 % for crystalloid and 11.7 % for colloid on the average. The goodness of fit observed for BV, ISFV, RBCV, and hematocrit suggests the validity of abstracting the inter-compartmental fluid shift (which involves many complex physiological mechanisms) into a simple closed-loop (PI) control action, while the goodness of fit observed for SV and CO illustrates the appropriateness of minimum-complexity physics-based expression for the relationship between BV versus SV and CO (Figure 4-2). Overall, the model exhibited remarkable performance in reproducing the experimental hemodynamic responses despite its simple architecture, indicating its potential to offer complementary value to the class of highly complex white-box models currently available in the field, e.g., (Abram et al., 2007; Kofránek and Rusz, 2010). Close scrutiny of the fully individualized model showed that the model parameters are physiologically relevant. First, the values of α_u^* associated with crystalloid (LR) infusion versus colloid (Hex) infusion were significantly different ($p<0.05$). This observation is consistent with what is anticipated from physiology that colloid, compared with crystalloid, enhanced BV expansion via reduced fluid shift from BV to ISFV due to large molecules it contains (Bighamian et al., 2016; Hedin and Hahn, 2005). This finding highlights the potential need for fluid-dependent models in the design and evaluation of closed-loop fluid resuscitation controllers. Second, V_{BU}

derived from the identified CO model parameters

Table 10: RMSEs associated with the fully and partially individualized models (mean (SD)). Full: fully individualized model. Partial: partially individualized model.

	Model	BV Error [l]	Hematocrit Error [-]	SV Error [ml]	CO Error [lpm]	BP Error [mmHg]
Crystalloid	Full	0.08 (0.05)	0.79 (0.28)	4.7 (3.4)	0.47 (0.21)	7.5 (2.2)
	Partial	0.09 (0.05)	0.87 (0.26)	5.1 (3.6)	0.50 (0.23)	7.8 (2.2)
Colloid	Full	0.05 (0.02)	0.49 (0.06)	3.5 (1.9)	0.30 (0.09)	6.8 (3.0)
	Partial	0.06 (0.02)	0.50 (0.04)	3.8 (1.9)	0.33 (0.08)	6.1 (2.6)

Table 11: model parameter values associated with the fully and partially individualized models.

	Model	α_u^*† [·]	α_v^* [·]	K_p^* [min^{-1}]	K_l^* [min^{-2}]	θ_1^* [ml]	θ_2^* [min/ml]	θ_3^* [ml^{-1}]	θ_4^* [·]	R_0^* [mmHg·min/l]	$P_{m,0}^*$[mmHg]
Crystalloid	Full	2.3 (2.0)	1.1 (0.9)	0.1 (0.1)	17e-4 (1e-3)	12.2 (5.4)	-0.048 (0.046)	0.28 (0.12)	-422 (231)	16.5 (6.12)	82.9 (7.14)
	Partial	1.56 (0.67)	1.09 (0.83)	0.13 (0.10)	31e-4 (0)	13.0 (0)	-0.045 (0.044)	0.27 (0.13)	-421 (246)	17.4 (6.66)	82.2 (7.59)
Colloid	Full	-0.20 (0.26)	0.93 (0.52)	0.15 (0.13)	63e-4 (41e-4)	14.7 (5.46)	-0.063 (0.041)	0.31 (0.12)	-410 (165)	14.7 (3.88)	91.1 (22.4)
	Partial	-0.20 (0.23)	0.90 (0.37)	0.20 (0.11)	31e-4 (0)	13.0 (0)	-0.072 (0.043)	0.32 (0.13)	-442 (228)	17.0 (7.56)	94.5 (31.2)

†: significantly different between fully versus partially individualized models ($p<0.05$).

($V_{BU}^* = (1 - \theta_4^*)/\theta_3^*$) was closely correlated with measured V_{B0} (r=0.87). This observation is consistent with what is anticipated from physiology that individuals with small (large) V_{B0} tend to have small (large) V_{BU} (Peterson and Bronzino, 2007). Third, R_{VR} derived from the identified CO model parameters ($C_S^* R_{VR}^* = -\theta_2^*/\theta_3^*$) was correlated positively with measured V_{B0} (r=0.59), which is consistent with an earlier finding that R_{VR} has a tendency to be proportional to V_{B0} (Chirinos et al., 2009). Finally, the agreement between $P_{m,0}^*$ and R_0^* versus their steady-state experimental values was adequate with average discrepancy of 12.3 % for $P_{m,0}^*$ and 29.3 % for R_0^*. Overall, these observations indicate that some, if not all, of the parameters in the proposed systems-level model are physically transparent and physiologically interpretable, rendering the model appropriate for the development of decision-assist and control algorithms as well as in-silico testing tools for investigational closed-loop

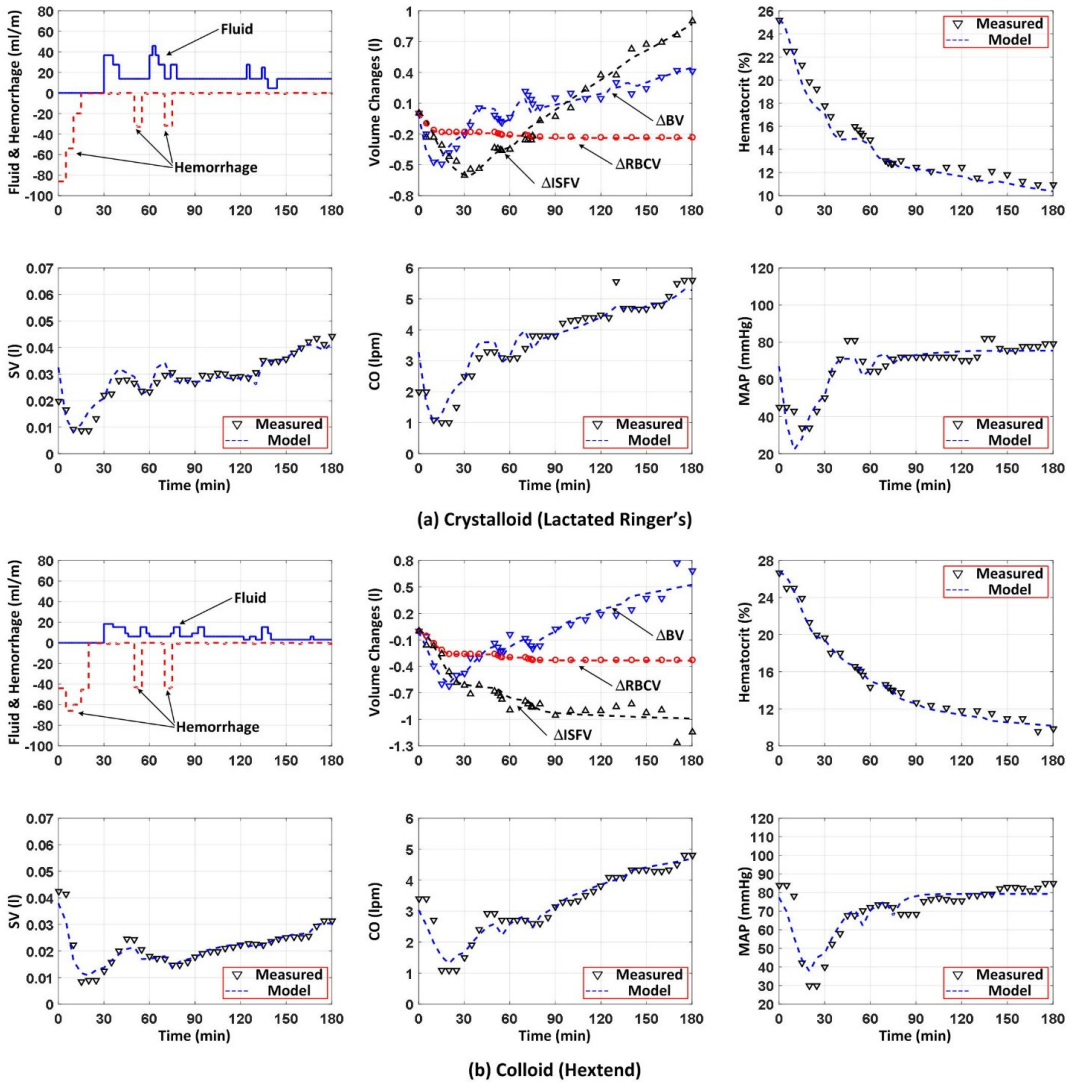

Figure 4-2: Measured versus model-reproduced hemodynamic responses to (a) crystalloid (Lactate Ringer's) and (b) colloid (Hextend) infusion.

controllers.

Comparing fully and partially individualized models, RMSE associated with the former was comparable to RMSE associated with the latter. Specifically, RMSEs associated with BV (p=0.24), hematocrit (p=0.20), SV (p=0.26), CO (p=0.50), and MAP (p=0.29) responses were not significantly different. In addition, AIC preferred partially

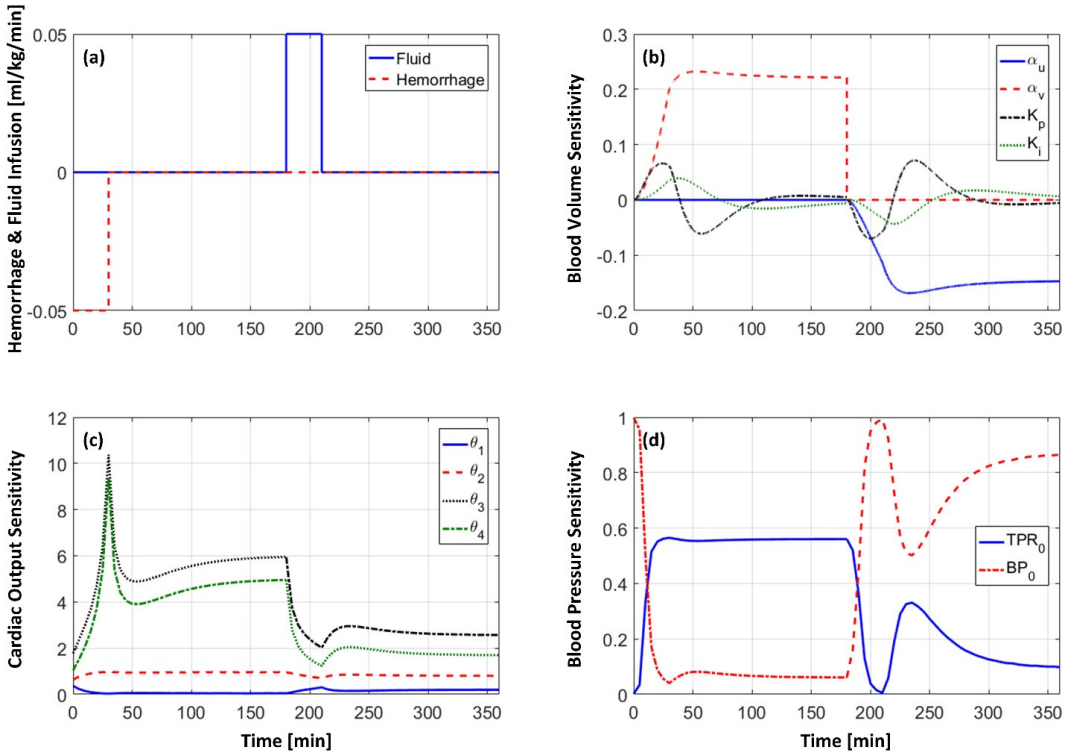

Figure 4-3: Time evolution of normalized parametric sensitivity functions (indicating percent change in the hemodynamic responses caused by unit percent perturbation in each parameter from the nominal value) in response to simulated hemorrhage and crystalloid infusion.

individualized model to its fully individualized counterpart (see Section 4.4). The difference in the 8 tunable parameters was minimal and mostly insignificant ($p>0.05$ for both LR and Hex, except K_p associated with Hex ($p=0.03$)). Further, the physiological relevance of parameters observed for the fully individualized model was preserved in the partially individualized model. In sum, the impact of fixing K_i and θ_1 to their nominal values on the validity and physiological relevance of the model was minimal. Considering that the partially individualized model involves less number of tunable parameters, it may be claimed that it is equipped with superior accuracy-complexity trade-off to fully individualized model.

4.5.2. Parametric Sensitivity

Examining the time evolution of the parametric sensitivity functions offered additional insights as to the relative importance and identifiability properties of the model parameters. First, the time evolution of $\mathcal{S}_{V_B}(t)$ indicates that BV response in the steady-state is primarily sensitive to α_u and α_v while the same response during transients is also influenced by K_p and K_i (Figure 4-3(b)). This is plausible in that α_u and α_v specify steady-state changes in BV and ISFV, whereas K_p and K_i are parameters dictating dynamic inter-compartmental fluid shift. In addition, the amplitudes of the sensitivity functions associated with K_p and K_i are relatively smaller than those associated with α_u and α_v, suggesting the relative importance of the latter parameters compared to the former parameters. In particular, K_i appears to be the least important parameter in the control-theoretic BV model, suggesting that the inter-compartmental fluid shift may be adequately described by individualizing the proportional control action alone. Second, the time evolution of $\mathcal{S}_{CO}(t)$ indicates that CO response is sensitive to θ_3 and θ_4 relative to θ_1 and θ_2 (Figure 4-3(c)). This observation is plausible in that θ_3 and θ_4 are related to BV and unstressed BV, the changes in which directly influences SV and CO. The amplitude of sensitivity functions was overall larger under hemorrhage than fluid infusion condition (except $\frac{\partial CO(t)}{\partial \theta_1}$ which exhibited the opposite trend), which may be attributed to an increase in the denominator term $(\theta_2 CO(t) + \theta_3 V_B(t) + \theta_4) - \theta_1\theta_2 HR(t)$ in $\mathcal{S}_{CO}(t)$ in response to BV expansion associated with fluid infusion. In sum, θ_1 appears to be the least important parameter in the lumped-parameter SV-CO model. Third, the time evolution of $\mathcal{S}_{P_0}(t)$ indicates

that both R_0 and $P_{m,0}$ make a large influence on MAP response (Figure 4-3(d)). In particular, noting that (4-13) is a saturating function in the MAP-TPR plane (Figure 4-3(c)), perturbing R_0 and $P_{m,0}$ shifts the function (4-13) in vertical and horizontal directions, respectively. Hence, the function, and thus MAP response as well, is more sensitive to R_0 than $P_{m,0}$ when BP is far away from $P_{m,0}$ (i.e., the saturating ends of the function) while it is more sensitive to $P_{m,0}$ than R_0 when MAP is near $P_{m,0}$. The sensitivity functions in Figure 4-3(d) clearly follow this anticipated behaviors: $\frac{\partial P_m(t)}{\partial R_0}$ exhibited larger amplitude during hemorrhage (with which BV decreases away from its baseline value) than during fluid infusion (with which BV increases back towards its baseline value), while $\frac{\partial P_m(t)}{\partial P_{m,0}}$ exhibited the opposite behaviors. Though R_0 and $P_{m,0}$ influence MAP response in different regimes, their peak amplitudes were quite comparable. Thus, both parameters were deemed important in reproducing MAP response accurately.

5. Development and Validation of a Dose-Response Model of Vasopressor Infusion

This chapter presents a new analytic tool for automated control of vasopressor infusion, which uses measured changes in BP to infer changes in the underlying CV state and then estimate their dose-response relationships. Ultimately, BP as a function of vasopressor dose is predicted based on the estimated underlying CV state by extrapolating the dose-response relationship. This tool can adapt to individual subjects with a minimum of individualized training data. The proof-of-principle is provided using experimental epinephrine dose-response data from four different sets of subjects. The proposed analytic tool may provide a meaningful step towards automated control of vasopressor therapy.

5.1.Goal, Need and Mechanism of Vasopressor Therapy

Vasopressors are medications that act to elevate arterial BP in critically ill patients suffering from a body-wide reduction in blood circulation. Vasopressors can act through one or more physiological mechanisms, including increasing resistance to blood exiting the arteries (i.e., TPR) and increasing CO through increased HR, cardiac contractility and decreased venous capacitance. The ultimate medical benefit of vasopressors is not increased BP per se, but increased blood flow to peripheral tissues driven by the increase in BP. In today's clinical practice, the infusion rate of vasopressor medications is adjusted by human clinicians. A complicating factor is that vasopressors can either improve blood flow to hypo-perfused peripheral tissues via the increase in BP or, in some cases, can decrease blood flow via excessive increase in

blood vessel resistance, depending on which effect is predominant (Meier-Hellmann et al., 1997; Nevière et al., 1996; Ruokonen et al., 1993). The second complicating factor is that there is substantial individual variability in the physiological response to vasopressor therapy (Bockenstedt et al., 2012; Rech et al., 2011). Therefore, standard clinical practice is to iteratively, and empirically, adjust the infusion rate in a given patient, seeking to maximize the expected beneficial effects relative to deleterious effects.

Control of BP as an endpoint has been the focus of clinical practice guidelines for vasopressor use, where current advice is to adjust infusion rates to achieve a minimal MAP of at least 65 mmHg [e.g., (Takala, 2010)]. In practice, clinicians empirically adjust vasopressor dose levels to achieve this target for MAP (see Chapter 2); in theory, such a tool could help clinicians make superior adjustments to vasopressor doses, avoiding dose-adjustments that are too small or too large. However, an appropriate BP can be resulted from low CO and excessive TPR, which can lead to inadequate level of blood delivery to the tissues. Therefore, developing a method of vasopressor therapy that works based on both underlying CV state and measurable hemodynamic endpoints would be of interest to biomedicine researchers.

In this chapter, we describe an analytic tool that satisfies the following specifications: (i) as inputs, it requires nothing more than the basic vital signs of HR, SBP, MAP and diastolic BP (DBP); and (ii) it adapts to individual patients with minimal observations. The feasibility and validity of this physiologic-phenomenological methodology are demonstrated using the experimental epinephrine dose-response data collected from four different sets of subjects. Its performance,

potential usefulness, and limitations are explained in the subsequent sections. Potentially, this analytic methodology may offer a meaningful step towards automated control of vasopressor therapy.

5.2.Development of the Vasopressor Model

Three basic steps involved in the proposed analytic tool are explained in Sections 5.2.1-5.2.3.

5.2.1. Estimation of the Complete Cardiovascular State.

Clinicians typically titrate the vasopressor drug level based on BP, even though changes in BP actually reflect changes in underlying state of CV, i.e., CO and TPR; from hereafter we call CO and TPR parameters or their corresponding trends as cardinal parameters. The proposed methodology is predicated on estimating a dose-response relationship for these underlying cardinal parameters. If CO and TPR are not directly measured, then the effects of the vasopressor agent on the cardinal parameters must be inferred. Therefore, a specific algorithm that uses non-continuous measurements of SBP, MAP, DBP, and HR will be developed and employed to infer cardinal parameters related to CO and TPR. This methodology is based on the assumption that the relationships between vasopressor dose level and the cardinal parameters are more consistent than the relationship between vasopressor dose and BP. It is noted that since a model of CV to infer cardinal parameters using rudimentary BP and HR measurement will be presented in the next chapter, in this chapter cardinal parameters are assumed to be known; we assume that cardinal parameters $\overline{\mathrm{R}}\overline{\mathrm{C}}^{*}$ and $\frac{\delta\overline{\mathrm{V}}^{*}}{\overline{\mathrm{C}}}$ are the optimal scaled

TPR index (TPRI) and SV index (SVI) associated with a particular vasopressor dose, which can be inferred from the physiologic CV model presented in Chapter 6.

5.2.2. Estimating Phenomenological Dose-Response Relationships

Here, we describe an approach to estimate a set of phenomenological models between the vasopressor dose level and the cardinal CV parameters. By design, this methodology permits the estimation of individualized dose-responses after observations from as few as two vasopressor dose levels. Of note, because different vasopressors affect the cardinal CV parameters differently, specific phenomenological models used to reproduce the phenomena are vasopressor-dependent, i.e., a different specific model must be employed for epinephrine versus norepinephrine, etc. As discussed later, it may also be appropriate to modify the methodology for low-dose epinephrine (where beta effects are more significant than alpha effects) versus high-dose epinephrine (where alpha effects are more significant than beta effects).

To demonstrate the general approach, we apply the analytic tool to a previously reported dataset describing low-to-moderate dose epinephrine's hemodynamic dose-response relationship ((Leenen et al., 2007; White and Leenen, 1997)). The aforementioned epinephrine dataset (Leenen et al., 2007; White and Leenen, 1997) reports hemodynamic responses of 14 normotensive young (NY; 30+/-2yr) and 18 normotensive old (NO; 60+/-2yr) subjects as well as 10 hypertensive young (HY; 36+/-1yr) and 17 hypertensive old (HO; 59+/-1yr) subjects. As per the original report, normotensive and hypertensive BP were defined as <130mmHg SBP/85mmHg DBP and >140mmHg SBP/95mmHg DBP, respectively.

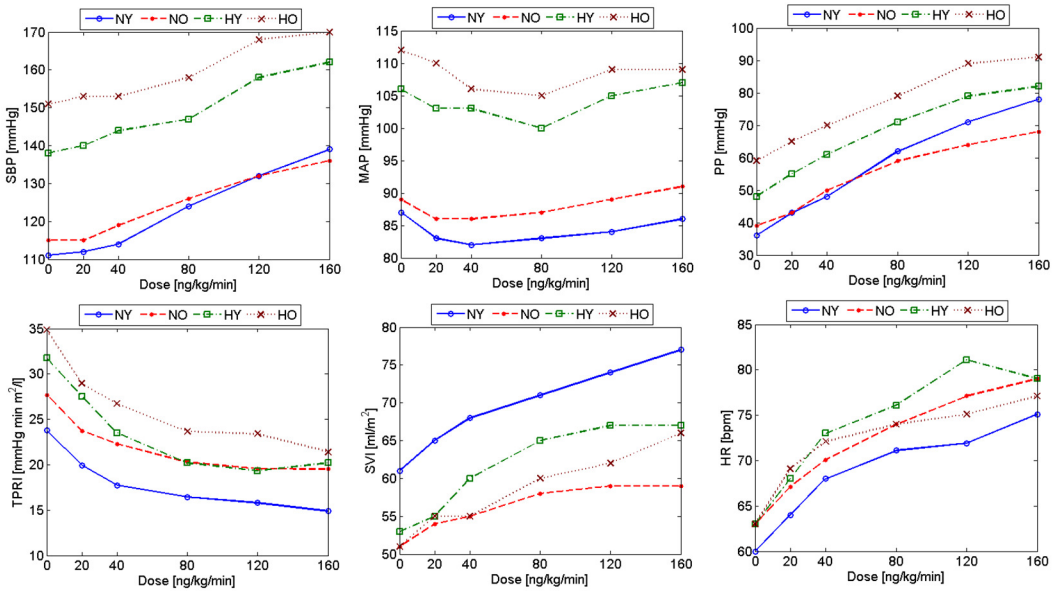

Figure 5-1: True hemodynamic responses of four sets of subjects to epinephrine administration.

The dataset provides BP data as a function of epinephrine dose (SBP, MAP and DBP), measured using an oscillometric arm BP cuff. The dataset also includes measurements of HR and SVI, measured using echocardiography (N.B., the SVI data are not inputs to the analytic tool, but rather, provide the gold-standard measurements against which the accuracy of the prediction of the analytic tool is evaluated). In the original experimental protocol, following a rest period of at least 60min, epinephrine was administered in consecutive 8 min intervals, at 20 ng/kg/min, 40 ng/kg/min, 80 ng/kg/min, 120 ng/kg/min and 160 ng/kg/min. (Typically, epinephrine's beta effects are dominant when the dose is less than 50 ng/kg/min, while its alpha effects do not dominate until doses of 100 ng/kg/min (Miller, 2010)). In this dataset, hemodynamic measurements were made at steady-state before epinephrine administration and then during the last 2-3min of each consecutive epinephrine dosing interval.

Table 12: Physiological range of epinephrine dose-dependent hemodynamic responses.

		HR [bpm]	SBP [mmHg]	MAP [mmHg]	DBP [mmHg]	SVI [ml/m^2]
Baseline Value		60-63	111-151	87-112	75-92	51-61
Hemodynamic Responses	020ng/kg/min	64-69	112-153	83-110	69-88	54-65
	040ng/kg/min	68-73	114-153	82-106	66-83	55-68
	080ng/kg/min	71-76	124-158	83-105	62-79	58-71
	120ng/kg/min	72-81	132-168	84-109	61-79	59-74
	160ng/kg/min	75-79	136-170	86-109	61-80	59-77

Figure 5-1 shows the pooled hemodynamic responses from the four sets of subjects to different epinephrine doses, including SBP, MAP and PP as well as TPRI, SVI and HR. Their ranges are summarized in Table 12. Note that detailed individual subject data were not reported, thus inter-individual variability was not considered in this study.

The challenge of estimating an individualized dose-response relationship with only two observations is the complexity of epinephrine's effects. Lower doses of epinephrine (e.g. < 50 ng/kg/min) decrease TPR over its baseline value (beta agonist effect), whereas higher doses (e.g., > 100 ng/kg/min) activate alpha receptors and increase TPR (Ellender and Skinner, 2008). HR and inotropy (affecting SV) are primarily increased by beta agonist action. To reproduce the anticipated responses of HR, TPRI and SVI accurately while minimizing the amount of a priori data required to train the models, we developed the following phenomenological models dictating the dose dependence of HR, $\overline{R}\overline{C}$ and $\frac{\delta\overline{V}}{\overline{C}}$:

$$HR = f_1(d, \theta_1) = (k_{1H}d + k_{2H})^{0.1},\ \theta_1 = \{k_{1H}, k_{2H}\} \quad (5\text{-}1a)$$

$$\overline{RC} = f_2(d, \theta_2) = \frac{1}{k_{1R}d + k_{2R}} + [k_{3R}d + k_{4R}]\sigma(d, d_0),\ \theta_2 = \{k_{1R}, k_{2R}\} \quad (5\text{-}1b)$$

$$\frac{\delta\overline{V}}{\overline{C}} = f_3(d, \theta_3) = k_{1V}d + k_{2V} - [k_{3V}d + k_{4V}]\sigma(d, d_0),\ \theta_3 = \{k_{1V}, k_{2V}\} \quad (5\text{-}1c)$$

where $\delta\overline{V}$ is SVI, and $\overline{R}$ (in mmHg·min·m^2/l) and $\overline{C}$ (in ml/mmHg/m^2) are defined as TPR index (TPRI, MAP divided by SVI and HR) and arterial compliance index (ACI), d is the drug dose level, k_{1H}, k_{2H}, k_{1R}, k_{2R}, k_{1V} and k_{2V} are empirical constants that quantify the beta agonist effects, whereas k_{3R}, k_{4R}, k_{3V} and k_{4V} are constants dictating the alpha agonist effects. The function $\sigma(d, d_0)$ in (5-1b) and (5-1c) is intended to activate the alpha agonist action in the high dose region and is defined as follows:

$$\sigma(d, d_0) = \begin{cases} 0, & d < d_0 \\ 1, & d \geq d_0 \end{cases} \quad (5\text{-}1d)$$

Overall, these phenomenological models are able to capture the following behaviors:

- Increasing HR with increasing d, tapering off at higher dose levels
- Increasing SVI with increasing d, tapering off at higher dose levels

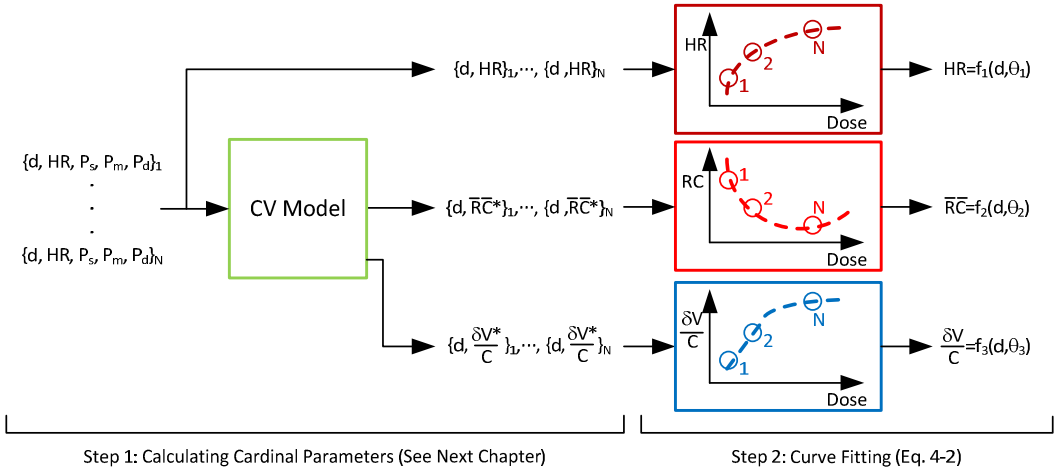

Figure 5-2: Training of phenomenological dose-response relationships using vasopressor dose and BP data.

- Decreasing TPRI with increasing d due to beta agonist effects, until alpha agonism becomes evident (e.g., note the increasing TPRI in NO and HY group at 160 ng/kg/min; see Figure 5-1).

This analytic tool was designed to provide subject-specific predictions using a minimum of observations (i.e., two). However, even these simplified dose-response models have too many unknowns to be estimated with just two observations. Accordingly, we employ the following strategy: solve the model parameters that drive the most inter-subject variability, and use population-based values for other model parameters, to reduce the number of unknowns. Examining this dataset, i.e., Figure 5-1, it is apparent that the alpha agonist effects (i.e., vasoconstriction causing increased TPR) did not drive the subjects' CV responses, and given this dosing regime (≤ 160 ng/kg/min), most of the inter-subject CV variability was driven by the beta agonist effects (k_{1H}, k_{2H}, k_{1R}, k_{2R}, k_{1V} and k_{2V}). Our analytic tool estimated parameters for the beta agonist effects, while relying on population-averaged values for the alpha effects (i.e., k_{3R}, k_{4R}, k_{3V}, k_{4V} and d_0). Ultimately, each of the phenomenological models (5-1) was left with only two unknowns and could be solved given only two individualized observations.

Quantitatively, the phenomenological models (5-1) (more specifically, the unknown beta agonist effect parameters therein) dictating the reliance of HR, $\overline{R}\overline{C}$ and $\frac{\delta\overline{V}}{\overline{C}}$ on vasopressor dose level can be fitted to the data obtained from Step I (see Section 5.2.1). Given the pairs of data $\left\{d,\ HR,\ \overline{R}\overline{C}^{*},\ \frac{\delta\overline{V}^{*}}{\overline{C}}\right\}_i$, $i = 1, \cdots N$, the optimal θ_1, θ_2 and θ_3 in (5-1) are determined using the following least-squares optimization process:

$$\theta_1^* = \arg\min_{\theta_1} \sum_{i=1}^{N} [HR - f_1(d, \quad \theta_1)]_i^2 \tag{5-2a}$$

$$\theta_2^* = \arg\min_{\theta_2} \sum_{i=1}^{N} [\overline{R}\overline{C}^* - f_2(d, \quad \theta_2)]_i^2 \tag{5-2b}$$

$$\theta_3^* = \arg\min_{\theta_3} \sum_{i=1}^{N} \left[\frac{\delta\overline{V}^*}{\overline{C}} - f_3(d, \quad \theta_3)\right]_i^2 \tag{5-2c}$$

where $[\cdot]_i$ is the expression evaluated using $\left\{d,\ HR,\ \overline{R}\overline{C}^*,\ \frac{\delta\overline{V}^*}{\overline{C}}\right\}_i$. The process of training the tool to individual subject (Steps I and II) is graphically demonstrated in Figure 5-2. The way the phenomenological dose-response models are determined is as follow: First, the beta agonist component of the phenomenological models (5-1b) and (5-1c) were modeled using the epinephrine dose and BP response data at 0 ng/kg/min and 20 ng/kg/min as follows: (i) dose and BP responses were used to calculate $\overline{R}\overline{C}^*$ and $\frac{\delta\overline{V}^*}{\overline{C}}$ corresponding to 0 ng/kg/min and 20 ng/kg/min (see next chapter), and (ii) $\overline{R}\overline{C} = \frac{1}{k_{1R}d+k_{2R}}$ and $\frac{\delta\overline{V}}{\overline{C}} = k_{1V}d + k_{2V}$ were fitted to $\overline{R}\overline{C}^*$ and $\frac{\delta\overline{V}^*}{\overline{C}}$ at the two dose levels using (5-2b) and (5-2c), respectively (note that the alpha agonist components were not considered since their effects are negligible in low epinephrine dose levels). Second, $\overline{R}\overline{C}$ and $\frac{\delta\overline{V}}{\overline{C}}$ associated with high epinephrine dose levels (80 ng/kg/min, 120 ng/kg/min and 160 ng/kg/min) were predicted using the beta agonist model thus obtained. Third, the discrepancy between direct versus model-predicted $\overline{R}\overline{C}$ and $\frac{\delta\overline{V}}{\overline{C}}$ was calculated for all the subject groups, which was regarded as the contribution from the alpha agonist action. Finally, the alpha agonist components of (5-1b) and (5-1c), i.e., k_{3R}, k_{4R}, k_{3V}

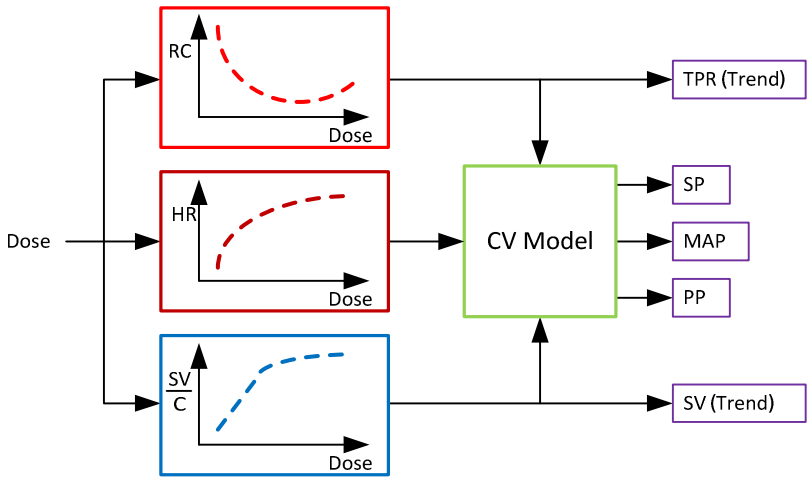

Figure 5-3: CV model with phenomenological relationship between vasopressor dose versus cardinal CV parameters HR, TPRI ($\overline{R}\overline{C}$) and SVI ($\frac{\delta\overline{V}}{\overline{C}}$).

and k_{4V}, were optimized to minimize the discrepancy in $\overline{R}\overline{C}$ and $\frac{\delta\overline{V}}{\overline{C}}$. Once the alpha agonist parameters were determined as described above, the phenomenological model was trained as follows. First, the alpha agonist parameters in (5-1b) and (5-1c) were fixed at the optimal population values. Second, $\overline{R}\overline{C}^*$ and $\frac{\delta\overline{V}^*}{\overline{C}}$ obtained from CV model directly from measurable BP and HR together with HR measurements were used to train the phenomenological models (5-1) via the optimization (5-2). Third, the analytic tool with the CV model and the trained phenomenological dose-response models was used to predict the hemodynamic responses including SBP, MAP and DBP as well as trend of TPR, SVI and COI as described in Section 5.2.3.

5.2.3. Prediction of Hemodynamic Responses

Using the CV model with the phenomenological dose-response relationships (5-1) individualized with $\theta_i^*, i = 1, \cdots 3$ obtained by (5-2), the hemodynamic responses for vasopressor dose levels not used in the training phase can be predicted solely based

on the vasopressor dose as follows (see Figure 5-3). HR, $\overline{R}\overline{C}$ and $\frac{\delta\overline{V}}{\overline{C}}$ are extrapolated using the trained (i.e., individualized) phenomenological models in (5-1) with the new vasopressor dose as input. Next, HR, $\overline{R}\overline{C}$ and $\frac{\delta\overline{V}}{\overline{C}}$ thus extrapolated are substituted in CV model (see next chapter) to predict SBP, MAP and PP associated with the vasopressor dose. Further, assuming that the short-term variability of arterial compliance (AC) is small and it can essentially be regarded as constant over short time window (Shoukas and Sagawa, 1971), $\overline{R}\overline{C}$ and $\frac{\delta\overline{V}}{\overline{C}}$ predicted from the phenomenological models in (5-1) can be regarded as predictions of TPRI and SVI (with unknown scale). Finally, the CO index (COI) can be predicted as the product of HR and $\frac{\delta\overline{V}}{\overline{C}}$ predicted with the phenomenological models in (5-1).

5.3.Validation of the Model

In this section, we demonstrate the application of the analytic tool to predict the responses to epinephrine infusion. We employed discrete BP measurements (SBP, MAP, DBP) and HR from only two different epinephrine dose levels - 0 ng/kg/min and X ng/kg/min - to train the phenomenological dose-response models (5-1). Then these models were used to predict cardinal CV parameters TPRI, SVI and HR for dose levels not used in the training phase, with which BP was predicted using the CV model (see next chapter).

We applied the analytic tool to each set of subjects described in Section 5.2. The hemodynamic responses predicted by the analytic tool were compared with in-vivo experimental data: MAP and HR were as reported in Leenen et al. (Leenen et al., 2007);

RC and SVI/C were estimated using a CV model (see next chapter) with the BP data reported in Leenen et al.

For each set of subjects, we studied different ways of training the tool, as follows:

- To explore performance for a patient requiring a vasopressor wean (i.e. prediction for a reduced dosage), we trained with BP and HR data from {0 ng/kg/min, 160 ng/kg/min} to predict TPRI, SVI, HR and BP responses to 20, 40, 80 and 120 ng/kg/min

- To explore performance for a patient in flux (i.e. prediction required for both increasing and decreasing doses), we trained with BP and HR data from {0 ng/kg/min, 80 ng/kg/min} to predict TPRI, SVI, HR and BP responses to 20, 40, 120 and 160 ng/kg/min

- To explore performance for a patient receiving an inadequate vasopressor dose, we trained with BP and HR data from {0 ng/kg/min, 20 ng/kg/min} to predict TPRI, SVI, HR and BP responses to 40, 80, 120 and 160 ng/kg/min.

The validity of the analytic tool was assessed in terms of prediction errors on SBP, MAP and PP, as well as the goodness of fits between measured versus model-predicted TPRI, SVI and COI in terms of the coefficient of determination (CoD; r^2 value) and the Bland-Altman statistics (i.e., the limits of agreement). It is noted that linear regression analysis was conducted on $\overline{R}\overline{C}^*$ and $\frac{\delta\overline{V}^*}{\overline{C}}$ to calibrate them against measured TPRI and SVI before quantifying the goodness of fits, thereby eliminating the effect of unknown AC.

Overall, the proposed analytic tool was able to accurately predict absolute responses of BP and HR (see Figure 5-4). Most remarkably, the phenomenological dose-response models could reproduce the biphasic behavior of MAP expected in response to epinephrine infusion, i.e. decrease MAP under low dose levels and increase under high dose levels. In terms of RMSE, the difference between actual versus model-predicted SBP, MAP and PP, aggregated across the four sets of subjects, were less than 6% of the respective underlying values when trained with {0 ng/kg/min, 20 ng/kg/min}, less than 4% when trained with {0 ng/kg/min, 80 ng/kg/min}, and less than 4% when trained with {0 ng/kg/min, 160 ng/kg/min}, respectively.

We also compared the ability of the analytic tool to estimate cardinal CV parameters' responses to new doses (Figure 5-4). Overall, the performance was encouraging (there was one exception to the successful prediction of cardinal parameters as a function of epinephrine dose: SVI in the NO subject group, trained with {0 ng/kg/min, 20 ng/kg/min} (see Figure 5-4(b)). The correlation between actual versus model-predicted cardinal CV parameters (TPRI, SVI, and CO index (COI) as calculated by the product of SVI and HR) were high: the r^2 values aggregated across the four sets of subjects, were higher than 0.96 regardless of the training doses used in this study. These results also support our strategy to individualize beta agonist parameters while fixing alpha agonist parameters to population-averaged values. To confirm the dominance of subject-specific beta effects (and the relative acceptability of using population-averaged alpha coefficients), we tested a reversal of our methodology. Specifically, we individualized alpha agonist parameters in the phenomenological dose-response models, while we fixed the beta agonist parameters

using population-averaged values. Consequently, the RMSE values associated with actual versus model-predicted SBP, MAP and PP were increased by 89%, 236% and 314%, respectively, when trained with {0 ng/kg/min, 160 ng/kg/min}.

Finally, the Bland-Altman analysis indicated that the model-predicted hemodynamic responses were in good agreement with their actual counterparts (see Figure 5-5). The biases were shown to be very small (see the solid horizontal lines Figure 5-5). In addition, the limits of agreement were also tight: the confidence intervals associated with SBP, MAP and PP as well as TPRI, SVI and COI were consistently less than 8% of the respective underlying values (calculated as the average between actual versus model-predicted values).

5.4.Model's Characteristics and Performance

An analytic tool that can accurately predict how an individual patient will respond to different doses of vasopressor infusions would be valuable in today's clinical practice and tomorrow's automated closed-loop infusion systems. Moreover, the ideal method would predict the patient's complete CV state rather than just a single parameter. Finally, the ideal method would require minimal observational data to adapt to the physiology of the individual patient.

In this chapter, we developed a methodology to satisfy these specifications. The method did not generate a direct relationship between BP versus drug dose; rather, it yielded a relationship between cardinal CV parameters versus drug dose, which could be applied to estimate BP versus drug dose. This approach yielded promising experimental results in a preliminary proof-of-principle evaluation.

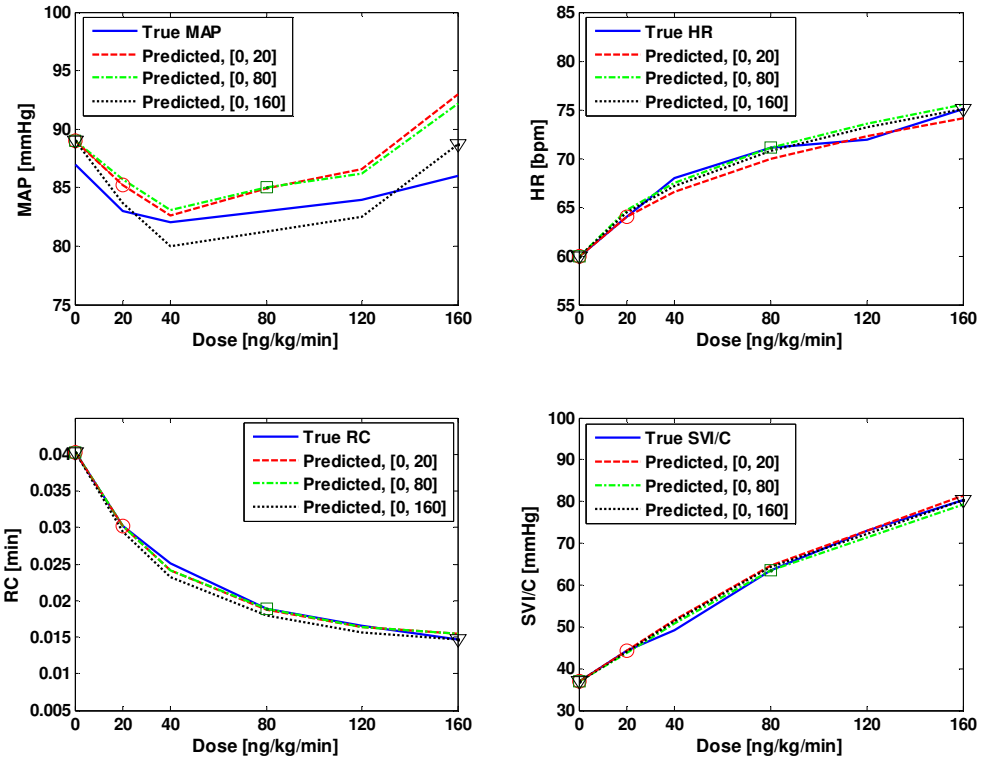

(a) Normotensive Young (NY) subject group

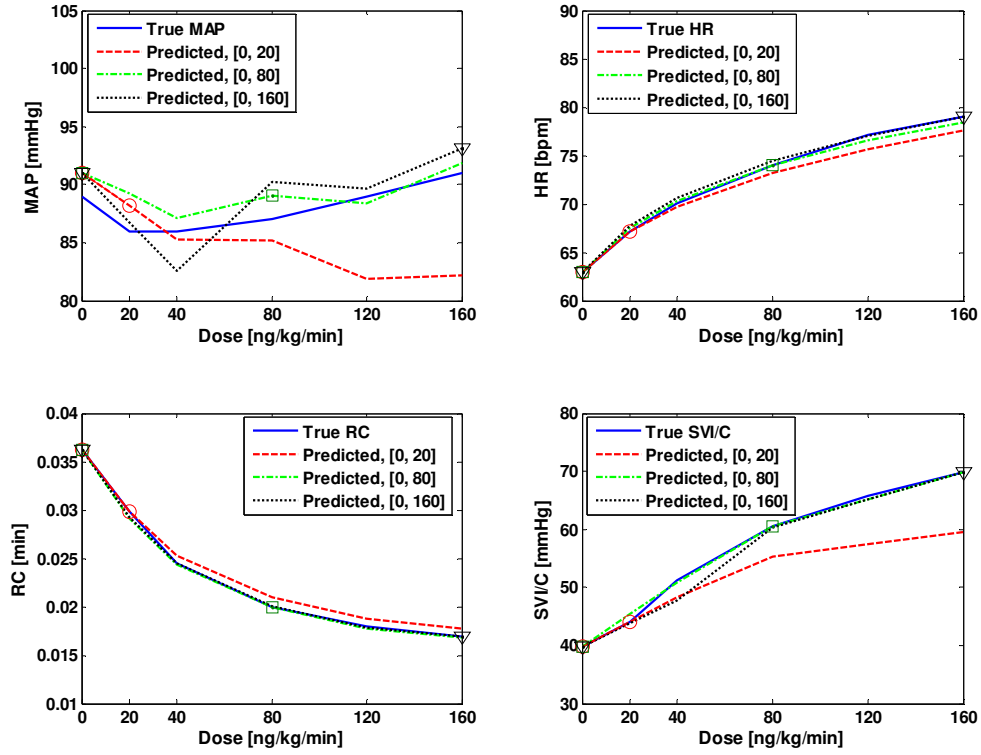

(b) Normotensive Old (NO) subject group

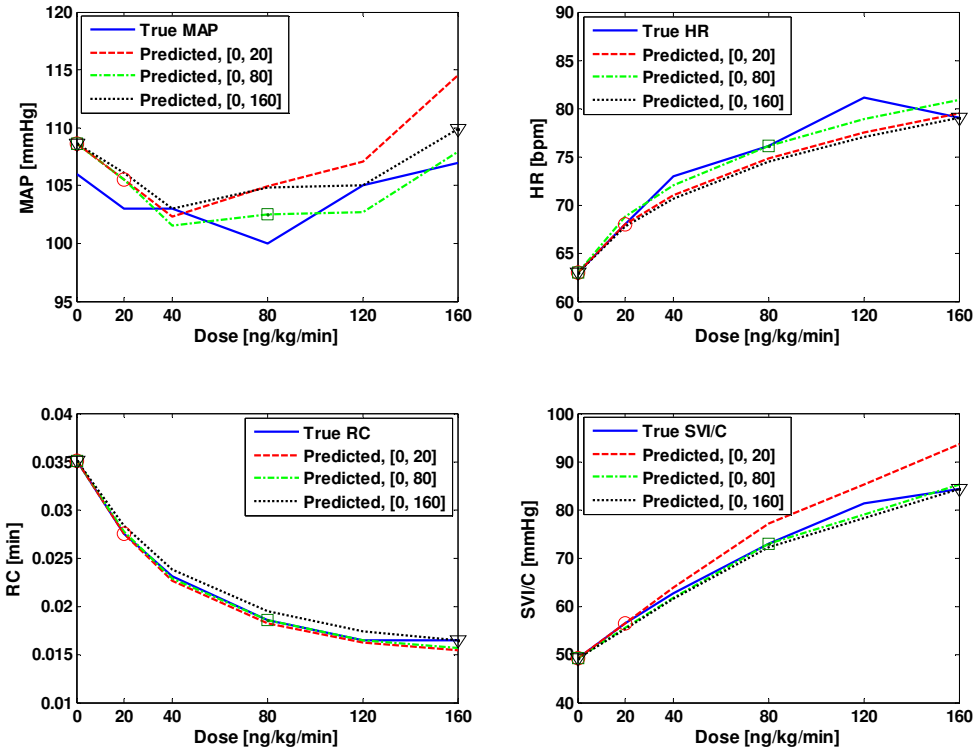

(c) Hypertensive Young (HY) subject group

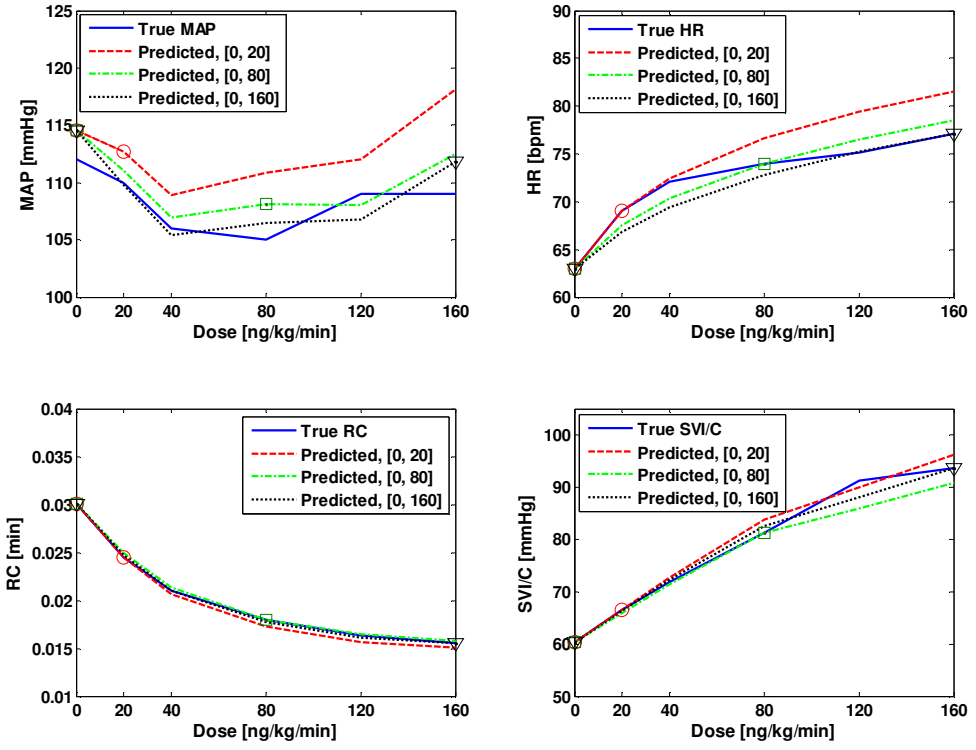

(d) Hypertensive Old (HO) subject group

Figure 5-4: Actual versus predicted hemodynamic responses for each set of subjects. The blue solid lines indicate actual responses. Markers indicate the dosage levels that were used in training the analytic tool; only BP and HR data were used as training inputs.

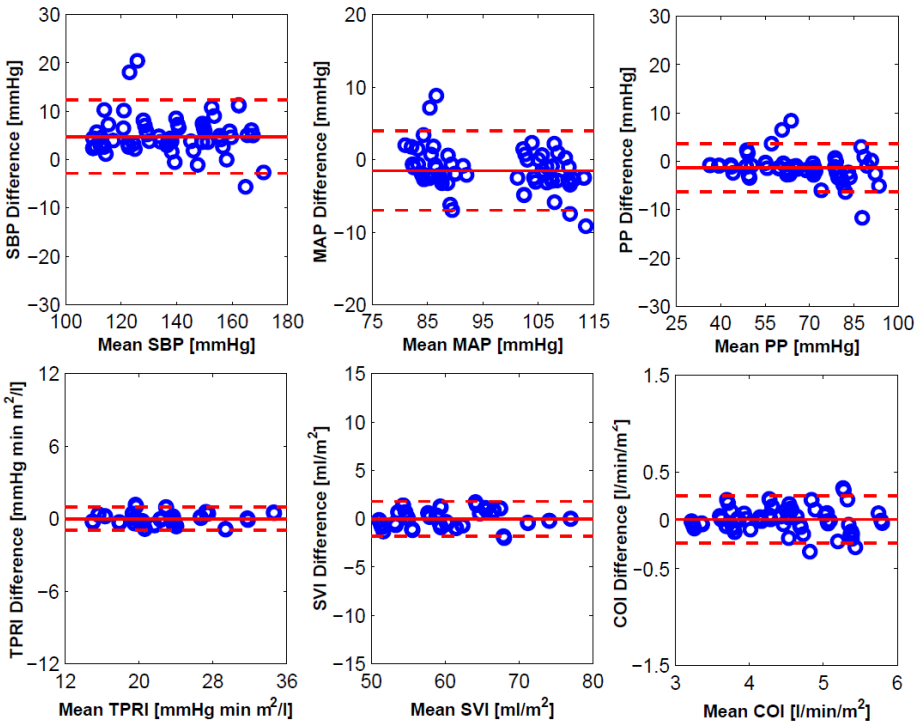

Figure 5-5: Bland-Altman plots associated with actual versus model-predicted SBP, MAP, PP, TPRI, SVI and COI in four sets of subjects, aggregated across three different scenarios. The biases and the limits of agreement are marked as solid and dashed lines, respectively.

In the section, we address the following: (a) the potential clinical benefits of such a methodology; (b) the performance of our specific solution; and (c) what generalizable lessons can be drawn from the current work that are applicable to future work.

5.4.1. Potential Clinical Benefits

Today, vasopressor doses are titrated by clinicians to achieve rudimentary endpoints. For instance, today's sepsis management guidelines suggest vasopressors should be infused until MAP $\geq$ 65 mmHg (Takala, 2010). At the same time, clinicians avoid excessive infusion rates because of possible deleterious effects, including excessive arterial pressures that strain the heart, excessive peripheral vasoconstriction that reduce peripheral perfusion, and possible cardiac tachyarrhythmias. In practice, today's vasopressor dosing changes are made on an informal, ad hoc basis.

There are several potential benefits of the analytic tool described in this chapter. Current clinical practice involves ad hoc dosage adjustments for vasopressor infusion rates, and there are intervals, inevitably, when the dosage adjustment isn't optimal and consequently the CV state of the patient is suboptimal. A good computational method should suggest dosage changes that can quickly move the patient to the optimal CV state, with minimal dosage changes that are either inadequate or excessive. Rapidly iterating to an optimal infusion rate should lead to superior outcomes for critically-ill patients, because their organs will be spared from intervals of hypo-perfusion (i.e., infusion rate too low), and of excessive vasoconstriction with reduced perfusion (i.e., infusion rate too high). The benefit of a computational algorithm, over the subjective judgment of the clinician, might be especially pronounced for patients being managed by clinicians without extensive critical care expertise (Hennings et al., 2010; Siegal et al., 2012). Lastly, if reliable, such a computational tool could also be installed into a closed-loop system for controlling infusion rates, and help enable a new generation of critical care delivered by "auto-pilot". Having a robust tool for determining how to adjust infusion dosages will be an essential component of such a closed-loop system.

Also, we conjecture that computational tools will enable a new generation of more sophisticated (and more effective) strategies for optimizing vasopressor dosages, as suggested by recent investigations (Parkin and Leaning, 2008; Uemura et al., 2006). Today's guidelines for dose adjustment are quite vague. Consider that the Surviving Sepsis campaign advises that, for patients in septic shock, clinicians infuse vasopressors to a MAP of at least 65 mmHg. This broad hemodynamic target has the advantage that the typical clinician can readily comply. Yet consider the wide variety

of CV states that satisfy this rather general criterion. In a patient with shock, MAP could be elevated by organ vasoconstriction alone, which would improve essential perfusion to the brain and heart (these specific organs are relatively insensitive to vasopressors) but at the expense of perfusion to other vasoconstricted organs. In many cases, it might be preferable to optimize CO, and not just MAP, since improved CO could translate to improved blood flow to all the organs of the body. Moreover, excessive increases in MAP have a cost, causing strain on the heart, i.e., increased oxygen requirement for the cardiac muscle tissues and the risk of reduced pump function. Increasing doses of vasopressors can likewise raise HR, which also can strain the heart. In summary, there are theoretical reasons why a sophisticated strategy of adjusting vasopressor infusion rates would be superior to today's coarse management strategies. More sophisticated therapeutic strategies can potentially balance the trade-offs between perfusing the heart and brain (i.e., adequate MAP), perfusing other organs (i.e., adequate CO), and cardiac work (i.e., non-excessive MAP and HR). Yet today's clinician simply lacks the capability to do much more than adjust, and re-adjust, to hit broad CV targets. An analytic tool that adapts to the individual patient and accurately predicts the proper vasopressor infusion rate to achieve tight optimized targets for MAP and CO will make it practical to employ more sophisticated therapeutic strategies.

5.4.2. Performance of the Proposed Model

We predicate that an ideal analytic tool to predict hemodynamic responses as a function of vasopressor dose should (i) infer the complete CV state rather than mere BP to allow for enhanced vasopressor dosing strategies, and (ii) adapt easily to the

physiology of each individual patient to effectively cope with large inter-individual variability.

In this work, we did not directly develop a dose-response relationship between BP versus vasopressor dose, but rather, we inferred the dose-response relationship of unmeasured cardinal CV parameters and used the inferred relationship to predict the BP response to vasopressor doses. This approach offers two potential advantages. First, the estimation of multiple CV parameters could, in theory, allow for more sophisticated dose adjustment (as discussed above). Second, this approach could, in theory, lead to more accurate predictive capability, especially if the relationship between vasopressor dose level and the unmeasured, cardinal parameters, e.g., SVI and TPRI, are in fact more consistent than the relationship between vasopressor dose and the measured parameters, e.g., BP.

This chapter is not intended to answer whether or not the novel analytic tool is superior to alternative approaches. Rather, the intent is to report a novel methodology and provide a proof-of-principle (the generalizability of this methodology is discussed below). We find that indeed the analytic tool demonstrates reasonable preliminary performance: consider how the analytic tool was able to extrapolate reliably beyond its training region. Given training data during low-to-medium dose (beta-receptor agonist) infusion, this approach was still able to anticipate that medium-dose infusion would lead to further reduction in MAP (due to maximum beta agonist effect) whereas high-dose infusion would then increase MAP (since alpha agonist effect becomes dominant). This effect was consistently seen for each of the three studies involving the NY, HO, and HY groups, and two of the studies involving the NO group. It was only in one of

sixteen trials that this anticipated trend of MAP was not seen (in the isolated NO group study with training data from {0ng/kg/min and 20 ng/kg/min} due to limited accuracy in SVI prediction for higher epinephrine doses).

It must be emphasized that reproduction of this physiologically relevant dose-dependent MAP behavior was not trivial, since our model was not fitted directly to the pair of epinephrine dose and MAP, and only two sets of observations were used to train the model. Specifically, MAP was inferred via the CV model (see next chapter) from HR, TPRI and SVI, which are predicted from the phenomenological models (5-1). This demonstrates how the combination of the CV model and phenomenological dose-response relationships for cardinal CV parameters can yield advantageous performance.

5.4.3. Generalizable Lessons

This study describes a framework for individualized dose-response prediction, and should be interpreted as a (potentially meaningful) first step towards the development of an analytic tool for automated control of vasopressor infusion, rather than a study to report an actual tool for decision support. This method is predicated on extrapolation of dose-response relationships for the cardinal CV parameters, where we estimate some parameters by fitting the model using a limited number of observations, while constraining the model using population-averaged values for other parameters that do not drive as much inter-subject variability. In this section, we examine both the limitations and the generalizable lessons from this work.

CV Model: Analyzing a dataset with non-continuous measurements of SBP, MAP, DBP, and HR, we sought to infer the complete CV state. Given these rudimentary

measurements, a rudimentary CV model was deemed reasonable; it provided a means to infer the underlying CV state in terms of the cardinal CV parameters related to CO and TPR. For more details, see next chapter.

Here, a question may arise to the reader: is an analytic tool that relies on a CV model superior to a more empiric method? When cardinal CV parameters are unmeasured, a CV model provides a rational basis for estimation and can reproduce some complex phenomenon (e.g., consider how the simple models in (5-1) are able to predict the drop, then rise, in MAP as epinephrine dose is increased). Predicting the patient's dose-response in terms of underlying cardinal parameters may yield reliable predictions, but whether this approach is better than a strictly empiric dose-response relationship remains an open question which should be examined in a larger dataset of clinical data.

Phenomenological Dose-Response Relationships: We sought a methodology for individualized dose-response relationships, because there is significant variability between patients (Kellum and Pinsky, 2002). At the same time, we sought a method that could operate with a minimal number of individualized observations, so that the analytic tool would be useful even during the earliest stages of critical care.

To determine dose-response relationships given just two observations, our phenomenological dose-response models could only contain two unknown parameters. Opportunistically, we decided to use the measurements to solve for parameters that were the biggest drivers of inter-subject variability, while relying on prior knowledge as a constraint that allowed for mathematical solution. This approach was optimized for this dataset: we decided to apply population-averaged values for the alpha agonist

effects, because they were less dominant than their beta counterparts. The result was encouraging performance as indicated by Figures 5-4 and 5-5.

To apply this strategy more broadly, different phenomenological models would be necessary for different vasopressors. Moreover, the decision to solve for individual beta effects versus alpha effects is likely a function of the dosing regime. For patients receiving high-dose epinephrine, it is quite likely that inter-subject variability will be driven more by alpha effects, hence it may be preferable to individualize the alpha effect models and employ population-based coefficients for the beta effects (or to require additional observations, which would allow for solution of additional unknowns). New datasets will need to be examined to evaluate whether there are specific approaches, in terms of how to employ a priori knowledge, that are broadly generalizable.

There is an important limitation of this work to consider. In this study, we reproduced group-averaged dose-response relationships, because the hemodynamic responses of each individual subjects were not available from the dataset. Given individual subjects, it is reasonable to anticipate additional variability. Will the models (5-1), and the use of population-averaged parameters therein, be efficacious to accommodate individual variability? This is another open question. Although we speculate that the basic (qualitative) relationships between the CV parameters versus vasopressors are unlikely to change, and two degrees of freedom should be adequate for reasonable predictions, whether or not the generic pattern of the hemodynamic responses assumed in the phenomenological models applies to all patient population (especially those exhibiting large inter-individual variability, e.g., diseases such as

heart failure (Lamba and Abraham, 2000) and septic shock (Price et al., 1999)) is an issue that needs to be further investigated in the follow-up study.

5.5.Further Model Validation using Dynamic Transient Data

As a follow up study to better assess the validity of the analytic tool proposed in this chapter, now we move to accommodate complex dynamic transients. To cope with the complexity of the data, we extended the model (5-1) to derive a hybrid model called the "latency-dose-response-CV" (LDC) model. This hybrid model includes a low-order lumped latency model, as well as several other enhancements to reproduce dose-response behavior under diverse physiological states. In this section, we conduct a rigorous investigation to test the capability of the LDC model to reproduce not only BP but also other CV parameter responses measured under diverse physiological states, and also examine the efficacy of the LDC model in predicting the hemodynamic response to epinephrine, and the relative importance of individualizing latency versus dose-response models in achieving a low-order but high-fidelity LDC model.

The hybrid model "LDC" incorporates (i) a low-order lumped latency model to reproduce the delay associated with the transport of vasopressor-inotrope agent and the onset of physiological effect, (ii) extended phenomenological dose-response model (5-1) to dictate the steady-state inotropic, chronotropic and vasoactive responses as a function of vasopressor-inotrope dose, and (iii) a physiological CV model to translate the agent's actions into the ultimate response of BP which will be explained in the next chapter. The validity of the LDC model to fit vasopressor-inotrope dose-response data is assessed using data collected from five piglet subjects during variable epinephrine

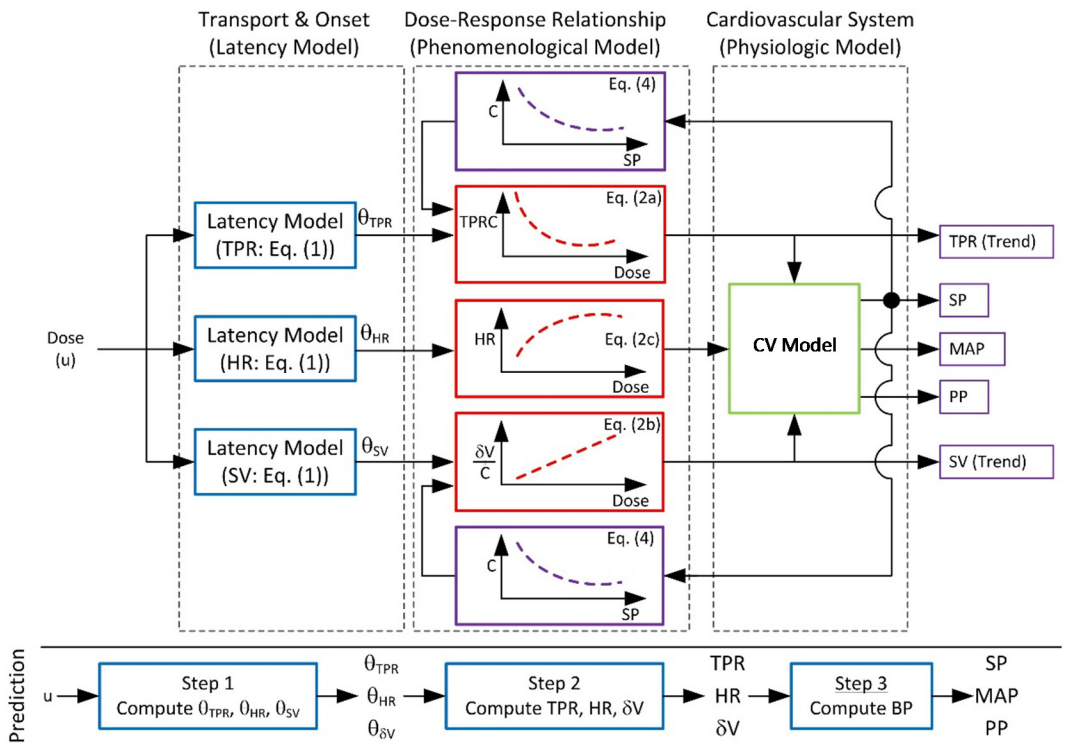

Figure 5-6: Hybrid LDC model.

infusion rates.

5.5.1. Hybrid Latency-Dose-Response-Cardiovascular Model Development

The LDC model is an extended version of the preliminary model (5-1) (Figure 5-6). As before, a CV model relates cardinal parameters (SV, TPR and HR) to BP. However, to account for dynamic transients and widely changing physiological state, the preliminary model (which could analyze only the steady-state dose-response) was strengthened by incorporating (i) the dynamics associated with the transport of agents and their onset of physiological effects, and (ii) the improved phenomenological dose-response models through pressure-dependent AC and the interaction among multiple receptor effects.

Lumped Latency Model: The lumped latency model we employed in the LDC model is distinct from classical pharmacological models in that it does not explicitly involve blood concentration of the agent. In the classical pharmacological models, multi-compartmental models are used to relate the infusion dose of an agent to its blood concentration by describing the mixing and elimination of the agent in the blood in response to its infusion dose (Hill, 2004). The blood concentration is then mapped to the concentration at the site of action via a first-order system (e.g., (Burnette, 1992)) often accompanied by a time delay (e.g., (Toutain and Bousquet-Mélou, 2004)). In contrast, the lumped latency model employed in the LDC model relates the actual infusion dose directly to the hypothetical "steady-state-equivalent" infusion dose acting at the site of action (i.e., the "steady-state-equivalent" infusion dose is the steady-state dose that would yield the physiological effects that are observed at a given time t). The lumped latency model incorporates simple first-order dynamics and a time delay.

This lumped latency model is based on a low-order model that was developed in a previous study, which was shown to be a promising approach to individualized dose-response modeling (Hahn et al., 2012). The model describes the dynamics associated with the transport of an agent and its elicitation of clinical effect as a lumped 1-compartment model with delay:

$$\tau_X \dot{\theta}_X(t) + \theta_X(t) = u\left(t - t_{D,X}\right), \tag{5-3}$$

where $\theta_X \in \{\theta_{TPR}, \theta_{\delta V}, \theta_{HR}\}$ are the hypothetical steady-state equivalent doses associated with vasoactive (TPR), inotropic (SV) and chronotropic (HR) effects, respectively, while τ_X and $t_{D,X}$ are the process time constant and the transport delay dictating the dynamics associated with the transport of the agent and physiological

onset latency, and u denotes the actual intravenous vasopressor-inotrope dose.

Dose-Response Relationship: To predict hemodynamic responses from the hypothetical steady-state equivalent vasopressor-inotrope infusion doses necessitates dose-response models. Vasopressor-inotropes alter BP by stimulating the CV adrenergic receptors (Ellender and Skinner, 2008; Fedida and Bouchard, 1992; Nagashima et al., 1996; Rudis et al., 1996) and ultimately modulating the CV parameters of TPR, SV and HR. In this study, we modeled the dose-response relationship of epinephrine. However, the computational methodology could be modified (using alternative dose-response models) for different agents.

The dose-response model employed in the LDC model includes all the known clinical effects elicited by epinephrine: vasoactive (TPR), inotropic (SV) and chronotropic (HR) effects (see (5-4)). Its effect on MAP is dependent on the administered infusion dose (Ellender and Skinner, 2008; Noori and Seri, 2012; Rudis et al., 1996). Specifically, TPR response (R) consists of a baseline term (R_0), a vasodilation term (ΔR_1) elicited in the low dose, i.e., predominant beta-agonist, range and a vasoconstriction term (ΔR_2) elicited in the high dose, i.e. predominant alpha-agonist, range:

$$R = R_0 + \Delta R_1(\theta_R) + \Delta R_2(\theta_R) = \underbrace{\frac{1}{k_{1,R}\theta_R + 1/R_0}}_{R_0 + \Delta R_1(\theta_R)} + \underbrace{(k_{2,R}\theta_R + k_{3,R})^{k_{4,R}} \cdot \frac{{\theta_R}^{k_{5,R}}}{\left({\theta_R}^{k_{5,R}} + k_{6,R}\right)}}_{\Delta R_2(\theta_R)}, \quad (5\text{-}4a)$$

where $k_{i,R}$ ($i = 1, \cdots, 6$) are unknowns to be determined from dose-response data.

Also, SV response consists of a baseline term (δV_0), a term representing the increase in SV due to inotropy and enhanced preload ($\Delta\delta V_1$) and a term representing the decrease in SV due to afterload ($\Delta\delta V_2$):

$$\delta V = \delta V_0 + \Delta\delta V_1(\theta_{\delta V}) + \Delta\delta V_2(\theta_{\delta V}) = \delta V_0 + \underbrace{\log\left(k_{1,\delta V}\theta_{\delta V} + 1\right)}_{\Delta\delta V_1} + \underbrace{\left\{-(k_{2,\delta V}\theta_{\delta V} + k_{3,\delta V})^{k_{4,\delta V}} \frac{{\theta_{\delta V}}^{k_{5,\delta V}}}{\left({\theta_{\delta V}}^{k_{5,\delta V}} + k_{6,\delta V}\right)}\right\}}_{\Delta\delta V_2}, \quad \text{(5-4b)}$$

where δV_0 is the baseline values, while $k_{i,\delta V}$ $(i = 1, \cdots, 6)$ are unknowns to be determined from dose-response data. Note that in (5-4a) and (5-4b), the Hill equation models (or the E_{max} models; see, e.g., (Dayneka et al., 1993)) were included to reproduce the recognition that vasoconstriction (ΔR_2) and afterload ($\Delta\delta V_2$) effects are activated only at high dose region. According to the Hill equation model, $\sqrt[k_{5,R}]{k_{6,R}}$ and $\sqrt[k_{5,\delta V}]{k_{6,\delta V}}$ are epinephrine infusion doses corresponding to 50% clinical effects.

Finally, HR response consists of a baseline term (HR_0) and a chronotropic term (ΔHR_1):

$$HR = HR_0 + \Delta HR_1(\theta_{HR}) = HR_0 + k_{1,HR}\frac{{\theta_{HR}}^{k_{2,HR}}}{\left({\theta_{HR}}^{k_{2,HR}} + k_{3,HR}\right)}, \quad \text{(5-4c)}$$

where HR_0 is the baseline value, while $k_{i,HR}$ $(i = 1, \cdots, 3)$ are unknowns to be determined from dose-response data.

The baseline values (R_0, δV_0, HR_0) in the dose-response relationships above are regarded as known quantities, because they can be deduced from the baseline

physiological state and thus can be expressed via baseline BP and HR measurements and the remaining parameters in (5-4) (see Section 5.7 for details).

Physiological CV Model: Once the responses of CV parameters (TPR, SV and HR) are determined from the phenomenological dose-response models (5-4), a CV model is used to compute the resulting BP response including SBP, MAP and PP. For more details, see next chapter. C is AC modeled as a function of SBP:

$$C = \frac{1}{k_1 P_S + k_2}, \tag{5-5}$$

To examine the validity of the LDC model, we conducted a secondary analysis of existing data collected from piglet subjects (Nachar et al., 2011). The data were collected from five neonatal Yorkshire Duroc piglets (age 10+/-3 d and weight 2.4+/-0.6 kg). For each piglet, after a baseline period, an escalating dose of epinephrine was administered, which ranged from low (0.25 mcg/kg/min), medium (0.5 and 0.75 mcg/kg/min) and high doses (1, 1.5 and 2 mcg/kg/min). Each dose was maintained for 15min before new dose was applied. BP and HR responses were collected in real time at a sampling rate of 0.2 Hz. The full details of the experimental protocol can be found in Nachar et al. (Nachar et al., 2011). Before analyzing the data, we manually identified the artifacts in the measurement that manifested as isolated large, sudden increases in BP (> 30 mmHg). In addition, we visually examined the data together with the event logs to identify the data associated with blood draws and seizure activity. In sum, the data corresponding to the artifacts amounted to only 1.6 % of the data, and they were not included in the subsequent analysis.

5.5.2. Model Identification of Dynamic Transient Data

The LDC model was adapted to data corresponding to an individual subject as follows. First, cardinal parameters $\mathrm{TPR}\cdot\mathrm{C}$ and $\frac{\delta V}{C}$ were computed from MAP and SBP data using a CV model presented in next chapter. Second, the unknown parameters in the lumped latency models (5-3), the dose-response models (5-4) and the AC model (5-5) were determined by minimizing the discrepancy between $\mathrm{TPR}\cdot\mathrm{C}$ and $\frac{\delta V}{C}$ predicted by the models versus those directly computed from MAP and SBP data. Specifically, the models of $\mathrm{TPR}\cdot\mathrm{C}$ and $\frac{\delta V}{C}$ were implemented by combining (5-4a), (5-4b) and (5-5):

$$R\cdot C=\left[\frac{1}{k_{1,R}\theta_R+1/R_0}+(k_{2,R}\theta_R+k_{3,R})^{k_{4,R}}\cdot\frac{{\theta_R}^{k_{5,R}}}{\left({\theta_R}^{k_{5,R}}+k_{6,R}\right)}\right]\cdot\frac{1}{(k_1P_s+k_2)}, \tag{5-6a}$$

$$\frac{\delta V}{C}=\left[\delta V_0+\log\left(k_{1,\delta V}\theta_{\delta V}+1\right)-(k_{2,\delta V}\theta_{\delta V}+k_{3,\delta V})^{k_{4,\delta V}}\frac{{\theta_{\delta V}}^{k_{5,\delta V}}}{\left({\theta_{\delta V}}^{k_{5,\delta V}}+k_{6,\delta V}\right)}\right]\cdot(k_1P_s+k_2), \tag{5-6b}$$

Then, the dose-response models (5-6) and (5-4c) together with the lumped latency models (5-3) were fitted to $R\cdot C$ and $\frac{\delta V}{C}$ computed from BP via the CV model and the measured HR through the optimization problem (5-7):

$$K^*=\arg\min_K J(u,P_s,P_m,HR,K), \tag{5-7}$$

where $K\triangleq\{\tau_X,t_{D,X},k_{i,\delta V},k_{i,R},k_{j,HR},k_l\}$ is the set of unknown parameters, K^* is the optimal value of K as the solution to (5-7), $i=1,\cdots,6$, $j=1,\cdots,3$, $l=1,2$, $J=J_R+J_{\delta V}+J_{HR}$, and

$$J_R(u, P_s, K) = w_R \left\| R \cdot C - \left[\frac{1}{k_{1,R}\theta_R + 1/R_0} + (k_{2,R}\theta_R + k_{3,R})^{k_{4,R}} \cdot \frac{{\theta_R}^{k_{5,R}}}{\left({\theta_R}^{k_{5,R}} + k_{6,R}\right)} \right] \cdot \frac{1}{(k_1 P_s + k_2)} \right\|, \tag{5-8a}$$

$$J_{\delta V}(u, P_s, K) = w_{\delta V} \left\| \frac{\delta V}{C} - \left[\delta V_0 + \log\left(k_{1,\delta V}\theta_{\delta V} + 1\right) - (k_{2,\delta V}\theta_{\delta V} + k_{3,\delta V})^{k_{4,\delta V}} \frac{{\theta_{\delta V}}^{k_{5,\delta V}}}{\left({\theta_{\delta V}}^{k_{5,\delta V}} + k_{6,\delta V}\right)} \right] \cdot (k_1 P_s + k_2) \right\|, \tag{5-8b}$$

$$J_{HR}(u, K) = w_{HR} \left\| HR - HR_0 - k_{1,HR} \frac{{\theta_{HR}}^{k_{2,HR}}}{\left({\theta_{HR}}^{k_{2,HR}} + k_{3,HR}\right)} \right\|, \tag{5-8c}$$

The optimization (5-7) was solved using the DE algorithm (Storn and Price, 1997). The weights w_R, $w_{\delta V}$ and w_{HR} were chosen so that the magnitudes of J_R, $J_{\delta V}$ and J_{HR} would be comparable. In solving (5-7), HR_0 was set to the baseline HR measurement (i.e., at $u = 0$), while R_0 and δV_0 were expressed via K by (i) first deriving the baseline values of $R \cdot C$ and $\frac{\delta V}{C}$ from the baseline measurements of SBP, MAP and HR using the CV model, and then (ii) expressing R_0 and δV_0 by K and the baseline values of $R \cdot C$ and $\frac{\delta V}{C}$ using (5-6). Further, constraints were imposed on a subset of the parameters in K for physiological relevance: (i) all the parameters were constrained to assume positive values; (ii) $0 < k_{4,R}, k_{4,\delta V} < 1$ was assumed to prevent the unboundedness of vasoconstriction effects in TPR (ΔR_2) and SV ($\Delta \delta V_2$) at high epinephrine doses. Then, (5-7) was solved by employing multiple initial conditions (in terms of the population size and mutation characteristics in the DE algorithm) to derive a number of candidate solutions, and the one with the minimum J value was chosen as the optimal solution, K^*. The data corresponding to artifacts were not used in solving (5-7).

Once adapted to a subject, the model was validated by applying it to predict the subject's hemodynamic responses solely based on the epinephrine infusion dose as follows. First, the lumped latency model (5-3) predicted the hypothetical steady-state equivalent vasopressor-inotrope infusion doses θ_X responsible for the onset of changes in TPR, SV and HR (Step 1 in Figure 5-6). Second, the phenomenological dose-response models (5-4) predicted the CV cardinal parameters (TPR, SV) and HR using the steady-state equivalent doses computed by the lumped latency models, while AC was computed by (5-5) (Step 2 in Figure 5-6). Third, the CV model (see next chapter) predicted the resulting BP responses based on the CV parameter responses (Step 3 in Figure 5-6).

Once individual-specific model parameters were obtained for all the subjects, the impact of inter-subject variability in lumped latency models and in dose-response

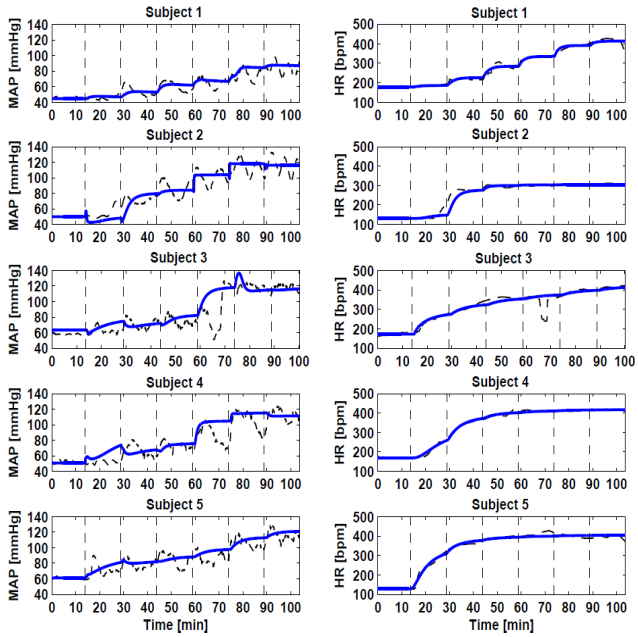

Figure 5-7: Measured and model-predicted MAP and HR in all piglets. Black dashed: measured; blue solid: model-predicted using fully-individualized LDC model (IL-ID). Each instant at which the epinephrine dose was increased is shown by a vertical dashed line.

models on the predictive efficacy of the LDC model was examined as follows. First, we predicted hemodynamics responses using (i) fully individualized LDC models (Individualized Latency and Individualized Dose-Reponse (IL-ID)), (ii) LDC model with average latency parameters ("Population-Based Latency and Individualized Dose-Response (PL-ID)), and (iii) LDC model with average dose-response model for TPR, SV and HR (IL-PD_X, $X \in \{R, \delta V, HR\}$). Then, we computed the r^2 values between measured versus model-predicted CV parameter and BP responses. Finally, we examined these r^2 values to assess the benefit of individualizing the parameters in the LDC model (see Table 14).

5.5.3. Generalizable Lessons

Table 13 summarizes the physiological data obtained in the piglets, including SBP, MAP, DBP and HR (which were directly measured) as well as $R \cdot C$ and $\frac{\delta V}{C}$ (which were computed from the CV model (see next chapter)). Figure 5-7 shows measured and model-predicted MAP and HR responses in all piglets[1], in which the RMSEs in MAP prediction associated with the IL-ID, PL-ID and IL-PD_{HR} models were 9.1+/-2.1 mmHg, 10.6+/-3.2 mmHg and 17.0+/-5.7 mmHg, respectively, while the RMSEs in HR prediction associated with the same models were 10.4+/-3.6 bpm, 21.3+/-9.9 bpm and 63.6+/-26.1 bpm, respectively (mean+/-SD). In addition, the limits of agreement between measured versus predicted MAP and HR were -19.9 mmHg to 15.2 mmHg and -19.3 bpm to 23.0 bpm (IL-ID), -24.1 mmHg to 16.3 mmHg and -50.0 bpm to 37.6 bpm (PL-ID) and -32.0 mmHg to 37.1 mmHg and -93.8 bpm to 149 bpm (IL-PD_{HR}),

[1] It is noted that the jumps in BP and HR responses in Subject 3 at ~65min is a measurement artifact.

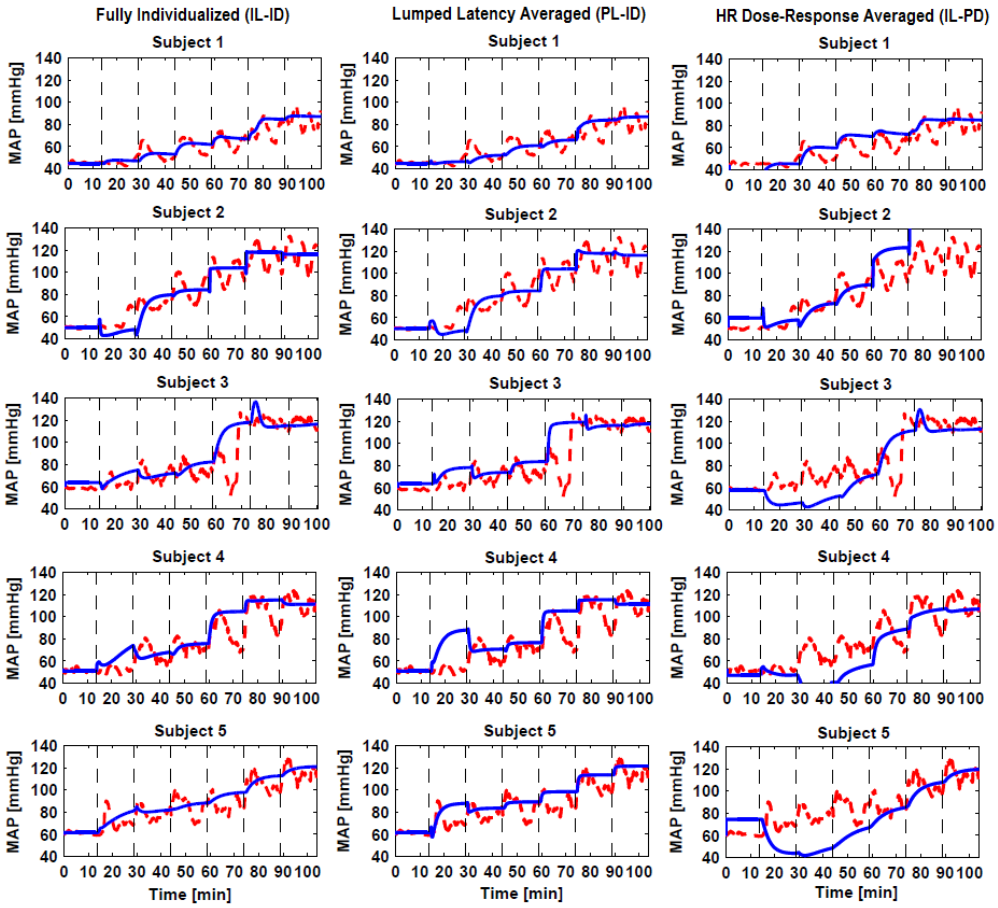

Figure 5-8: Measured and model-predicted MAP in all piglet subjects based on IL-ID, PL-ID and IL-PD LDC models. Red dashed: measured; blue solid: model-predicted.

respectively. Table 14 shows the r^2 values between measured MAP and HR responses versus those predicted by the IL-ID, PL-ID and IL-PD_X LDC models, and Figure 5-8 shows measured and model-predicted MAP responses for these models. Table 15 summarizes the distributions of the parameters in the LDC model.

One primary finding of this investigation was that the LDC model offered a reasonable prediction of the relationship between epinephrine dosage versus CV parameters including MAP and HR. The LDC model exhibited the anticipated phenomena such as a biphasic TPR response, monotonic chronotropic effect, and the effect of afterload in the high infusion dose region.

This encouraging performance is notable for two reasons. First, the LDC models predicted each subject's CV trends despite substantial individual variability. Consider that Subject #2 had a HR ranging between 252+/-72.6 bpm (mean+/-SD) while Subject #5 had a HR ranging between 334+/-100 bpm (see Table 13); the distributions of their HR values were quite distinct. Despite such variability, HR prediction was quite accurate using the LDC models with r^2 values > 0.90 for every subject. The prediction of dynamic HR response to changing epinephrine dosage was also promising; compare the actual HR versus predicted HR for Subjects #1-#5 in Figure 5-7 (second column) where it is evident that the latency model captured the dynamics of the system properly.

On the other hand, Figure 5-8 also reveals the limitation of these approaches. During the escalating doses of epinephrine infusions, measured MAP was a fundamentally oscillatory signal without a "true" steady-state. Importantly, such oscillations were not present in the pre-epinephrine (baseline) period, and the cause of this oscillatory response is unclear (Nachar et al., 2011). During each interval of constant epinephrine infusion, there were 1-2 cycles of MAP oscillation that could not be modeled by the LDC model. Further, when the epinephrine dose was changed, the

Table 13: Physiological conditions spanned by the piglets (mean+/-SD)

Subject ID	SBP [mmHg]	MAP [mmHg]	DBP [mmHg]	HR [bpm]	R·C [min]	δV/C [mmHg]
1	92.2+/-18.6	61.1+/-14.4	44.5+/-11.1	283+/-88.7	4.2e-3+/-1e-3	54.3+/-8.50
2	105+/-28.1	84.6+/-26.0	70.8+/-24.1	252+/-72.6	9.2e-3+/-2e-3	38.4+/-8.07
3	103+/-28.6	83.9+/-25.0	68.7+/-22.7	316+/-81.3	7.8e-3+/-2e-3	36.3+/-9.58
4	97.6+/-23.9	78.0+/-23.3	62.1+/-21.7	336+/-97.1	6.8e-3+/-2e-3	36.1+/-7.85
5	109+/-21.5	86.2+/-18.8	69.1+/-16.7	334+/-100	6.8e-3+/-2e-3	42.6+/-8.60
All Subjects	102+/-25.1	78.7+/-23.8	63.1+/-22.3	295+/-105	7.0e-3+/-2e-3	41.5+/-10.9

Table 14: r^2 values between measured and model-predicted MAP and HR. IL-ID: LDC model with individualized latency and dose-response parameters; PL-ID: LDC model with average latency parameters; IL-PD_X: LDC model with average dose-response model on X ($X \in \{\mathbf{R}, \boldsymbol{\delta V}, \mathbf{HR}\}$)

Subject ID			1	2	3	4	5
MAP	IL-ID		0.80	0.86	0.84	0.73	0.79
	PL-ID		0.75	0.85	0.79	0.57	0.72
	IL-PD	IL-PD_{HR}	0.64	0.20	0.63	0.45	<0
		IL-PD_R	<0	<0	0.12	0.46	0.05
		IL-$PD_{\delta V}$	<0	<0	<0	<0	<0
HR	IL-ID		0.99	0.95	0.98	1.00	0.99
	PL-ID		0.98	0.95	0.97	0.91	0.93
	IL-PD	IL-PD_{HR}	0.92	0.42	0.41	0.28	0.17
		IL-PD_R	0.99	0.95	0.98	1.00	0.99
		IL-$PD_{\delta V}$	0.99	0.95	0.98	1.00	0.99

dynamic response in the measured MAP was masked by these oscillations. Overall, our analysis suggests that the benefit of an individualized latency model (IL-ID) seems modest, and to avoid the over-fitting of MAP response corrupted by un-modeled oscillations, it may be appropriate to use group-averaged terms for latency reflective of typical mixing times and physiological onset delays.

While our findings don't entirely support the usefulness of the individualized latency model (which is in part due to epinephrine-specific oscillations), the findings strongly support the need for individualized dose-response models. When one examines the inter-subject inconsistencies in physiological response as a function of epinephrine dose (see Table 13), it is obvious that substantial individualization would be necessary to predict each subject's dose-response. Table 15 demonstrates that there was considerable variability between the model parameters fitted to different subjects. This trend was consistent for the parameters in the AC model (5-5): $k_1 = 1.3 \times 10^{-2}$

Table 15: Distribution of model parameters (mean+/-SD, SD in % of mean) for the IL-ID model

X	Latency Parameters		Dose-Response Parameters						
	τ_X	$t_{D,X}$ [sec]	X_0	k_{1X}	k_{2X}	k_{3X}	k_{4X}	k_{5X}	k_{6X}
δV	329±52%	29.1±90%	33.4±21%	2.3e3±109%	0.64±250%	4.3e3±205%	0.49±57%	25.1±127%	14.3±245%
R	264±70%	48.6±36%	76.4±74%	96.8±35%	7.7e-4±143%	4.0e-3±78%	0.96±7.0%	31.1±116%	14.7±237%
HR	511±52%	25.1±99%	155.±16%	239.±23%	4.05±91%	0.18±150%	-	-	-

with 17% SD and $k_2 = 7.8 \times 10^{-2}$ with 227% SD, respectively. Moreover, when HR dose-response parameters were group-averaged (see Figure 5-8), the MAP prediction efficacy unacceptably deteriorated. Prediction efficacy was even worse when TPR and SV dose-response parameters were averaged (Table 15). In particular, the group-averaged SV dose-response model predicted a non-physiological (i.e., negative) SV in the high epinephrine dose region due to the exaggerated afterload effect, resulting in an unacceptable MAP response for all the subjects with r^2 values lower than zero. Altogether, these findings indicate that the dose-response models must be individualized: it is evident that different subjects had different quantitative responses to epinephrine (Table 13) and that the LDC model, when using population-averaged parameter values, yielded non-physiological predictions (Table 15).

In sum, these findings lead us to a generalizable lesson regarding the tradeoff between model complexity and individualization capability. Complex subject-specific models can offer adequate individualization capability, but its large degrees of freedom may result in non-physiological and even unstable responses unless properly fitted to each individual. Simple group-averaged models can provide physiologically acceptable responses, but they cannot be as accurate as complex subject-specific models. Therefore, appropriate balance between individualized and group-averaged

components is essential to achieve stable and accurate prediction of physiological responses to medication agents.

There is a remaining question, which although outside the scope of the current investigation, is important to consider for future work: is the LDC model suitable for predicting hemodynamic responses to epinephrine? Due to the presence of BP oscillations associated with epinephrine administration, the LDC model could not perfectly predict BP response to epinephrine. However, it is unknown how the LDC model would have performed in the absence of these oscillations. Future work on data not resulting in an oscillatory BP (such as dopamine and dobutamine (Nachar et al., 2011)) will be able to answer this question. Regardless, we can conceptually contemplate if this model is too simple, too complex, or generally appropriate for practical use.

We do not think the model is too simple: it includes terms to quantify most of the known effects of epinephrine, including a biphasic TPR response, pressure-dependent AC, monotonic chronotropic effect, and the effect of afterload in the high infusion dose region. We have found that a simpler version of this model (see Section 5.2) and the current iteration (e.g., Figure 5-6) can yield favorable predictive capability (though, as noted above, the current model could not capture the oscillations in MAP specific to epinephrine, leading to the one shortcoming in MAP prediction).

More likely, the current model may be too complicated to serve as a practical tool for dose selection. The usefulness of the model will further be exacerbated if additional mechanisms to model the oscillatory MAP behavior (such as autonomic reflex mechanism) are being taken into account. In theory, even highly complicated

models can be determined as long as persistently exciting dose-response data (e.g., having many dose changes) are available (Ljung, 1999). However, multiple changes in infusion dose may not be commonly available in real clinical setting when epinephrine-dosing changes are made to treat the patient rather than to facilitate dose-response modeling. In the future, therefore, it will be appropriate to reduce model complexity allowing for individual predictive capability without extensive training data from each subject.

Finally, the validity of the LDC model in vasopressor-inotropes other than epinephrine must be examined in the future. Since vasopressor-inotropes commonly exhibit latency, dose-response and physiological (CV) mechanisms, the methodological framework presented in this study should be universally applicable to a range of vasopressor-inotropes. However, due to the differences in the specific mechanisms of action associated with each vasopressor-inotrope, dose-response models specific to each vasopressor-inotrope must be derived and validated independently. In this regard, future effort on dose-response modeling of a wide spectrum of vasopressor-inotropes will be necessary to facilitate the real-world application of the LDC model.

6. Modeling of Cardiovascular Endpoint Responses to Vasopressor Infusion

Section 6.1 presents a method relating the changes in CV measurable endpoints to changes in cardinal parameters in response to vasopressor infusion. This method was utilized in Chapter 5 to infer cardinal CV parameters from measured hemodynamic responses, e.g., BP and HR, and also estimate BP via predicted cardinal parameters in response to different doses of vasopressor. In Section 6.2 it is shown that this method may not adequately work for fluid infusion.

6.1. Estimation of Cardinal Parameters

Clinicians typically titrate the BV and vasopressor dose level based on BP, even though changes in BP actually reflect changes in CO and TPR, the underlying cardinal parameters. The methodology defined in Chapter 5 was based on estimating a dose-response relationship for the underlying cardinal parameters. If CO and TPR are not directly measured, then the effects of the vasopressor agent on the cardinal parameters must be inferred. Here, we develop a specific algorithm based on Windkessel model that uses measurements of SBP, MAP, DBP, and HR to infer cardinal parameters related to CO and TPR.

Approximating the aortic flow as a train of impulses (Parlikar et al., 2007), the Windkessel model equipped with a resistor and a capacitor, each representing TPR and AC, is mathematically expressed as follows:

$$\frac{dP(t)}{dt} = -\frac{1}{R.C}P(t) + \frac{1}{C}\delta V \cdot \delta(t), \tag{6-1}$$

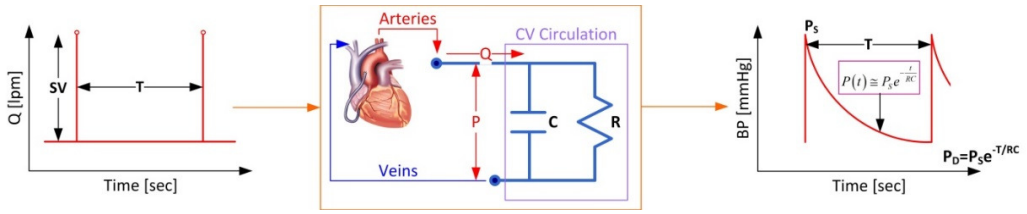

Figure 6-1: A two-parameter Windkessel model subject to aortic flow approximated as a train of impulses.

where $0 \leq t \leq T$, $P(t)$ is BP, R, C and δV represent TPR, AC and SV, respectively, $\delta(t)$ is the Dirac delta function, and T is the heart period. To use SVI, (which is available from the dataset used in previous chapter, Section 5.2) rather than SV in the CV model, (6-1) is re-written as follows:

$$\frac{dP(t)}{dt} = -\frac{1}{\bar{R}.\bar{C}}P(t) + \frac{1}{\bar{C}}\delta\bar{V} \cdot \delta(t), \tag{6-2}$$

where $\delta\bar{V}$ is SVI, and $\bar{R}$ (in mmHg·min·m^2/l) and $\bar{C}$ (in ml/mmHg/m^2) are TPRI, MAP divided by SVI and HR) and AC, respectively. Solving (6-2) for BP using the convolution integral (Chen, 1984) yields:

$$P(t) = P_d e^{-\frac{t}{\bar{R}.\bar{C}}} + \int_{\tau=0}^{t} e^{-\frac{1}{\bar{R}.\bar{C}}(t-\tau)} \frac{1}{\bar{C}}\delta\bar{V} \cdot \delta(\tau)d\tau = P_d e^{-\frac{t}{\bar{R}.\bar{C}}} + \frac{\delta\bar{V}}{\bar{C}} e^{-\frac{t}{\bar{R}.\bar{C}}}, \tag{6-3}$$

which is valid for each heart period (see Figure 6-1). From (6-3), the following relationships between BP versus TPRI and SVI (scaled by ACI) are obtained:

$$P_m = \bar{R} \cdot HR \cdot \delta\bar{V} = \bar{R}.\bar{C} \cdot HR \cdot \frac{\delta\bar{V}}{\bar{C}}, \tag{6-4a}$$

$$P_s = \left(1 - e^{-\frac{T}{\bar{R}.\bar{C}}}\right)^{-1} \frac{\delta\bar{V}}{\bar{C}}, \tag{6-4b}$$

$$P_P = P_s - P_d = \frac{\delta\bar{V}}{\bar{C}}, \tag{6-4c}$$

where P_s, P_m and P_d are SBP, MAP and DBP, respectively, and P_P is PP. Given measurements of SBP, MAP and PP as well as HR for a given vasopressor dose level, the corresponding values of $\bar{R}.\bar{C}$ and $\frac{\delta\bar{V}}{\bar{C}}$ can be determined by solving (6-4). For this purpose, the following multi-objective optimization problem is formulated based on the relationship between BP versus $\bar{R}.\bar{C}$ and $\frac{\delta\bar{V}}{\bar{C}}$:

$$\left\{\bar{R}.\bar{C}^*, \frac{\delta\bar{V}^*}{\bar{C}}\right\} = \arg\min J\left(\bar{R}.\bar{C}, \frac{\delta\bar{V}}{\bar{C}}\right) = \arg\min\left\{\left\|\begin{bmatrix} F_1\left(\bar{R}.\bar{C}, \frac{\delta\bar{V}}{\bar{C}}\right) \\ F_2\left(\bar{R}.\bar{C}, \frac{\delta\bar{V}}{\bar{C}}\right) \\ F_3\left(\frac{\delta\bar{V}}{\bar{C}}\right) \end{bmatrix}\right\|_\infty\right\}, \tag{6-5}$$

where $\bar{R}\bar{C}^*$ and $\frac{\delta\bar{V}^*}{\bar{C}}$ are the optimal scaled TPRI and SVI associated with a particular dose response, and F_i, $i = 1,2,3$ are specified as follows:

$$F_1\left(\bar{R}.\bar{C}, \frac{\delta\bar{V}}{\bar{C}}\right) = \left[P_m - \bar{R}.\bar{C} \cdot HR \cdot \frac{\delta\bar{V}}{\bar{C}}\right]/P_m, \tag{6-6a}$$

$$F_2\left(\bar{R}.\bar{C}, \frac{\delta\bar{V}}{\bar{C}}\right) = \left[P_s - \left(1 - e^{-\frac{T}{\bar{R}.\bar{C}}}\right)^{-1} \frac{\delta\bar{V}}{\bar{C}}\right]/P_s, \tag{6-6b}$$

$$F_3\left(\frac{\delta\bar{V}}{\bar{C}}\right) = \left[P_P - \frac{\delta\bar{V}}{\bar{C}}\right]/P_P. \tag{6-6c}$$

which are derived from (6-4). Thus, we obtain $\left\{\bar{R}.\bar{C}^*, \frac{\delta\bar{V}^*}{\bar{C}}\right\}_i$ from $\{d, HR, P_s, P_m, P_d\}_i$, $i = 1, \cdots N$, where $\{\cdot\}_i$ denotes dose (d) and CV responses (HR and BP as well as scaled TPRI and SVI) corresponding to the i-th dose, while N is the number of dose levels at which BP measurements are taken to train the model.

Analyzing a dataset with non-continuous measurements of SBP, MAP, DBP, and HR in response to vasopressor infusion (see chapter 5, Section 5.2), a rudimentary

model, i.e. the Windkessel, was deemed reasonable; it provided a means to infer the underlying CV state in terms of the cardinal CV parameters related to CO and TPR. A model of additional complexity would have been fruitless without additional measurement data available for identification of more sophisticated model. For other datasets with more profound and richer data (such as BP and flow waveforms), more advanced models and methods to infer CV state could be appropriate. For instance, given a BP waveform, the current Windkessel model could be replaced by the long-time interval analysis (Mukkamala et al., 2006) or the improved Windkessel-model-based method (Fazeli and Hahn, 2012) to better estimate TPR and SV. For patients with a Swann-Ganz catheter, direct CO and TPR measurements could be used.

In addition, the model was able to yield reasonable predictions of the dose-response relationship of the cardinal CV parameters (i.e., related to CO and TPR) as well as BP and HR (see Sections 5.2 and 5.5). This provides the proof-of-principle for the general approach of this chapter. Is this specific approach generalizable to other populations and physiological states? This is an open question and will be answered in the next sections of this chapter.

6.2. Pulse Pressure Underestimates Stroke Volume

The CV model presented in Section 6.1 was based on the assumption that SV and PP are linearly proportional; see (6-4c) and also (Bataille et al., 2012; Ishihara et al., 2004; Mathews and Singh, 2008; Papaioannou et al., 2012). In fact, there are many existing evidences supporting this assumption (Fazeli and Hahn, 2012; Marquez et al., 2008; Parlikar et al., 2007). Due to this reason, PP has been widely used as a convenient

surrogate of SV during diagnostic and therapeutic procedures, such as fluid therapy (Convertino et al., 2006), ventricular resynchronization therapy (Kass, 2002) and vasopressor/inotrope therapy (Bighamian et al., 2014a). However, some recent experimental investigations suggest that although SV and PP are proportionally correlated during BV perturbation, the relationship may not be strictly linear, and PP may underestimate SV in response to BV changes (Convertino et al., 2006; Monnet et al., 2011; Reisner et al., 2011). Since the mechanisms underlying the relation between the two have not been clearly understood, in this section we elucidate how arterial PP and SV respond to a perturbation in the LV BV based on a systematic mathematical analysis. Our mathematical analysis showed that the relative change in arterial PP due to a LV BV perturbation was consistently smaller than the corresponding relative change in SV, due to the nonlinear LV pressure-volume (P-V) relation during diastole that reduces the sensitivity of arterial PP to perturbations in the LV BV. Therefore, arterial PP must be used with care when used as surrogate of SV in guiding fluid therapy. P-V loop framework employed as the basis of the mathematical analysis is presented in the next section.

6.2.1. Left-Ventricular Pressure-Volume Framework

We use the LV P-V loop framework (Sagawa et al., 1988) to mathematically analyze how changes in SV and PP are related during volume perturbation. In the context of LV P-V loop, the so-called “maximum” LV pressure (Hay et al., 2005; Sagawa et al., 1988; Santamore and Burkhoff, 1991) is given by the weighted average of end-systolic pressure (ESP) and EDP:

$$P_{LV}^{max} = \phi(t)P_S\big(V(t)\big) + \big(1 - \phi(t)\big)P_D\big(V(t)\big) \tag{6-7}$$

where $\phi(t)$ is the activation function (Piene, 1984; Sagawa et al., 1988; Santamore and Burkhoff, 1991), and P_S and P_D are the pressures corresponding to end-systolic and end-diastolic P-V relationships at a LV volume $V(t)$ (Sagawa et al., 1988; Santamore and Burkhoff, 1991). P_S and P_D are given by (see red and blue dashed lines in Figure 6-2):

$$\begin{aligned} P_S\big(V(t)\big) &= E_S(V(t) - V_0) \\ P_D\big(V(t)\big) &= B\big[e^{A(V(t)-V_0)} - 1\big] \end{aligned} \tag{6-8}$$

where E_S is the end-systolic LV elastance, A and B are constants specifying the end-diastolic P-V relationship, and V_0 is the LV volume corresponding to zero LV pressure (Piene, 1984; Sagawa et al., 1988; Santamore and Burkhoff, 1991).

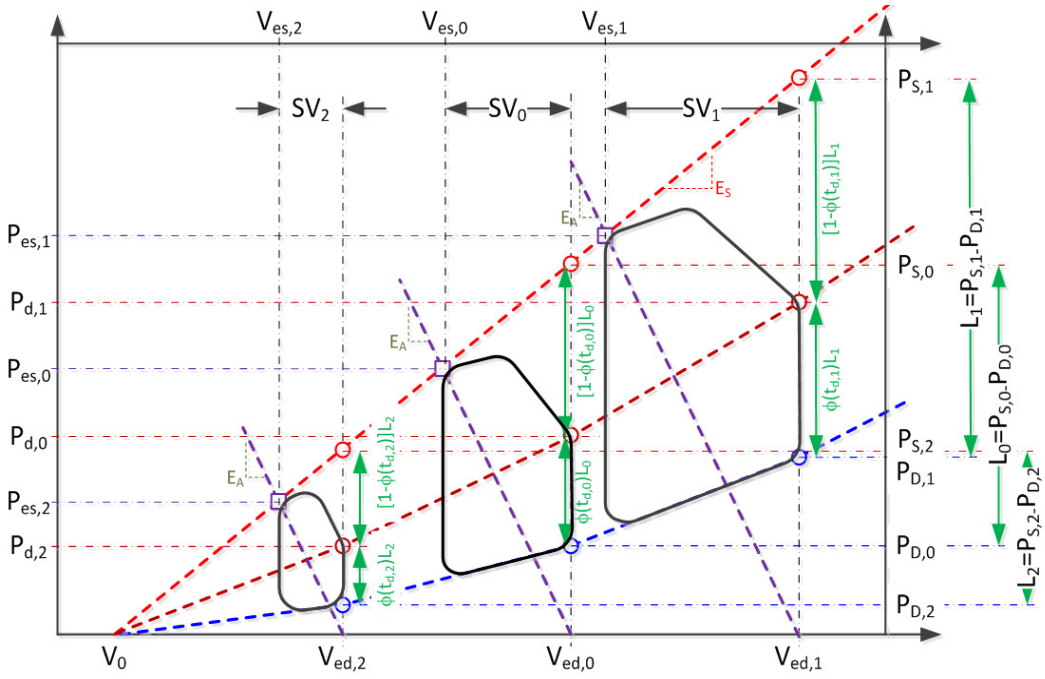

Figure 6-2: Left ventricular pressure-volume loop for different end-diastolic volumes.

6.2.2. Stroke Volume Response to Volume Perturbation

In the context of P-V loop, SV can be computed from EDV as follows. By definition, SV is given by the difference between EDV and ESV:

$$\delta V = V_{ed} - V_{es} = V(t_{ed}) - V(t_{es}) \tag{6-9}$$

where $V_{ed} = V(t_{ed})$ and $V_{es} = V(t_{es})$ are EDV and ESV, and t_{ed} and t_{es} are the time instants corresponding to end-diastole and end-systole, respectively. Alternatively, SV is given from mean MAP as follows:

$$\delta V = \frac{P_m}{R} T \tag{6-10}$$

where P_m is MAP, R is TPR and T is heart period. At end-systole ($t = t_{es}$), the P-V loop intersects with the systolic P-V relationship $P_S = E_S(V(t) - V_0)$ (Sagawa et al., 1988; Santamore and Burkhoff, 1991), where $P_S = P_{es}$ and $V(t) = V(t_{es}) = V_{es}$. Therefore, we have:

$$P_{es} = E_S(V_{es} - V_0) \tag{6-11}$$

On the other hand, since ESP is typically very close in value to MAP (Kass and Beyar, 1991; Maurer et al., 2009), we have, from (6-4):

$$\delta V = V_{ed} - V_{es} \cong \frac{P_{es}}{R} T \tag{6-12}$$

Combining (6-11) and (6-12) yields the following expression for V_{es}:

$$V_{es} = \frac{E_A}{E_S + E_A} V_{ed} + \frac{E_S}{E_S + E_A} V_0 \tag{6-13}$$

where $E_A = \frac{R}{T}$ is called the arterial elastance (Maurer et al., 2009; Sagawa et al., 1988; Santamore and Burkhoff, 1991). Therefore, SV can be computed from EDV as

$$\delta V = V_{ed} - V_{es} = \frac{E_S}{E_S + E_A}(V_{ed} - V_0) \tag{6-14}$$

Thus, SV is related to EDV by the proportionality constant $\frac{E_S}{E_S+E_A}$, which depends on LV and arterial elastances. Therefore, it can be concluded that a change in EDV caused by volume perturbation results in a change in SV whose magnitude is linearly proportional to that of EDV, if LV and arterial elastances remain constant during volume perturbation. In Figure 6-2, this can be illustrated as the linear proportionality between the triangles defined by ($V_{ed,j}$, 0), (V_0, 0) and ($V_{es,j}$, $P_{es,j}$), j=0,1,2: as long as E_S and E_A remain constant, SV ($= V_{ed,j} - V_{es,j} = P_{es,j}\cot^{-1} E_A = \frac{E_S E_A}{E_S+E_A}\left(V_{ed,j} - V_0\right)\cot^{-1} E_A$) is proportional to the EDV ($= V_{ed,j} - V_0$).

6.2.3. Pulse Pressure Response to Volume Perturbation

To understand the PP response to volume perturbation, we first analyze the responses of ESP and DBP to changes in EDV, and then show the response of PP by formulating it to the difference between ESP response and DBP response. The rationale for using ESP and DBP rather than SBP and DBP is because, in contrast to ESP and DBP which always occur at ESV and EDV (see Fig. 24), the value of volume on the P-V loop where SBP occurs is not straightforward to specify. It will be demonstrated that PP can be, at least approximately, obtained from ESP and DBP by assuming that ESP is typically very close in value to MAP.

At diastole ($t = t_d$ where t_d is the time instant corresponding to DBP), the maximum LV pressure is equal to DBP, and LV volume is equal to EDV (V_{ed}). Therefore, (1) reduces to:

$$\begin{aligned} P_d(V_{ed}) &= \phi(t_d)P_S(V_{ed}) + \big(1 - \phi(t_d)\big)P_D(V_{ed}) \\ &= \phi(t_d)E_S(V_{ed} - V_0) + \big(1 - \phi(t_d)\big)B\big[e^{A(V_{ed} - V_0)} - 1\big] \end{aligned} \tag{6-15}$$

For simplicity of analysis, assume that t_d relative to T remains constant during volume perturbation (see Section 6.7 for what happens if this assumption is relaxed). Then, it is obvious from (6-15) that, for a given value of EDV, DBP is determined as the weighted average of ESP and EDP corresponding to that EDV:

$$\begin{aligned} P_d(V_{ed}) &= \sigma P_S(V_{ed}) + (1 - \sigma)P_D(V_{ed}) \\ &= \sigma E_S(V_{ed} - V_0) + (1 - \sigma)B\big[e^{A(V_{ed} - V_0)} - 1\big] \end{aligned} \tag{6-16}$$

where $\sigma = \phi(t_d)$ is constant if t_d relative to T remains constant. Now, if we note that the end-systolic P-V relationship, $E_S(V_{ed} - V_0)$, is linear in V_{ed} whereas the end-diastolic P-V relationship, $B\big[e^{A(V_{ed} - V_0)} - 1\big]$, is exponential in V_{ed}, and also that $P_d(V_{ed})$ is simply the weighted average between the two, it can be concluded that the rate of change in DBP increases as EDV increases (see Figure 6-2). This is illustrated in Figure 6-2 by the brown dashed line connecting $P_{d,j} = P_d\big(V_{ed,j}\big)$, j=0,1,2, whose slope becomes steeper as EDV increases.

The response of ESP to changes in EDV can be obtained by combining (6-11) and (6-13), which yields:

$$P_{es}(V_{ed}) = E_S(V_{es} - V_0) = \frac{E_S E_A}{E_S + E_A}(V_{ed} - V_0) \tag{6-17}$$

Thus, ESP is related to EDV by the proportionality constant $\frac{E_S E_A}{E_S+E_A}$, which depends on LV and arterial elastances. Therefore, it can be concluded that ESP is linearly proportional to EDV if LV and arterial elastances remain constant during volume perturbation.

To relate ESP and DBP to PP, we use a widely accepted relationship between SBP, MAP and DBP: $P_m \cong P_d + \frac{1}{3}(P_s - P_d)$. As for Section 6.2.2, if we assume that ESP is very close to MAP ($P_{es} \approx P_m$), we get the following relationship between PP, ESP and DBP:

$$P_{es} \cong P_d + \frac{1}{3}(P_s - P_d) \rightarrow P_p = P_s - P_d \cong 3(P_{es} - P_d) \tag{6-18}$$

which indicates that PP is linearly proportional to the difference between ESP and DBP. Finally, combining the conclusions drawn from (6-16)-(6-18), we can conclude that the rate of change in PP decreases as EDV increases, because the rate of change in DBP becomes steeper than that in ESP as EDV increases (see Figure 6-2). This can be illustrated in Figure 6-2 as follows: as long as LV and arterial elastances as well as $\phi(t_d)$ remain constant, the rate of change in $P_{es,j} - P_{d,j}$ decreases with an increase in EDV (see the left vertical axis), since the difference between the slopes of red (P_{es}) and brown (P_D) lines decreases as EDV increases.

6.2.4. Relation between Stroke Volume and Pulse Pressure

The analyses performed in Sections 6.2.2 and 6.2.3 indicate that, under the assumption that 1) both LV and arterial elastances as well as t_d relative to T remain constant during volume perturbation, and 2) ESP is close in value to MAP, SV shows

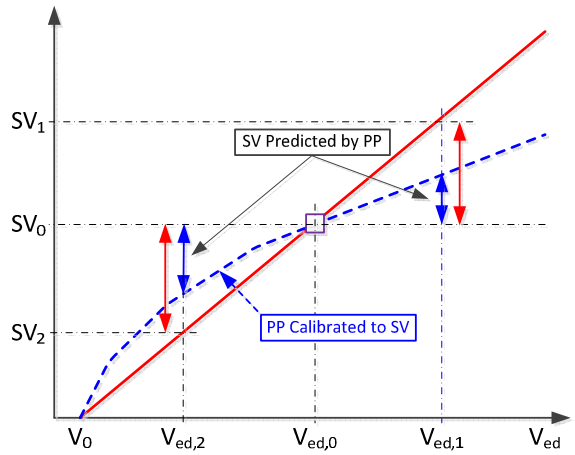

Figure 6-3: Relationship between SV and PP.

constant proportionality to EDV as indicated in (6-14) (i.e., it is a linear function of EDV). In contrast, PP exhibits decreasing proportionality to EDV with an increase in EDV, thereby decreasing the rate of change in PP response to EDV as it increases (in other words, PP shows a gradually decreasing slope when it is plotted against EDV). Since SV and PP exhibit constant versus decreasing slopes against EDV, respectively, the relationship between SV and PP is concave towards SV. Therefore, SV and PP are NOT linearly proportional to each other, and the rate of change in PP is not a good quantitative indicator of the rate of change in SV. In fact, our analyses suggest that the rate of change in PP underestimates the rate of change in SV in the neighborhood of a given operating EDV (see Figure 6-3). Indeed, Figure 6-3 illustrates that, the slope of SV with respect to EDV is steeper than that of PP around the vicinity of an operating EDV.

Relaxation of Assumptions

In our analysis, we made the following assumptions: during changes in EDV due to volume perturbation, (i) the time instant corresponding to DBP relative to the

heart period ($\frac{t_d}{T}$) is constant (A1); (ii) ESP is close in value to MAP (A2); and (iii) LV and arterial elastances remain constant (A3). In this section, these assumptions are relaxed and their effects are incorporated to the conclusion drawn in Section 6.2.4.

Relaxation of Assumption A1

It has been suggested that the shape of the activation function $\phi(t)$ is highly consistent among different individuals, i.e., its inter-individual variability is small (Georgakopoulos et al., 1998; Kjørstad et al., 2002). However, the timing values associated with cardiac events, e.g., diastole ($t = t_d$) may be subject to change due to mechanisms such as baroreflex. This may invalidate the assumption A1 above. Thus, it is worthwhile to examine how the timing-related variability in $\phi(t)$ alters the relationship between SV and PP.

It is obvious from (6-14) that SV is not influenced by $\phi(t)$. In addition, (6-16)-(6-18) indicates that PP is related to $\phi(t)$ only via DBP but not via ESP. So, uncertainty in $\phi(t)$ affects the relationship between SV and PP by altering DBP (which occurs at $t = t_d$). Consequently, variability in the time instant corresponding to diastole ($t = t_d$) turns out to be the main parameter to be analyzed. In this study, we perform sensitivity analysis to quantitatively assess how significantly the relationship between SV and PP is altered by the variability in t_d. Using (6-16)-(6-18), PP can be rewritten as follows:

$$\begin{aligned} P_p &= P_s - P_d \cong 3(P_{es} - P_d) \\ &= 3\left\{\frac{E_S E_A}{E_S + E_A}(V_{ed} - V_0) - [\sigma P_S(V_{ed}) + (1-\sigma)P_D(V_{ed})]\right\} \end{aligned} \tag{6-19}$$

Then, the sensitivity of PP with respect to $\frac{t_d}{T}$ is given by:

$$\frac{\partial P_p}{\partial(t_d/T)} \cong -3\frac{\partial P_d}{\partial(t_d/T)} = -3\frac{\partial \sigma}{\partial(t_d/T)}[P_S(V_{ed}) - P_D(V_{ed})] \quad (6\text{-}20)$$

In (6-20), $[P_S(V_{ed}) - P_D(V_{ed})]$ does not depend on t_d; it is a function of V_{ed} only. Since the term $\frac{\partial \sigma}{\partial(t_d/T)}$ (i.e., the sensitivity of the activation function with respect to $\frac{t_d}{T}$) is always positive (Hay et al., 2005), it can be concluded that PP decreases as $\frac{t_d}{T}$ increases.

Relaxation of Assumption A2

The effect of discrepancy between MAP and ESP on the relationship between SV and PP can be examined as follows. It is clear from (6-14) and (6-18) that only PP but not SV is affected. The error in PP ($\widetilde{P_p}$) due to the difference between MAP and ESP is given by:

$$\widetilde{P_p} = 3(P_{es} - P_d) - 3(P_m - P_d) = 3\widetilde{P_m} \quad (6\text{-}21)$$

where $\widetilde{P_m} = P_{es} - P_m$. Thus, an error in MAP (caused by approximating it to ESP) is propagated to the PP error with an amplification factor of 3 (e.g., 1% error in MAP results in 3% error in PP), which can be deleterious if the MAP error is large. However, the absolute magnitude of alteration in PP due to the discrepancy between MAP and ESP is not expected to be significant, since MAP is indeed close in value to ESP over a wide range of physiologic conditions (Kass and Beyar, 1991; Maurer et al., 2009).

Table 16: Effect of arterial elastance on the responses of ESP, PP and SV

	R	T	E_A	$\frac{E_S E_A}{E_S + E_A}$	$\frac{E_S}{E_S + E_A}$	P_{es}	P_p	δV
V_{ed} ↑	↓	↑	↓	↓	↑	↓	↓	↑
V_{ed} ↓	↑	↓	↑	↑	↓	↑	↑	↓

Relaxation of Assumption A3

First, the effect of arterial elastance on the responses of ESP, PP and SV anticipated due to the changes in EDV is summarized in Table 16. In theory, TPR and the HR (the inverse of heart period) are altered by the autonomic baroreflex in response to alterations in V_{ed} (Kumar et al., 2004; Reil et al., 2009). Specifically, an increase in EDV results in a decrease in TPR and HR, whereas they increase to a decrease in EDV (Kumar et al., 2004; Reil et al., 2009). Therefore, the arterial elastance decreases during an increase in EDV, which then yields a decrease in ESP (with respect to its value predicted under constant arterial elastance) via a decrease in $\frac{E_S E_A}{E_S+E_A}$. This then results in a decrease in PP, since DBP is not affected by the arterial elastance. On the other hand, a decrease in arterial elastance yields an increase in SV (again, with respect to its value predicted under constant arterial elastance) via an increase in $\frac{E_S}{E_S+E_A}$. Therefore, should there be any notable impact of EDV on arterial elastance, the underestimation of SV based on PP will be exacerbated during an increase in EDV, e.g., during fluid therapy. In contrast, it can be deduced, based on the reasoning consistent with the above, that PP and SV will, respectively, increase and decrease from their values predicted under constant arterial elastance if EDV decreases.

Table 17: Effect of LV elastance on the responses of ESP, PP and SV

	E_S	$\frac{E_S E_A}{E_S + E_A}$	$\frac{E_S}{E_S + E_A}$	P_{es}	P_d	P_p	δV
V_{ed} ↑	↓	↓	↓	↓	↓	↑	↓
V_{ed} ↓	↑	↑	↑	↑	↑	↓	↑

Thus, the underestimation of SV based on PP will be alleviated during a decrease in EDV, e.g., hemorrhage.

Second, the effect of LV elastance on the responses of ESP, PP and SV anticipated due to the changes in EDV is summarized in Table 17. Similarly to TPR and HR, LV elastance is altered by the autonomic baroreflex in response to alterations in V_{ed} (Klabunde, 2005). In particular, LV elastance typically decreases if EDV increases, and it increases if EDV decreases (Klabunde, 2005). It can then be shown that both $\frac{E_S E_A}{E_S+E_A}$ and $\frac{E_S}{E_S+E_A}$ decrease in response to an increase in EDV. Consequently, an increase in EDV will result in a decrease in ESP and SV (with respect to their values predicted under constant LV elastance), whereas a decrease in EDV will result in an increase in EDP and SV (again, with respect to their values predicted under constant LV elastance). In addition, DBP is also affected by the LV elastance, because a change in LV elastance alters the value of $P_S(V_{ed})$ (see Figure 6-2). Therefore, the effect of LV elastance on PP can be elucidated by combining its impacts on ESP and DBP. To quantify the effect of LV elastance on PP, consider the following equations for ESP and DBP in response to a perturbation on LV elastance:

$$\begin{aligned}(P_{es} + \Delta P_{es}) &= \frac{(E_S + \Delta E_S)E_A}{(E_S + \Delta E_S) + E_A}(V_{ed} - V_0) \\ (P_d + \Delta P_d) &= \sigma(E_S + \Delta E_S)(V_{ed} - V_0) + (1-\sigma)B\left[e^{A(V_{ed}-V_0)} - 1\right]\end{aligned} \tag{6-22}$$

Thus, alterations in ESP and DBP can be written as follows:

$$\begin{aligned}\Delta P_{es} &= \left[\frac{(E_S + \Delta E_S)E_A}{(E_S + \Delta E_S) + E_A} - \frac{(E_S)E_A}{(E_S) + E_A}\right](V_{ed} - V_0) \\ &\approx \left(\frac{E_A}{E_S + E_A}\right)^2 \Delta E_S(V_{ed} - V_0) \\ \Delta P_d &= \sigma \Delta E_S(V_{ed} - V_0)\end{aligned} \tag{6-23}$$

where the expression for ΔP_{es} was simplified using the Taylor series expansion. Consequently, the alteration of PP due to a perturbation in LV elastance can be quantified as follows:

$$\frac{\partial P_p}{\partial E_S} = 3\left[\left(\frac{E_A}{E_S + E_A}\right)^2 - \sigma\right](V_{ed} - V_0) \tag{6-24}$$

So, whether PP increases or decreases depends on the sign of $\left[\left(\frac{E_A}{E_S+E_A}\right)^2 - \sigma\right]$. Though not definitive, it can be shown numerically that $\left[\left(\frac{E_A}{E_S+E_A}\right)^2 - \sigma\right]$ takes negative values over the space of physiologically nominal parameter values. Therefore, should there be any notable impact of EDV on LV elastance, the underestimation of SV based on PP will be alleviated during an increase in EDV, e.g., during fluid therapy. In contrast, the underestimation of SV based on PP will be exacerbated during a decrease in EDV, e.g., hemorrhage.

6.2.5. Simulation Study

To numerically examine the results of the analysis in this section, a simulation model developed by Ursino et al. (Ursino, 1998; Ursino and Magosso, 2000, 2003) was used to create SV and PP responses to a wide range of hypothetical volume perturbations. The model includes a time-varying elastance model of the heart, arterial and venous vessels lumped into 12 compartments, and a nonlinear baroreflex feedback model. In the simulation model, BV was varied from 3.5L to 6.5L (with nominal volume of 5.0L), and the corresponding BP and SV responses in the steady-state were obtained. A representative result is shown in Figure 6-4, where PP has been scaled to SV so that their values at 3.5L match.

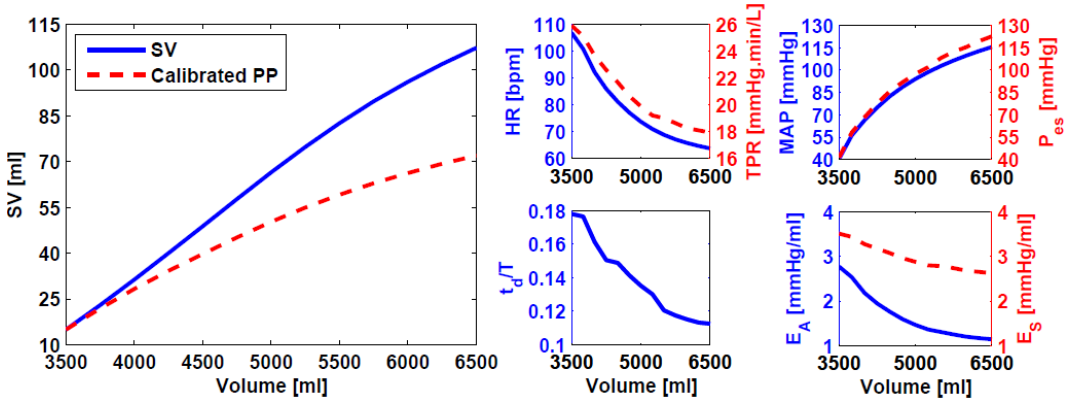

Figure 6-4: A representative result of SV, BP and baroreflex responses to a wide range of perturbation in blood volume (3.5L-6.5L).

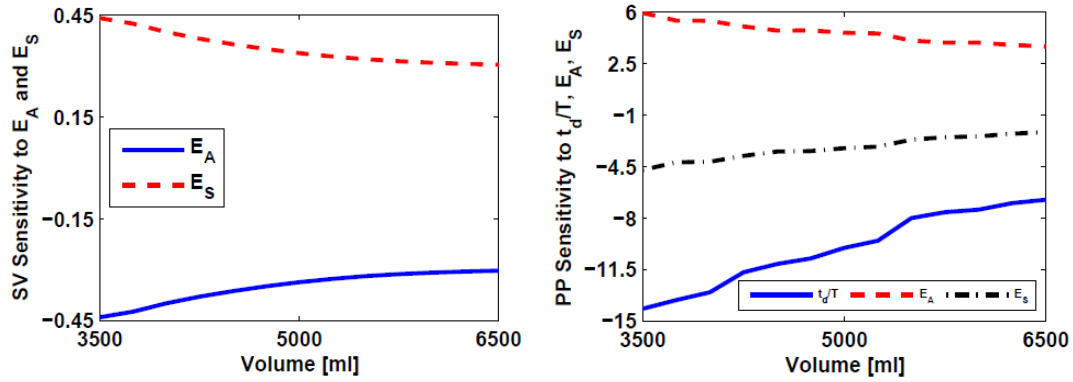

(a) SV (b) PP

Figure 6-5: Sensitivity of SV and PP to $\frac{t_d}{T}$, $\mathbf{E_A}$ and $\mathbf{E_S}$.

First of all, the simulation result shown in Figure 6-4 reassures that the change in PP underestimates that in SV. For example, the change in SV as predicted by the change in PP in response to the added BV of 3.0L (from 3.5L to 6.5L) was only ~60% of the actual change in SV. Therefore, PP must not be used as a linear predictor of SV. It is noted that the result shown in Figure 6-4 was obtained in the presence of realistic variability in $\frac{t_d}{T}$, E_A and E_S. Indeed, the baroreflex feedback responses in Figure 6-4 indicate that these parameters were subject to non-negligible variability during BV perturbation. In particular, $\frac{t_d}{T}$ decreased by large amount in response to an increase in

BV, which was attributed to a large decrease in HR (thus a large increase in T). Also, TPR as well as arterial and LV elastances decreased as BV increased, which was anticipated. Compared with LV elastance, however, the variability in arterial elastance was significantly larger due to large changes in HR and TPR.

To quantitatively examine the effect of variability in $\frac{t_d}{T}$, E_A and E_S on our analysis, the sensitivity of SV and PP to these parameters were computed and scrutinized (see Figure 6-5). Overall, the sensitivity of SV on E_A and E_S was very small (see Fig. 27a). Also, it does not explicitly depend on $\frac{t_d}{T}$ as indicated by (6-14). Thus, we predicted that the assumptions A1-A3 made in Section 6.2.1 would not affect SV. Indeed, simulated SV as shown in Figure 6-5 was very close in value to SV predicted from (6-14) under constant E_A and E_S (not shown). On the other hand, PP turned out to be largely affected by these parameters (see Figure 6-5(b)). Considering that the absolute amount of change in E_A was much larger than that in E_S (see Figure 6-4),it turned out that the effect of changes in $\frac{t_d}{T}$ and E_A on PP was dominant in comparison with the effect of change in E_S. Now that the direction of changes in $\frac{t_d}{T}$ and E_A is the same (i.e., both decrease for positive volume perturbation but increase for negative volume perturbation) but their impact on PP is opposite (as indicated by opposite signs in sensitivity; see Figure 6-5(b)), it was observed that their effects were approximately canceled by each other. So, together with the observation that ESP was consistently higher than MAP (see Figure 6-4), PP was overestimated based on (6-21). Summarizing all these observations, relaxation of the assumptions A1-A3 appear to further pronounce PP's underestimation of SV.

6.3. Need for General Model of Cardiovascular Responses to Combined Fluid and Vasopressor Infusion

This chapter mathematically demonstrated that PP, a readily available NIBP measurement, may fail to guide a major fluid resuscitation. In the same way, the Windkessel model shown in Section 6.1 may fail in other populations than those used in Section 5.2. For instance, AC changes as a function of BP (Langewouters et al., 1984; Stergiopulos et al., 1995). In the dataset used in Section 5.2, the range of BP was small, and so, presumably, was the range of AC. This may not be the case for patients with drastic BP changes as might be observed in circulatory shock, hemorrhage or fluid resuscitation events. If so, modifications of the methodology and/or CV model may need to be considered.

7. Modeling of Cardiovascular Endpoint Responses to Blood Volume Perturbation and Vasopressor Infusion

This chapter presents a platform to reproduce hemodynamic responses to fluid and vasopressor infusion. Chapters 4 and 5 presented methodologies to estimate cardinal parameters and hemodynamic responses to fluid and vasopressor administration. Chapter 4 combined Guyton's model of venous return and LV P-V relationship to achieve a transparent model of SV with 4 tunable parameters in which each parameter was lumped via a combination of physiological parameters (e.g., θ_1 included E_S and E_A). Chapter 5 employed receptor-based phenomenological models to replicate the behavior of cardinal parameters including SV. Although both methods led to adequate estimations of hemodynamic endpoints, systematic way of merging them as a single model to reproduce hemodynamic endpoints to both fluid and vasopressor infusion is not practical. In fact, the feasibility of considering the effects of vasopressors on the lumped physiological parameters of the SV model in Chapter 4 is dubious. As demands for ACCS necessitate development of a single platform to replicate cardinal parameters in subjects under hemodynamic management, this chapter develops a universal platform for both fluid and vasopressor administration. Compared to the models of hemodynamic endpoints to BV and vasopressor, this universal platform necessitates (i) adding new model complexities and parameters, and (ii) a unique set of data from left-ventricle to validate it. To evaluate the platform, we recorded high resolution unique data from 4 pig animals. Although the order of fluid and vasopressor infusion in the pig subjects is consecutive, we speculate that this tool may be potentially employed in case of concurrent fluid and vasopressor infusion as well.

7.1. Modeling of Universal Platform to Fluid and Vasopressor Infusion

The model proposed in this Chapter includes two sub-models: a) the model of LV preload response to the fluid and vasopressor infusion, and b) the model of SV and BP response to change in preload. The second sub-model is built based on LV P-V relationship framework. Since the model of BV is validated in Chapters 3 and 4, we assume BV measurements are given and only preload, SV and MAP are estimated in response to BV and vasopressor dose perturbation.

7.1.1. Model of Preload Response to Fluid and Vasopressor Infusion

Change in LV preload is known to be a proportional but delayed response to BV perturbation (see Figure 7-1(a)). An increase in BV increases CVP. Based on Guyton's model of venous return, increase in CVP corresponds to increase in pulmonary venous blood flow to the left ventricle, thereby increasing LV EDV. Compared to the increase in LV preload, change in V_0 (LV volume at zero LV pressure) is modest. We define the effective LV preload as $V_{LV} = V_{ed} - V_0$. The effective preload in response to BV is modeled as a linear function:

$$[V_{LV}(t)]_{BV} = \left[V_{LV,0}\right]_{BV} + \lambda(\theta_B(t) - V_{B0}) \tag{7-1a}$$

where $[V_{LV}(t)]_{BV}$ and $\left[V_{LV,0}\right]_{BV}$ are effective preload and its baseline when subject is under BV perturbation, $\theta_B(t)$ is delayed BV perturbation, and V_{B0} is baseline BV. The latency observed between the dynamics of preload and BV response is reproduced via a second-order mixing model that is shown below in the frequency domain:

$$\theta_B(s) = \frac{K_Z s + 1}{\frac{1}{\omega^2}s^2 + \frac{2\zeta}{\omega}s + 1} V_B(s) \tag{7-1b}$$

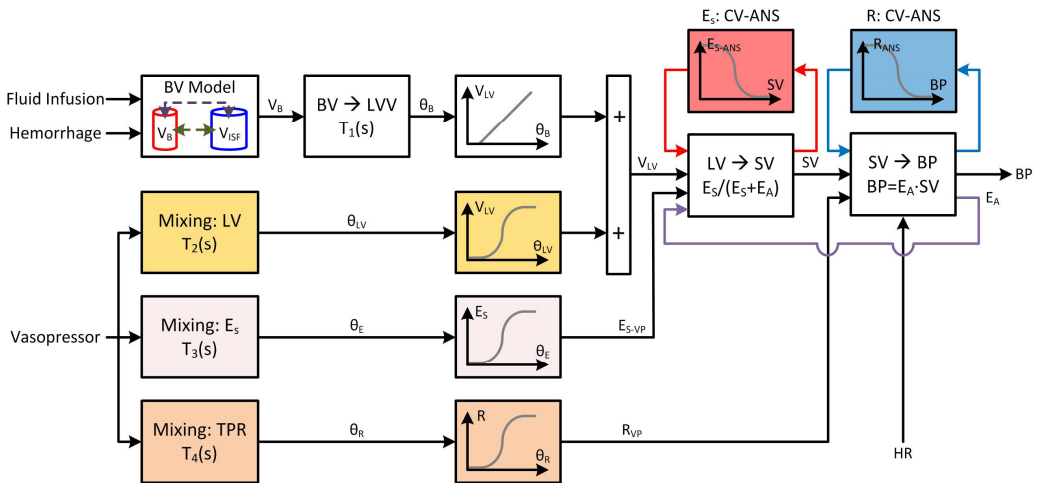

Figure 7-1: Schematic of the universal platform. CV: cardiovascular, ANS: autonomic nervous system

Norepinephrine (NE) is a potent alpha-adrenergic receptor agonist with modest beta-agonist activity, which renders it a powerful vasoconstrictor with less potent direct inotropic properties. As far as the LV preload is concerned, when inotropy is increased SV increases, which reduces the ESV. This is accompanied by a secondary reduction in EDV because when SV is increased the ventricle contains less residual BV after ejection (decreased ESV), which can be added to the incoming venous return during filling. Therefore, ventricular filling (EDV) is slightly reduced due to inferior inotropic effects. On the other hand, NE results in increase in ESP via enhanced TPR (dominant), SV and HR (secondary) as well as slight increase in LV elastance E_S due to inotropy. While ESV drops, the significant increase in ESP is compensated by slight increase in E_S and large reduction of V_0. (see (6.11), $P_{es} = E_S(V_{es} - V_0)$). In sum, effective preload shows increase in response to NE administration (see Figure 7-1):

$$[V_{LV}(t)]_{vaso} = [V_{LV,0}]_{vaso} + \frac{E_{max}[\theta_{LV}(t)]^n}{I_{50}{}^n + [\theta_{LV}(t)]^n} \tag{7-2a}$$

where I_{50} is NE infusion dose corresponding to 50% clinical effects and $\left[V_{LV,0}\right]_{vaso}$ is baseline effective preload when subject Is under vasopressor infusion. θ_{LV} is the hypothetical mixing NE dose and defined in the frequency domain as follow:

$$\theta_{LV}(s) = \frac{1}{\tau s + 1} D(s) \tag{7-2b}$$

where $D(s)$ is vasopressor dose (d) in frequency domain. If we combine (7-1a) and (7-2a), the model of preload in response to both fluid and vasopressor infusion would be:

$$V_{LV}(t) = V_{LV,0} + \lambda(\theta_B(t) - V_{B0}) + \frac{E_{max}[\theta_{LV}(t)]^{n_{LV}}}{{I_{50}}^{n} + [\theta_{LV}(t)]^{n_{LV}}} \tag{7-3}$$

Suppose fluid and vasopressor infusion occur in a consecutive order and E_{max} is equal to the effective preload before vasopressor infusion starts, (7-3) is simplified to:

$$V_{LV}(t) = \left(V_{LV,0} + \lambda(\theta_B(t) - V_{B0})\right)\left(1 + \frac{[\theta_{LV}(t)]^{n_{LV}}}{{I_{50}}^{n} + [\theta_{LV}(t)]^{n_{LV}}}\right) \tag{7-4}$$

7.1.2. Model of Stroke Volume and Blood Pressure Responses to Change in Preload

Perturbation in LV preload leads to change in SV and BP. In this section, we build the models of SV and BP based on the LV P-V framework. Given that the effective preload can be estimated by (7-4), TPR and E_S are the two essential parameters required to elucidate SV and BP in response to change in LV preload. In general, these two parameters are subject to two sources of perturbation, baroreflex and vasopressor-driven stimulation:

Baroreflex regulation or autonomic nervous system (ANS), the rapid negative feedback mechanism to buffer endpoints against excessive rise or fall, primarily persuades the cardinal parameters in which SV and BP stay at their normal level when a subject is under hemorrhage and fluid infusion, i.e., BV perturbation. To this end, change in TPR

and E_S are to ensure the negative feedback on SV and BP. It was shown in Chapter 4 that TPR as a phenomenological model of BP could adequately reproduces the baroreflex regulation of MAP.

In addition, NE, as a potent alpha-agonist activator with modest effects on beta receptors, actuates TPR, E_S and HR to achieve superior SV and BP. These sets of actuation are alongside the baroreflex system when subjects are under vasopressor infusions and can elevate SV and BP to more than normal levels in a short time.

Based on what is explained, we developed the models of TPR and E_S as follows:

$$R(t) = \left\{R_0 - \frac{\Delta R}{2}\frac{\mathrm{sgn}\left(P_m(t) - P_{m,0}\right)\left|P_m(t) - P_{m,0}\right|^{n_R}}{1 + \left|P_m(t) - P_{m,0}\right|^{n_R}}\right\} + K_R\theta_R(t) \tag{7-5}$$

$$E_s(t) = \left\{E_{S0} - \frac{\Delta E_S}{2}\frac{\mathrm{sgn}(\delta V(t) - \delta V_0)|\delta V(t) - \delta V_0|^{n_{E_S}}}{1 + |\delta V(t) - \delta V_0|^{n_{E_S}}}\right\} + K_{E_S}\theta_E(t) \tag{7-6}$$

where R_0, $E_{S,0}$, $P_{m,0}$ and δV_0 are baseline TPR, E_S, MAP and SV, and K_R and K_{E_S} determine the extent to which NE stimulates TPR and E_S. The first portion of the models shown in brackets indicates change in TPR and E_S due to baroreflex while the second portion determines the influence of NE stimulant. For simplicity, the same mixing effects as V_{LV} was considered for TPR and Es, i.e., $\theta_R(s) = \theta_E(s) = \frac{1}{\tau s+1}D(s)$.

Once LV preload, TPR and E_S are available, SV and BP can be estimated via LV P-V framework (see (6-14) and (6-17)):

$$\delta V(t) = V_{ed}(t) - V_{es} = \frac{E_S}{E_S + E_A}(V_{ed}(t) - V_0) = \frac{E_S}{E_S + E_A}V_{LV}(t) \tag{7-7}$$

$$P_m(t) \cong P_{es}(t) = \frac{E_S(t)E_A(t)}{E_S(t) + E_A(t)}(V_{ed}(t) - V_0) = \frac{E_S(t)E_A(t)}{E_S(t) + E_A(t)}V_{LV}(t) = E_A\delta V(t) \tag{7-8}$$

where $E_A(t) = R(t)HR(t)$ is arterial elastance. In (7-8) it was assumed that MAP≅ESP (see Section 7.2.2).

7.2. Experimental Data

To validate the proposed platform, we used experimental data collected from 4 pig animals under the protocol approved by the Institutional Animal Care and Use Committee (IACUC) at the University of North Carolina. The measurements included the rates of hemorrhage, infusion, as well as BV (hematocrit), BP, HR and LV pressure and volume under general anesthesia and mechanical ventilation. Each animal went under stepwise hemorrhage with the maximum total amount of 25% of the baseline BV. Blood withdrawn, ranging between 250 ml to 500 ml, was continued until either the maximum hemorrhage was achieved or MAP dropped to 40 mmHg. Colloid fluid resuscitation (6% Hetastarch) was administered shortly after the end of hemorrhage with the rate of 20 ml/min and was continued until MAP increased to ~75% of its baseline value. Once the hemodynamic responses were stabilized, the subjects received NE vasopressor at 4-5 distinct infusion rates of 10 min duration. The minimum and maximum infusion rates used ranged between 0.1 μg/kg/min and 0.3 mcg/kg/min.

7.2.1. Pressure-Volume Loop Data Feature Extraction

EDV, ESV and their difference SV, V_0 and E_S were extracted from LV P-V loop data. The feature extraction was performed every 1-2 min during the transient responses to hemorrhage and fluid infusion and every 5 min once the responses were stabilized to hemorrhage, fluid resuscitation, and vasopressor infusion. To be

consistent, other hemodynamic variables including BV, BP, and HR were extracted at the same time instants.

First, we automatically identified the corner points associated with the end of diastole (lower right corner), opening of aorta (upper right corner), end of systole (upper left corner) and lower left corner of each selected P-V loop. To this end, we defined two crossing points, one for the right corners and another one for the left corners. We specified the average pressure in the P-V loop as $P_{av} = \frac{P_{max}+P_{min}}{2}$, where P_{max} and P_{min} are the maximum and minimum pressure magnitudes among all the data points of the loop. The value of maximum (V_{max}) and minimum (V_{min}) volumes associated with the loop were also identified. Coordinates of the crossing points corresponding to the right and left corners were defined as $(1.2V_{max}, P_{av})$ and $(0.5V_{min}, P_{av})$, respectively (see Figure 7-2). To find the corners, we drew slope-varying lines through each crossing point toward their associated corners. The corners were identified as the intersections of the P-V loop and the crossing lines with the maximal slope (see Figure 7-2). Figure 7-2 shows that, for instance, the point of $(0.5V_{min}, P_{av})$ and the purple crossing lines were utilized to detect the ESP.

Second, the derivative of the pressure measurements corresponding to the points located between the lower and upper right corners as well as the lower and upper left corners were calculated. The points with maximum pressure variation were indicated as $Max(dP_D)$ and $Max(dP_S)$ (see Figure 7-2). EDV and ESV were thus computed as the numerical average of all the volume measurements corresponding to the points with LV pressure of +/-40% of $Max(dP_D)$ and $Max(dP_S)$, respectively (see

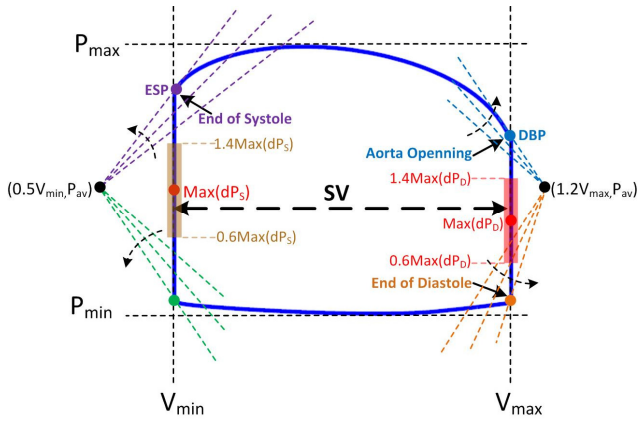

Figure 7-2: P-V loop feature extraction. EDV and ESV are averaged volume of data points within the red and brown bars.

Figure 7-2, shown as red and brown bars respectively).

Third, V_0 and $E_S$were identified via least square solution of the relationship between ESPs and corresponding volume measurement $P_{es} = E_S(V(t = t_{es}) - V_0)$. At each instant of feature extraction, 2 to 3 consecutive respiratory cycles of P-V loop data (about 30-40 loops in total) were selected and identified for their end of systole. Given that both pressure and volume measurements are under sensor noise, a total least square approach was employed to identify V_0 and E_S for that instant.

7.2.2. Data Evaluation

The hemodynamic responses employed to validate the platform were collected from different sensor measurements: LV pressure, volume and aortic pressure waveform measurements. Furthermore, LV measurement features were extracted via detached steps including P-V loop corner point identification, averaging volume measurements to obtain EDV, ESV and SV, and total least square estimation of V_0 and E_S. Therefore, it was uncertain whether these data can be replicated by the LV P-V loop

framework. To check the adequacy of the data and model's performance, a few initial steps were made. Details follow:

First, we examined how close ESP and MAP measurements are. All 4 animal data showed that MAP slightly underestimates ESP, in which in all the subjects ESP can be adequately approximated by 1.15MAP. Second, we utilized measured effective preload, E_S, HR, MAP and SV measurements to examine the LV P-V model performance to replicate the extracted SV and MAP data via equations (7-7) and (7-8). Our analysis showed that the LV P-V loop framework can adequately reproduce the MAP and SV data.

7.3. Model Evaluation and identification

In this section, methods to examine model performance to reproduce hemodynamic responses to BV perturbation and vasopressor infusion are presented. In particular, we evaluate how adequately the model proposed above estimates the LV preload, SV and BP.

7.3.1. Model Fitting

A numerical optimization approach was employed to fit the model to the hemodynamic responses. In particular, effective preload V_{LV}, SV and MAP were utilized as the endpoints to be gauged. In this work, we assumed BV is measured and available as the input to the model. All the parameters supposed to be identified were initiated by a random guess. Details follow.

First, we inputted BV and NE dose to the model of effective preload (7-4) (also see Figure 7-1). Along with the models associated with the dynamics of BV and

vasopressor dose (7-1b) and (7-2b), the model of preload contains 8 parameters, 4 corresponding to the PD model of effective preload $\{V_{LV,0}, \lambda, n_{LV}, I_{50}\}$ and the remaining 4 associated with the PK of BV and vasopressor infusion, i.e., $\{K_Z, \zeta, \omega, \tau\}$. It was assumed that baseline BV V_{B0} is known.

Second, computed preload was inputted to the models of SV. SV is a function of TPR (see (7-7)) and TPR is a function of MAP (see (7-5)). Therefore, the models of SV (7-7) and BP (7-8) are coupled and must be jointly solved alongside with the models of TPR and E_S. To this end, a numerical root finding approach was employed. After fixing ΔR and ΔE_S to cover experimentally observed maximal change in TPR and E_S in all 4 animals (30 [mmHg·min/l] and 1.4 [mmHg/ml]), the models of TPR and E_S include 8 parameters to tune: $\{R_0, P_{m,0}, K_R, n_R\}$ and $\{E_{S0}, \delta V_0, K_{E_S}, n_{E_S}\}$ corresponding to TPR and E_S, respectively. To count for the difference between ESP and MAP, (7-8) was scaled by a factor of 1.15 (see Section 7.2.2). The computed EDV, SV and MAP via the initial guess of the parameters were compared with their true measurements and the discrepancy between them was minimized by solving the following problem:

$$\begin{aligned}\Omega^* &= \{V_{LV,0}{}^*, \lambda^*, n_{LV}{}^*, I_{50}^*, \tau^*, K_Z^*, \zeta^*, \omega^*, R_0^*, P_{m,0}^*, K_R^*, n_R, E_{S0}^*, \delta V_0^*, K_{E_S}^*, n_{E_S}\} \\ &= \arg\min_{\Omega} \left\| \left[\left(\frac{\widetilde{V_{LV}}(t) - V_{LV}(t|\Omega)}{\overline{\widetilde{V_{LV}}(t)}} \right) \quad \left(\frac{\widetilde{\delta V}(t) - \delta V(t|\Omega)}{\overline{\widetilde{\delta V}(t)}} \right) \quad \left(\frac{\widetilde{P_m}(t) - P_m(t|\Omega)}{\overline{\widetilde{P_m}(t)}} \right) \right] \right\|_2 \end{aligned} \tag{7-9}$$

where $\widetilde{V_{LV}}(t)$, $\widetilde{\delta V}(t)$, and $\widetilde{P_m}(t)$ are measured preload, SV, and MAP, while $V_{LV}(t|\Omega)$, $\delta V(t|\Omega)$, and $P_m(t|\Omega)$ are the same parameters estimated by the model. In addition, $\overline{\widetilde{V_{LV}}(t)}$, $\overline{\widetilde{\delta V}(t)}$, and $\overline{\widetilde{P_m}(t)}$ are the same variables averaged over the entire study and utilized to normalize the error magnitude corresponding to each variable. DE algorithm was utilized for the

optimization, where it perturbs the initial parameters guess under frequent mutation and crossover until the fitting error (7-9) is minimized.

7.3.2. Model identification and Sensitivity

The model was analyzed from two standpoints: fitting performance and physiological relevance of identified parameters. First, to assess the model performance in reproducing the hemodynamic variables, RMSEs between measured versus estimated variables were calculated and reported. Second, the physiological relevance of the identified parameters was investigated. In particular, the relevance of the identified $V_{LV,0}$, δV_0, $P_{m,0}$ to their true counterparts was studied. In addition, the contribution of the NE stimulant on TPR and E_S change, i.e., K_R and K_{E_S} was studied.

From the perspective of variable identification, the physiological variables are all identifiable: First, both SV and MAP are given as the variables to be fitted. Therefore, the variable in between, i.e., TPR (see (7-8)), is identifiable. Second, given that TPR, and as a result E_A, is available, LV elastance E_S is also identifiable since V_{LV} and SV are both given as the reference variables (see (7-7)).

A parametric sensitivity analysis is needed to understand the importance of the parameters in each sub-model. Since fluid and vasopressor infusion occur in a consecutive order, the sensitivity of variables in response to fluid and vasopressor infusion can be performed separately. In this regard, we first studied the sensitivity of V_{LV} parameters to fluid infusion. As the model of V_{LV} with respect to fluid infusion is linear, a linear regression analysis was employed to examine whether the parameters of the model can be separately characterized. If we combine (7-1a) and (7-1b), we have:

$$s^2V_{LV}(s) = \begin{bmatrix} -sV_{LV}(s) & -V_{LV}(s) & sV_B(s) & V_B(s) & \frac{-1}{s} & -1 \end{bmatrix} \begin{bmatrix} 2\zeta\omega \\ \omega^2 \\ \lambda\omega^2 K_Z \\ \lambda\omega^2 \\ \omega^2(\lambda V_{B0} - V_{LV,0}) \\ 2\zeta\omega(\lambda V_{B0} - V_{LV,0}) \end{bmatrix} \quad (7\text{-}10)$$

Given that baseline BV V_{B0} is known, all the parameters in the above linear regression are identifiable (meaning they can be uniquely determined provided the input data are informative).

On the other hand, the model of V_{LV} in response to vasopressor infusion as well as the baroreflex-driven portions of SV and MAP models include nonlinear components and a parametric sensitivity analysis is essential. To this end, we constructed an average subject at which the sensitivity of V_{LV} to NE and baroreflex-oriented SV and MAP to BV and NE perturbation can be examined at its nominal operating condition. Since hemorrhage and fluid infusion scenario was consistent between 4 subjects, the average BV, as an input to the SV and MAP models, as well as V_{LV} response under BV perturbation were defined as the average BV and V_{LV} measurements among all four subjects. The order of vasopressor doses, however, was different between different subjects. Therefore, we defined the nominal vasopressor input as stepwise increase in NE dose ranging between 0 and 2 μg/kg/min with steps of 0.5 μg/kg/min increase, at which each dose lasted for 10 min. The nominal V_{LV}, SV, MAP and E_S responses at each NE dose were defined as the average of their corresponding measurement to that dose in all the subjects.

Then, we constructed the sensitivity functions associated with V_{LV} response to NE (7-2) and also SV (7-7) and MAP (7-8) models when TPR and E_S are only influenced by baroreflex mechanism. To this end, we computed partial derivative of models of NE-

driven V_{LV} as well as baroreflex-driven SV and BP with respect to their corresponding parameters. From (7-2) we have:

$$\left(\mathcal{S}_{V_{LV}}(t)\right)_{Vaso} = \begin{bmatrix} \frac{\partial V_{ed}(t)}{\partial n_{LV}} \\ \frac{\partial V_{ed}(t)}{\partial I_{50}} \\ \frac{\partial V_{ed}(t)}{\partial \tau} \end{bmatrix} = \begin{bmatrix} \frac{{I_{50}}^{n_{LV}} E_{max}}{({I_{50}}^{n_{LV}} + [\theta_{LV}(t)]^{n_{LV}})^2} \log\left(\frac{\theta_{LV}(t)}{I_{50}}\right) [\theta_{LV}(t)]^{n_{LV}} \\ \frac{-n_{LV} {I_{50}}^{n_{LV}-1} E_{max}}{({I_{50}}^{n_{LV}} + [\theta_{LV}(t)]^{n_{LV}})^2} [\theta_{LV}(t)]^{n_{LV}} \\ \frac{n_{LV} {I_{50}}^{n_{LV}} E_{max}}{({I_{50}}^{n_{LV}} + [\theta_{LV}(t)]^{n_{LV}})^2} [\theta_{LV}(t)]^{n_{LV}-1} \frac{\partial \theta_{LV}(t)}{\partial \tau} \end{bmatrix} \quad (7\text{-}11a)$$

where by taking the derivative of (7-2b) with respect to τ and then discretizing the outcome into a difference equation using the Euler's method we have:

$$\begin{aligned} \frac{\partial \theta_{LV}(t)}{\partial \tau}(i) = &\left(2 - 2\frac{T_S}{\tau}\right)\frac{\partial \theta_{LV}(t)}{\partial \tau}(i-1) + \left(2\frac{T_S}{\tau} - 1 - \frac{{T_S}^2}{\tau^2}\right)\frac{\partial \theta_{LV}(t)}{\partial \tau}(i-2) \\ &- \frac{T_S}{\tau^2}[d(i-1) - d(i-2)] \end{aligned} \quad (7\text{-}11b)$$

where T_S is sampling interval. From (7-5) to (7-8), sensitivity of baroreflex-driven SV can be computed as follows:

$$\left(\mathcal{S}_{\delta V}(t)\right)_{ANS} = \begin{bmatrix} \frac{\partial \delta V(t)}{\partial E_{S0}} \\ \frac{\partial \delta V(t)}{\partial \delta V_0} \\ \frac{\partial \delta V(t)}{\partial n_{E_S}} \\ \frac{\partial \delta V(t)}{\partial R_0} \\ \frac{\partial \delta V(t)}{\partial P_{m,0}} \\ \frac{\partial \delta V(t)}{\partial n_R} \end{bmatrix} = \begin{bmatrix} \frac{E_A(t)V_{ed}(t)\left(1+(|\delta V(t)-\delta V_0|)^{n_{E_S}}\right)^2}{0.7n_{E_S}E_A(t)V_{ed}(t)(|\delta V(t)-\delta V_0|)^{n_{E_S}-1}+\Psi_1(t)^2} \\ \frac{0.7n_{E_S}E_A(t)V_{ed}(t)(|\delta V(t)-\delta V_0|)^{n_{E_S}-1}}{0.7n_{E_S}E_A(t)V_{ed}(t)(|\delta V(t)-\delta V_0|)^{n_{E_S}-1}+\Psi_1(t)^2} \\ \frac{-0.7E_A(t)V_{ed}(t)sgn(\delta V(t)-\delta V_0)log(|\delta V(t)-\delta V_0|)(|\delta V(t)-\delta V_0|)^{n_{E_S}}}{0.7n_{E_S}E_A(t)V_{ed}(t)(|\delta V(t)-\delta V_0|)^{n_{E_S}-1}+\Psi_1(t)^2} \\ \frac{-E_S(t)HR(t)V_{ed}(t)}{(E_S(t)+E_A(t))^2} \\ \frac{-15n_RE_S(t)HR(t)V_{ed}(t)(|P_m(t)-P_{m,0}|)^{n_R-1}}{\left(1+(|P_m(t)-P_{m,0}|)^{n_R}\right)^2(E_S(t)+E_A(t))^2} \\ \frac{15E_S(t)HR(t)V_{ed}(t)sgn(P_m(t)-P_{m,0})log(|P_m(t)-P_{m,0}|)(|P_m(t)-P_{m,0}|)^{n_R}}{\left(1+(|P_m(t)-P_{m,0}|)^{n_R}\right)^2(E_S(t)+E_A(t))^2} \end{bmatrix} \quad (7\text{-}12)$$

$\Psi_1(t) = E_{S0}[1 + (|\delta V(t) - \delta V_0|)^{n_{E_S}}] - 0.7sgn(\delta V(t) - \delta V_0)(|\delta V(t) - \delta V_0|)^{n_{E_S}} + E_A(t)[1 + (|\delta V(t) - \delta V_0|)^{n_{E_S}}]$.

In the same way, for sensitivity of baroreflex-driven BP is as follows:

$$\left(\mathcal{S}_{P_m}(t)\right)_{ANS} = \begin{bmatrix} \frac{\partial P_m(t)}{\partial R_0} \\ \frac{\partial P_m(t)}{\partial P_{m,0}} \\ \frac{\partial P_m(t)}{\partial n_R} \\ \frac{\partial P_m(t)}{\partial E_{S0}} \\ \frac{\partial P_m(t)}{\partial \delta V_0} \\ \frac{\partial P_m(t)}{\partial n_{E_S}} \end{bmatrix} = \begin{bmatrix} \frac{E_S(t)^2 V_{ed}(t)\left(1+\left(|P_m(t)-P_{m,0}|\right)^{n_R}\right)^2}{15 n_R E_S(t)^2 V_{ed}(t)\left(|P_m(t)-P_{m,0}|\right)^{n_R-1}+\Psi_2(t)^2} \\ \frac{15 n_R E_S(t)^2 V_{ed}(t)\left(|P_m(t)-P_{m,0}|\right)^{n_R-1}}{15 n_R E_S(t)^2 V_{ed}(t)\left(|P_m(t)-P_{m,0}|\right)^{n_R-1}+\Psi_2(t)^2} \\ \frac{-15 E_S(t)^2 V_{ed}(t)\,sgn\left(P_m(t)-P_{m,0}\right)\log\left(|P_m(t)-P_{m,0}|\right)\left(|P_m(t)-P_{m,0}|\right)^{n_R}}{15 n_R E_S(t)^2 V_{ed}(t)\left(|P_m(t)-P_{m,0}|\right)^{n_R-1}+\Psi_2(t)^2} \\ \frac{E_A(t)^2 V_{ed}(t)}{(E_S(t)+E_A(t))^2} \\ \frac{0.7 n_{E_S} E_A(t)^2 V_{ed}(t)\left(|\delta V(t)-\delta V_0|\right)^{n_{E_S}-1}}{\left(1+\left(|\delta V(t)-\delta V_0|\right)^{n_{E_S}}\right)^2 (E_S(t)+E_A(t))^2} \\ \frac{-0.7 E_A(t)^2 V_{ed}(t)\,sgn(\delta V(t)-\delta V_0)\log\left(|\delta V(t)-\delta V_0|\right)\left(|\delta V(t)-\delta V_0|\right)^{n_{E_S}}}{\left(1+\left(|\delta V(t)-\delta V_0|\right)^{n_{E_S}}\right)^2 (E_S(t)+E_A(t))^2} \end{bmatrix} \quad (7\text{-}13)$$

$\Psi_2(t) = E_S(t)\left(1+\left(|P_m(t)-P_{m,0}|\right)^{n_R}\right) + 1e^{-3} HR(t) R_0\left(1+\left(|P_m(t)-P_{m,0}|\right)^{n_R}\right) - 15e^{-3} HR(t)\,sgn\left(P_m(t)-P_{m,0}\right)\left(|P_m(t)-P_{m,0}|\right)^{n_R}$.

We then numerically computed $\mathcal{S}_{V_{LV}}(t)$ to NE infusion, and $\mathcal{S}_{\delta V}(t)$ and $\mathcal{S}_{P_m}(t)$ to BV and NE perturbation by solving (7-11), (7-12), and (7-13) simultaneously with (7-4) to (7-8). Since the model parameter values exhibited diversity in terms of magnitude, we normalized the computed sensitivity variables using the respective nominal parameter values and time series sequence of $V_{LV}(t)$, $\delta V(t)$, and $P_m(t)$. For each sub-model, we compared the magnitudes of the normalized parametric sensitivity functions and compared the level of sensitivity between different parameters. Lastly, sensitivity of NE-driven portion of SV and BP models were determined via a linear regression model. Assuming baseline E_S and TPR at the start of NE infusion, i.e., $[E_{S0}]_{vaso}$ and $[R_0]_{vaso}$, are their measurements at the end of BV perturbation, from (7-5) to (7-7) and (7-2b) we obtain the following equation in discrete time:

$$[E_{S0}+E_{A0}]_{vaso}\delta V(i-1) - [E_{S0}]_{vaso} V_{LV}(i-1)$$
$$= \begin{bmatrix} [E_{S0}]_{vaso}\left(V_{LV}(i)-V_{LV}(i-1)\right) - [E_{S0}+E_{A0}]_{vaso}\left(\delta V(i)-\delta V(i-1)\right) \\ d(i-1)V_{LV}(i-1) \\ -d(i-1)\delta V(i-1) \end{bmatrix}^T \begin{bmatrix} \frac{\tau}{T_S} \\ K_{E_S} \\ K_{E_S}+K_R \end{bmatrix} \quad (7\text{-}14)$$

where $E_{A0} = e^{-3} HR_0 R_0$. Given that both $[E_{S0}]_{vaso}$ and $[E_{A0}]_{vaso}$ are known, from (7-14) and (7-15) it is evident that τ, K_{E_S} and K_R can be uniquely identified.

7.4. Model Fitting and Discussion

Once tuned the parameters, the model could adequately reproduce the hemodynamic variables. The RMSEs associated with preload, SV, and BP were 5.4 ml, 1.4 ml, and 4.2 mmHg, respectively, which, when normalized by their respective average response, were consistently smaller than 8.0%. Figure 7-3 shows the true and estimated hemodynamic variables for an individual subject, indicating the adequate goodness of fit. Table 18 shows the identified parameters averaged among 4 animal subjects.

From the physiological relevance perspective, the identified baseline values $V_{LV,0}$, δV_0 and $P_{m,0}$ were compared with their true counterpart. When

Table 18: Identified parameters (mean (SD)) averaged between 4 animal subjects

PK of Preload	PD of Preload	TPR	E_S
τ [min] 0.015 (0.017)	$V_{LV,0}$ [ml] 71.3 (11.8)	R_0 [mmHg] 15.6 (9.8)	E_{s0} [mmHg/ml] 1.03 (0.30)
K_Z [min] 144 (97)	λ [-] 0.03 (0.04)	$P_{m,0}$ [mmHg] 58.7 (23.3)	SV_0 [ml] 25.8 (3.8)
ω [1/min] 0.18 (0.09)	n_{LV} [-] 0.63 (0.44)	K_R [mmHg.min^2.kg/mcg.l] 43 (48)	K_{E_S} [mmHg.min.kg/mcg.ml] 1.8 (1.5)
ζ [-] 1.95 (0.96)	I_{s0} [µg/kg/min] 19.9 (31.1)	n_R [-] 0.78 (0.75)	n_{SV} [-] 0.81 (0.82)

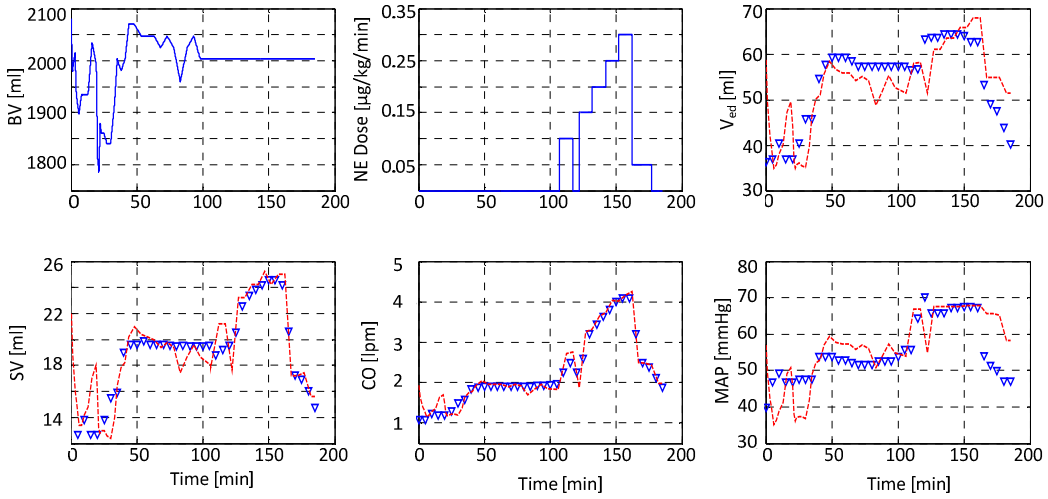

Figure 7-3: True and estimated hemodynamic variables in response to consecutive fluid and norepinephrine infusion for an individual subject. True: blue circles, Estimated: red dashed-line

normalized, the errors associated with the baseline values were consistently less than 20% on the average, indicating a good relevance between the identified parameters to their corresponding true values.

The importance of parameters associated with V_{LV}, SV and BP was also studied. First, the identified parameters associated with PK of V_{LV} due to BV and NE perturbation showed large distribution for the parameter τ (see Table 18, SD of τ was 113% of its nominal value) while less variation was seen in ω, ζ, and K_Z (SD were 50%, 49%, and 67% of their nominal values, respectively). It's speculated that among the parameters corresponding to PK of BV and vasopressor, the importance of the parameters ω, ζ, and K_Z is substantial. Figure 7-4(a) presents the sensitivity of V_{LV} model parameters under NE infusion. The normalized sensitivity of V_{LV} in response to NE infusion suggests that V_{LV} response is not sensitive to τ except at the time of changes in dose (see Figure 7-4(a)), while ω, ζ, and K_Z were shown to be identifiable via the regression model (7-10). Furthermore, the zero in the second order filter (7-1b), $\frac{-1}{K_Z}$, is close to zero, indicating its dominant impact on the BV distribution (see

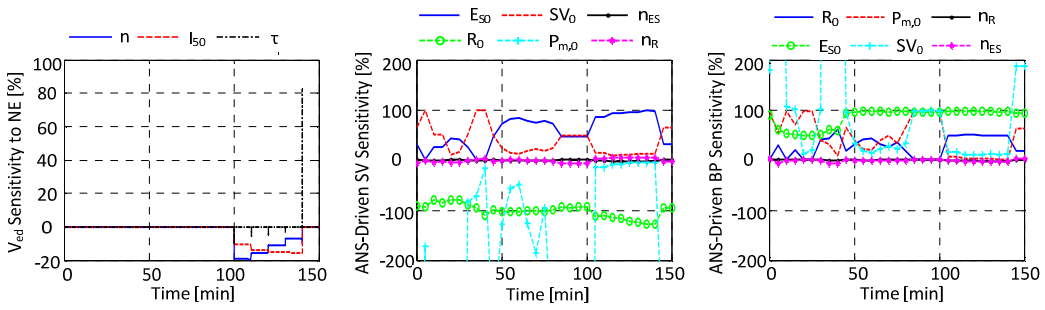

Figure 7-4: Time evolution of normalized parametric sensitivity functions (indicating percent change in the hemodynamic responses caused by unit percent perturbation in each parameter from the nominal value). (a) Sensitivity of LV effective preload to norepinephrine (NE) infusion, (b) sensitivity of SV to baroreflex-driven parameters, (c) sensitivity of BP to baroreflex-driven parameters.

Table 18). Figure 7-4(a) also shows the large sensitivity of EDV response with respect to n_{LV} and I_{50}. Figures 7-4(b) and 7-4(c) show the sensitivity of baroreflex-driven parameters in the models of TPR (7-5) and E_S (7-6), respectively. It is palpable that among all the parameters, the sensitivity of n_{E_S} and n_R is minimal, meaning these two parameters may be fixed at their nominal values between different subjects. In fact, this is consistent with what was found in chapter 4. In Chapter 4 we found that n_R as a low sensitive parameter could be fixed at its nominal value (0.33 in Chapter 4). It was also shown that vasopressor-driven parameters in TPR and E_S, that are τ, K_{E_S} and K_R, can be uniquely identified (see (7-14)).

The effects of NE on TPR and E_S on the average were significant, where, 2 and 3 subjects offered large contribution of NE on TPR and E_S increase, respectively (see Table 18).

It was shown that the proposed universal platform was adequate to reproduce hemodynamic endpoint responses to consecutive BV and NE. Regarding the generalizability of (7-3) as well as the P-V loop model, we hypothesize that this platform can be extended to concurrent BV and vasopressor perturbations. As the limitation of the work, our findings are preliminary results from only 4 pig animals and further investigation is needed using more experimental data.

8. Conclusions

Fluid resuscitation followed by vasopressor infusion is the first-line therapy in patient with hemorrhage and hypovolemia. In patients with decreased CV reserve, fluid resuscitation alone is not sufficient to augment CV performance. Therefore, vasopressor agents are utilized to supplement fluid infusion and force blood into the capillaries of all organs. Therefore, as a need for critical care treatment, a model of BV and tools to predict hemodynamic endpoints to fluid and vasopressor infusion were successfully developed and validated using experimental data. This dissertation developed a hybrid physiologic-phenomenological modeling paradigm to develop mathematical models for ACCS. The objectives of this modeling paradigm was shown to be in two fields. First, this paradigm can provide low-order models with adaptive personalization capability suited to develop ACCS control algorithms. Second, this paradigm can provide high-fidelity models with physiological relevance and transparency suited to interpret the underlying physiological principals. In other words, the model's transparency can make it possible to streamline the interpretation of the model during an ACCS event.

Mathematical model of physiological systems has potential to contribute to the design and evaluation of closed-loop hemodynamic management controllers. In the design phase, it enables the control designer to easily acquire insights on system dynamics and influence of each physiological component on the performance of closed-loop controllers via analysis and simulation. This in turn lends confidence to the efficacy of the model-based closed-loop controllers by conferring them sufficient

level of performance and robustness against conceivable physiological variability and challenging clinical scenarios, which are hard to achieve with empiric and rule-based controllers designed by iterative trial and error process. In the evaluation phase, mathematical model can facilitate the evaluation of closed-loop hemodynamic management controllers in the forms of in-silico and hardware-in-the-loop test methods similar to other types of closed-loop controlled systems (Dassau et al., 2009; Kovatchev et al., 2009b; León-Vargas et al., 2011). By leveraging such non-clinical test methods, it is possible to perform rigorous stress testing of closed-loop hemodynamic management controllers in a wide range of clinical scenarios, enabling the study of the behavior of the closed-loop controllers under worst-case clinical scenarios. Therefore, computational simulations incorporating mathematical models with established validity and utility for pre-clinical evaluation may be used as complementary evidence for the evaluation of closed-loop hemodynamic management controllers, while obviating the time and cost required to conduct a large-scale animal study. From these perspectives, the mathematical models developed in this dissertation may serve as a viable initial step towards model-based design and evaluation of closed-loop hemodynamic management controllers.

8.1. Summary of Dissertation Contributions

The contributions of this research can be summarized into the following folds:

Need for ACCS:

1) A retrospective analysis was performed on critical care patients receiving treatments by human clinicians. 224 ICU stays were extracted from MIMICII database and analyzed for the efficacy of the treatment they received. It was shown that treatment

by human clinicians was not optimum, in which 152 ICU stays included at least one episode of sustained hypotension. It was shown that ACCS is indeed required.

Model development for BV response to fluid infusion:

2) A control-oriented hybrid model of BV to fluid infusion was developed. This model was validated via human's BV responses to fluid infusion for three different states: (i) different BV states, (ii) different types of fluids, and (iii) different CV states. It was shown that once the model is fitted to the non-invasive fractional BV measurements in response to fluid infusion, it's accurate and interpretable in which the underlying physiological parameters of an individual patient could be adequately estimated. The model was also expanded to be adapted to hemorrhage scenario in addition to fluid infusion. The expanded model was validated via BV data obtained from 11 sheep subjects. The model was shown to be transparent and accurate.

Model development for hemodynamic endpoint responses to fluid infusion:

3) Physiologic-phenomenological hybrid models of hemodynamic endpoints, including CO and BP, to change in BV were developed. First, the Guyton's venous return model and model of LV P-V relationship were combined to develop the models of SV and CO in response to change in BV. Furthermore, a model of BP response to change in CO was developed. This model was developed based on the concept of baroreflex-based variation in TPR to regulate BP. A set of data from sheep animals under hemorrhage and fluid infusion were employed to validate the models of CO and BP. The model performance was satisfactory in which the CO and BP normalized RMSE among all the subjects was consistently less than 14.4% of their averaged responses. The low sensitivity parameters were also identified and averaged to their

nominal values. AIC showed a batter accuracy-complexity trade-off when the low sensitive parameters were fixed at their nominal values than fully individualized model.

Dose-dependent models of cardinal parameters in response to vasopressor infusion:

4) Dose-dependent and low-order phenomenological models of underlying CV state to vasopressor infusion were developed. A uniqueness of these models was that they were derived so that they can be tuned via only two dosages. It was shown the results were not trivial since these models were developed based on the receptor effects and were not simply fitted to the measured BP. Two sets of data were used for validation: (i) a dataset with sparse steady-state measurements and (ii) a dataset with high resolution dynamic transient. These models were shown to adequately reproduce the bi-phasic behavior of BP response to epinephrine infusion for individual subjects.

CV model derivation to estimate underlying CV state and predict endpoints

5) The Windkessel CV model was employed to derive a methodology to (i) estimate underlying CV state via measured NIBP, and (ii) predict hemodynamic endpoints to upcoming vasopressor doses using existing BP measurements to previous vasopressor dose levels. It was shown that the model performance is satisfactory for individual subjects, where r^2 values between true versus predicted endpoints were consistently higher than 0.96 regardless of the employed training doses. It was shown that the Windkessel model may fail when there is a wide variation of PP during fluid infusion.

Derivation of a universal platform for vasopressor and fluid infusion

6) A physiologic-phenomenological low-order platform was derived to reproduce the cardinal parameters and hemodynamic endpoints for consecutive fluid and vasopressor infusion. This model was built based on LV P-V relationship. The model

was shown to be adequate and transparent. It was hypothesized that the model can be employed for concurrent fluid and vasopressor infusion to test control algorithms, without involving real patients to which a patient's safety go under risk. The model was validated via 4 set of data from 4 pig subjects collected by our group.

8.2. Recommendations for Future Directions

The following areas are suggested for the future research:

1) The model of BV in this dissertation was only employed in response to fluid infusion and hemorrhage. It is of interest to explore new areas of BV model application. Burn and blood transfusion are among those critical care situations that clinician are always looking for better ways of BV resuscitation.

2) Hemorrhage inputted to the model of BV is assumed to be known and accurate. However, in reality, the amount of hemorrhage is often times unknown since it mostly occurs inside a human's body. Therefore, developing a technique to estimate hemorrhage based on measured endpoints, e.g., hematocrit, is highly rewarded.

3) Urine inputted to the model of BV is assumed to be known and accurate. This endpoint is commonly utilized to guide fluid resuscitation in burn patients. To develop an ACCS for BV management of burn patients the model of UO needs to be derived and validated. It's speculated that urine is delayed response to change in BV.

4) The controller used in BV model is linear PI controller. It's speculated that nonlinear controllers may lead to better BV estimation, in particular when there is oscillation in BV responses, e.g., BV response to fluid infusion under ISO administration.

5) It was shown that the identified baseline BV was slightly larger than its true value. The constant fluid distribution ratio estimated via steady-state portion of BV response to fluid infusion was regarded as the main reason for this discrepancy. Since there is no method estimating accurate baseline BV via fractional BV measurements, improvement of baseline BV estimation in the model of BV is of main interest.

6) The dose-dependent model of vasopressor infusion was only studied in subjects under epinephrine administration. The efficacy of this type of modeling should be further investigated in case of other vasopressors than epinephrine, including norepinephrine and dopamine as the most common medications in critical care.

7) The prediction of hemodynamic endpoints to vasopressor infusion was performed using observations from as few as two existing vasopressor dosages. The performance of the model needs to be further investigated when more than two dosages are available. It's anticipated that this step will enhance the accuracy of hemodynamic response prediction.

8) A more comprehensive validation of the models developed in this dissertation, including the models of BV and vasopressor infusion, is required. In particular, the universal platform for fluid and vasopressor infusion is only tested for 4 subjects. Additional animal experiments are required to perform sensitivity analysis and model cross validation between animals.

9) The ultimate goal of this research is to develop ACCSs that help clinician make better decision for dose adjustments (in case of decision support systems) and/or define the hemodynamic targets (in case of closed-loop systems). Therefore, the main upcoming research recommended for future work is to employ and refine the models

developed in this research as decision support systems and eventually design closed-loop systems that can achieve better treatments outcome.

Bibliography

1. Abram, S. R., Hodnett, B. L., Summers, R. L., Coleman, T. G., and Hester, R. L. (2007). Quantitative circulatory physiology: an integrative mathematical model of human physiology for medical education. *Adv. Physiol. Educ.* 31, 202–210. doi:10.1152/advan.00114.2006.
2. Arturson, G., Groth, T., Hedlund, A., and Zaar, B. (1989). Computer simulation of fluid resuscitation in trauma. First pragmatic validation in thermal injury. *J. Burn Care Rehabil.* 10, 292–299.
3. Asmussen, S., Salter, M., Prough, D. S., Kramer, G. C., Svensen, C., Sheffield-Moore, M., et al. (2014). Isoproternenol increases vascular volume expansion and urinary output after a large crystalloid bolus in healthy volunteers. *Shock Augusta Ga* 42, 407–414. doi:10.1097/SHK.0000000000000233.
4. Bajwa, S. S., and Kulshrestha, A. (2012). Diagnosis, prevention and management of postoperative pulmonary edema. *Ann. Med. Health Sci. Res.* 2, 180–185. doi:10.4103/2141-9248.105668.
5. Barrow, R. E., Jeschke, M. G., and Herndon, D. N. (2000). Early fluid resuscitation improves outcomes in severely burned children. *Resuscitation* 45, 91–96.
6. Bataille, B., Bertuit, M., Mora, M., Mazerolles, M., Cocquet, P., Masson, B., et al. (2012). Comparison of esCCO and transthoracic echocardiography for non-invasive measurement of cardiac output intensive care. *Br. J. Anaesth.* 109, 879–886. doi:10.1093/bja/aes298.
7. Beard, D. A., and Feigl, E. O. (2011). Understanding Guyton's venous return curves. *Am. J. Physiol. Heart Circ. Physiol.* 301, H629-633. doi:10.1152/ajpheart.00228.2011.
8. Bendjelid, K., and Romand, J. A. (2003). Fluid responsiveness in mechanically ventilated patients: a review of indices used in intensive care. *Intensive Care Med.* 29, 352–360. doi:10.1007/s00134-002-1615-9.
9. Bibian, S., Dumont, G. A., and Black, I. (2015). Closed-loop target-controlled infusion systems: stability and performance aspects. *Mil. Med.* 180, 96–103. doi:10.7205/MILMED-D-14-00380.
10. Bighamian, R., Reisner, A. T., and Hahn, J. O. (2014a). An analytic tool for prediction of hemodynamic responses to vasopressors. *IEEE Trans. Biomed. Eng.* 61, 109–118. doi:10.1109/TBME.2013.2277867.
11. Bighamian, R., Reisner, A. T., and Hahn, J. O. (2016). A lumped-parameter subject-specific model of blood volume response to fluid infusion. *Front. Physiol.* 7. doi:10.3389/fphys.2016.00390.
12. Bighamian, R., Rubbo, C., Thorsen, J. E., Hahn, J. O., and Reisner, A. T. (2014b). Is there opportunity for automated decision-support and closed-loop control in ICU patients receiving vasopressor infusion? *Conf. Proc. Annu. Int. Conf. IEEE Eng. Med. Biol. Soc. IEEE Eng. Med. Biol. Soc. Annu. Conf.* 2014, 1949–1952. doi:10.1109/EMBC.2014.6943994.
13. Blankenship, H. B., Wallace, F. D., and Pacifico, A. D. (1990). Clinical application of closed-loop postoperative autotransfusion. *Med. Prog. Technol.* 16, 89–93.

14. Bockenstedt, T. L., Baker, S. N., Weant, K. A., and Mason, M. A. (2012). Review of vasopressor therapy in the setting of vasodilatory shock. *Adv. Emerg. Nurs. J.* 34, 16–23. doi:10.1097/TME.0b013e31824371d3.
15. Bortolani, A., Governa, M., and Barisoni, D. (1996). Fluid replacement in burned patients. *Acta Chir. Plast.* 38, 132–136.
16. Bowman, R. J., and Westenskow, D. R. (1981). A microcomputer-based fluid infusion system for the resuscitation of burn patients. *IEEE Trans. Biomed. Eng.* 28, 475–479. doi:10.1109/TBME.1981.324822.
17. Burnette, R. R. (1992). Fundamental pharmacokinetic limits on the utility of using a sinusoidal drug delivery system to enhance therapy. *J. Pharmacokinet. Biopharm.* 20, 477–500.
18. Burnham, K. P., and Anderson, D. R. (2003). *Model Selection and Multimodel Inference: A Practical Information-Theoretic Approach*. 2nd edition. NY, USA: Springer.
19. Carlson, D. E., Kligman, M. D., and Gann, D. S. (1996). Impairment of blood volume restitution after large hemorrhage: a mathematical model. *Am. J. Physiol.* 270, R1163-1177.
20. Cervera, A. L., and Moss, G. (1974). Crystalloid distribution following hemorrhage and hemodilution: mathematical model and prediction of optimum volumes for equilibration at normovolemia. *J. Trauma* 14, 506–520.
21. Chaisson, N. F., Kirschner, R. A., Deyo, D. J., Lopez, J. A., Prough, D. S., and Kramer, G. C. (2003). Near-infrared spectroscopy-guided closed-loop resuscitation of hemorrhage. *J. Trauma* 54, S183-192. doi:10.1097/01.TA.0000064508.11512.28.
22. Champion, H. R., Sturdivan, L., Nolan, J., Stega, M., Cowley, R. A., Sacco, W., et al. (1975). A mathematical model for volume replacement in bleeding patients. *J. Surg. Res.* 19, 297–302.
23. Chase, J. G., Starfinger, C., Hann, C. E., Revie, J. A., Stevenson, D., Shaw, G. M., et al. (2010). Model-based prediction of the patient-specific response to adrenaline. *Open Med. Inform. J.* 4, 149–163. doi:10.2174/1874431101004010149.
24. Chen, C. T. (1984). *Linear System Theory And Design*. Fort Worth, TX, USA: Saunders College Publishing.
25. Cheng, L., Ivanova, O., Fan, H.-H., and Khoo, M. C. K. (2010). An integrative model of respiratory and cardiovascular control in sleep-disordered breathing. *Respir. Physiol. Neurobiol.* 174, 4–28. doi:10.1016/j.resp.2010.06.001.
26. Chien, S. (1971). Hemodynamics in hemorrhage: influences of sympathetic nerves and pentobarbital anesthesia. *Proc. Soc. Exp. Biol. Med. Soc. Exp. Biol. Med. N. Y. N* 136, 271–275.
27. Chirinos, J. A., Rietzschel, E. R., De Buyzere, M. L., De Bacquer, D., Gillebert, T. C., Gupta, A. K., et al. (2009). Arterial load and ventricular-arterial coupling: physiologic relations with body size and effect of obesity. *Hypertens. Dallas Tex 1979* 54, 558–566. doi:10.1161/HYPERTENSIONAHA.109.131870.
28. Classen, D. C., Pestotnik, S. L., Evans, R. S., Lloyd, J. F., and Burke, J. P. (1997). Adverse drug events in hospitalized patients. Excess length of stay, extra costs, and attributable mortality. *JAMA* 277, 301–306.
29. Coleman, T. G., and Guyton, A. C. (1969). Hypertension caused by salt loading in the dog. *Circ. Res.* 25, 153–160.

30. Convertino, V. A., Cooke, W. H., and Holcomb, J. B. (2006). Arterial pulse pressure and its association with reduced stroke volume during progressive central hypovolemia. *J. Trauma* 61, 629–634. doi:10.1097/01.ta.0000196663.34175.33.
31. Dassau, E., Palerm, C. C., Zisser, H., Buckingham, B. A., Jovanovic, L., and Doyle, F. J. (2009). In silico evaluation platform for artificial pancreatic beta-cell development--a dynamic simulator for closed-loop control with hardware-in-the-loop. *Diabetes Technol. Ther.* 11, 187–194. doi:10.1089/dia.2008.0055.
32. Dayneka, N. L., Garg, V., and Jusko, W. J. (1993). Comparison of four basic models of indirect pharmacodynamic responses. *J. Pharmacokinet. Biopharm.* 21, 457–478.
33. DeBey, R. K., Westenskow, D. R., Jordan, W. S., and McJames, S. W. (1987). Urine based control system for fluid infusion. *Biomed. Sci. Instrum.* 23, 195–198.
34. Drobin, D., and Hahn, R. G. (1999). Volume kinetics of Ringer's solution in hypovolemic volunteers. *Anesthesiology* 90, 81–91.
35. Drobin, D., and Hahn, R. G. (2002). Kinetics of isotonic and hypertonic plasma volume expanders. *Anesthesiology* 96, 1371–1380.
36. Dumont, G. A. (2014). Feedback control for clinicians. *J. Clin. Monit. Comput.* 28, 5–11. doi:10.1007/s10877-013-9469-y.
37. Dumont, G. A., and Ansermino, J. M. (2013). Closed-loop control of anesthesia: a primer for anesthesiologists. *Anesth. Analg.* 117, 1130–1138. doi:10.1213/ANE.0b013e3182973687.
38. Ellender, T. J., and Skinner, J. C. (2008). The use of vasopressors and inotropes in the emergency medical treatment of shock. *Emerg. Med. Clin. North Am.* 26, 759–786, ix. doi:10.1016/j.emc.2008.04.001.
39. Fazeli, N., and Hahn, J. O. (2012). Estimation of cardiac output and peripheral resistance using square-wave-approximated aortic flow signal. *Front. Physiol.* 3, 298. doi:10.3389/fphys.2012.00298.
40. Fedida, D., and Bouchard, R. A. (1992). Mechanisms for the positive inotropic effect of alpha 1-adrenoceptor stimulation in rat cardiac myocytes. *Circ. Res.* 71, 673–688.
41. Georgakopoulos, D., Mitzner, W. A., Chen, C. H., Byrne, B. J., Millar, H. D., Hare, J. M., et al. (1998). In vivo murine left ventricular pressure-volume relations by miniaturized conductance micromanometry. *Am. J. Physiol.* 274, H1416-1422.
42. Gingrich, K. J., and Roy, R. J. (1991). Modeling the hemodynamic response to dopamine in acute heart failure. *IEEE Trans. Biomed. Eng.* 38, 267–272. doi:10.1109/10.133208.
43. Görges, M., Westenskow, D. R., Kück, K., and Orr, J. A. (2010). A tool predicting future mean arterial blood pressure values improves the titration of vasoactive drugs. *J. Clin. Monit. Comput.* 24, 223–235. doi:10.1007/s10877-010-9238-0.
44. Guillamet, M. C. V., Rhee, C., and Patterson, A. J. (2012). Cardiovascular management of septic shock in 2012. *Curr. Infect. Dis. Rep.* 14, 493–502. doi:10.1007/s11908-012-0279-z.
45. Guyton, A. C., Coleman, T. G., and Granger, H. J. (1972). Circulation: overall regulation. *Annu. Rev. Physiol.* 34, 13–46. doi:10.1146/annurev.ph.34.030172.000305.

46. Guyton, A. C., Taylor, A. E., and Granger, H. J. (1975). *Dynamics and control of the body fluids*. W.B. Saunders.
47. Gyenge, C. C., Bowen, B. D., Reed, R. K., and Bert, J. L. (2003). Preliminary model of fluid and solute distribution and transport during hemorrhage. *Ann. Biomed. Eng.* 31, 823–839.
48. Hahn, J. O., Dumont, G. A., and Ansermino, J. M. (2012). A direct dynamic dose-response model of propofol for individualized anesthesia care. *IEEE Trans. Biomed. Eng.* 59, 571–578. doi:10.1109/TBME.2011.2177497.
49. Hahn, R. G. (2010). Volume kinetics for infusion fluids. *Anesthesiology* 113, 470–481. doi:10.1097/ALN.0b013e3181dcd88f.
50. Hahn, R. G. (2013). Why are crystalloid and colloid fluid requirements similar during surgery and intensive care? *Eur. J. Anaesthesiol.* 30, 515–518. doi:10.1097/EJA.0b013e328362a5a9.
51. Hay, I., Rich, J., Ferber, P., Burkhoff, D., and Maurer, M. S. (2005). Role of impaired myocardial relaxation in the production of elevated left ventricular filling pressure. *Am. J. Physiol. Heart Circ. Physiol.* 288, H1203-1208. doi:10.1152/ajpheart.00681.2004.
52. Hedin, A., and Hahn, R. G. (2005). Volume expansion and plasma protein clearance during intravenous infusion of 5% albumin and autologous plasma. *Clin. Sci.* 108, 217–224. doi:10.1042/CS20040303.
53. Hedlund, A., Zaar, B., Groth, T., and Arturson, G. (1988). Computer simulation of fluid resuscitation in trauma. I. Description of an extensive pathophysiological model and its first validation. *Comput. Methods Programs Biomed.* 27, 7–21.
54. Hennings, S., Romero, A., Erstad, B., Franke, H., and Theodorou, A. (2010). A comparison of automated infusion device technology to prevent medication errors in pediatric and adult intensive care unit patients. *Hosp. Pharm.* 45, 464–471. doi:10.1310/hpj4506-464.
55. Henschen, S., Busse, M. W., Zisowsky, S., and Panning, B. (1993). Determination of plasma volume and total blood volume using indocyanine green: a short review. *J. Med.* 24, 10–27.
56. Hill, S. A. (2004). Pharmacokinetics of drug infusions. *Contin. Educ. Anaesth. Crit. Care Pain* 4, 76–80. doi:10.1093/bjaceaccp/mkh021.
57. Hirshberg, A., Hoyt, D. B., and Mattox, K. L. (2006). Timing of fluid resuscitation shapes the hemodynamic response to uncontrolled hemorrhage: analysis using dynamic modeling. *J. Trauma* 60, 1221–1227. doi:10.1097/01.ta.0000220392.36865.fa.
58. Hollenberg, S. M., Kavinsky, C. J., and Parrillo, J. E. (1999). Cardiogenic shock. *Ann. Intern. Med.* 131, 47–59.
59. Hoskins, S. L., Elgjo, G. I. E., Lu, J., Ying, H., Grady, J. J., Herndon, D. N., et al. (2006). Closed-loop resuscitation of burn shock. *J. Burn Care Res. Off. Publ. Am. Burn Assoc.* 27, 377–385. doi:10.1097/01.BCR.0000216512.30415.78.
60. Hunter, J. D., and Doddi, M. (2010). Sepsis and the heart. *Br. J. Anaesth.* 104, 3–11. doi:10.1093/bja/aep339.
61. Ishihara, H., Okawa, H., Tanabe, K., Tsubo, T., Sugo, Y., Akiyama, T., et al. (2004). A new non-invasive continuous cardiac output trend solely utilizing routine cardiovascular monitors. *J. Clin. Monit. Comput.* 18, 313–320.

62. Johnston, A. J., Steiner, L. A., O'Connell, M., Chatfield, D. A., Gupta, A. K., and Menon, D. K. (2004). Pharmacokinetics and pharmacodynamics of dopamine and norepinephrine in critically ill head-injured patients. *Intensive Care Med.* 30, 45–50. doi:10.1007/s00134-003-2032-4.
63. Karar, M. E., and El-Brawany, M. A. (2011). Automated cardiac drug infusion system using adaptive fuzzy neural networks controller. *Biomed. Eng. Comput. Biol.* 2011, 1–11.
64. Kass, D. A. (2002). Ventricular dyssynchrony and mechanisms of resynchronization therapy. *Eur. Heart J.-Suppl.* 4, D23–D30.
65. Kass, D. A., and Beyar, R. (1991). Evaluation of contractile state by maximal ventricular power divided by the square of end-diastolic volume. *Circulation* 84, 1698–1708.
66. Kawada, T., Shishido, T., Inagaki, M., Tatewaki, T., Zheng, C., Yanagiya, Y., et al. (2001). Differential dynamic baroreflex regulation of cardiac and renal sympathetic nerve activities. *Am. J. Physiol. Heart Circ. Physiol.* 280, H1581-1590.
67. Kawada, T., Uemura, K., Kashihara, K., Kamiya, A., Sugimachi, M., and Sunagawa, K. (2004). A derivative-sigmoidal model reproduces operating point-dependent baroreflex neural arc transfer characteristics. *Am. J. Physiol. Heart Circ. Physiol.* 286, H2272-2279. doi:10.1152/ajpheart.00787.2003.
68. Kellum, J. A., and Pinsky, M. R. (2002). Use of vasopressor agents in critically ill patients. *Curr. Opin. Crit. Care* 8, 236–241.
69. Khalil, H. K. (2001). *Nonlinear Systems*. 3rd edition. N.J, USA: Pearson.
70. Kjørstad, K. E., Korvald, C., and Myrmel, T. (2002). Pressure-volume-based single-beat estimations cannot predict left ventricular contractility in vivo. *Am. J. Physiol. Heart Circ. Physiol.* 282, H1739-1750. doi:10.1152/ajpheart.00638.2001.
71. Klabunde, R. E. (2005). *Cardiovascular Physiology Concepts*. Lippincott Williams & Wilkins.
72. Kofránek, J., and Rusz, J. (2010). Restoration of Guyton´s diagram for regulation of the circulation as a basis for quantitative physiological model development. *Physiol. Res.* 59, 897–908.
73. Komajda, M., Hanon, O., Hochadel, M., Lopez-Sendon, J. L., Follath, F., Ponikowski, P., et al. (2009). Contemporary management of octogenarians hospitalized for heart failure in Europe: Euro Heart Failure Survey II. *Eur. Heart J.* 30, 478–486. doi:10.1093/eurheartj/ehn539.
74. Kovatchev, B. P., Breton, M., Man, C. D., and Cobelli, C. (2009a). In silico preclinical trials: a proof of concept in closed-loop control of type 1 diabetes. *J. Diabetes Sci. Technol.* 3, 44–55.
75. Kovatchev, B. P., Breton, M., Man, C. D., and Cobelli, C. (2009b). In silico preclinical trials: a proof of concept in closed-loop control of type 1 diabetes. *J. Diabetes Sci. Technol.* 3, 44–55.
76. Kramer, G. C., Kinsky, M. P., Prough, D. S., Salinas, J., Sondeen, J. L., Hazel-Scerbo, M. L., et al. (2008). Closed-loop control of fluid therapy for treatment of hypovolemia. *J. Trauma* 64, S333-341. doi:10.1097/TA.0b013e31816bf517.
77. Kumar, A., Anel, R., Bunnell, E., Habet, K., Neumann, A., Wolff, D., et al. (2004). Effect of large volume infusion on left ventricular volumes, performance and

contractility parameters in normal volunteers. *Intensive Care Med.* 30, 1361–1369. doi:10.1007/s00134-004-2191-y.
78. Lamba, S., and Abraham, W. T. (2000). Alterations in adrenergic receptor signaling in heart failure. *Heart Fail. Rev.* 5, 7–16. doi:10.1023/A:1009885822076.
79. Langewouters, G. J., Wesseling, K. H., and Goedhard, W. J. (1984). The static elastic properties of 45 human thoracic and 20 abdominal aortas in vitro and the parameters of a new model. *J. Biomech.* 17, 425–435.
80. Leenen, F. H., Fourney, A., Coletta, E., and White, R. (2007). Effects of hypertension on cardiovascular responses to epinephrine in humans. *Am. J. Physiol. Heart Circ. Physiol.* 292, H3025-3031. doi:10.1152/ajpheart.01200.2006.
81. Leonetti, P., Audat, F., Girard, A., Laude, D., Lefrère, F., and Elghozi, J. L. (2004). Stroke volume monitored by modeling flow from finger arterial pressure waves mirrors blood volume withdrawn by phlebotomy. *Clin. Auton. Res. Off. J. Clin. Auton. Res. Soc.* 14, 176–181. doi:10.1007/s10286-004-0191-1.
82. León-Vargas, F., Prados, G., Bondia, J., and Vehí, J. (2011). A new virtual environment for testing and hardware implementation of closed-loop control algorithms in the artificial pancreas. *Conf. Proc. Annu. Int. Conf. IEEE Eng. Med. Biol. Soc. IEEE Eng. Med. Biol. Soc. Annu. Conf.* 2011, 385–388. doi:10.1109/IEMBS.2011.6090124.
83. Lewis, F. R. (1986). Prehospital intravenous fluid therapy: physiologic computer modelling. *J. Trauma* 26, 804–811.
84. Ljung, L. (1999). *System Identification: Theory for the User*. Prentice Hall PTR.
85. Mackenzie, A. F., Colvin, J. R., Kenny, G. N., and Bisset, W. I. (1993). Closed loop control of arterial hypertension following intracranial surgery using sodium nitroprusside. A comparison of intra-operative halothane or isoflurane. *Anaesthesia* 48, 202–204.
86. Magosso, E., Biavati, V., and Ursino, M. (2001). Role of the baroreflex in cardiovascular instability: a modeling study. *Cardiovasc. Eng. Int. J.* 1, 101–115. doi:10.1023/A:1012574513589.
87. Mardel, S. N., Simpson, S. H., Kelly, S., Wytch, R., Beattie, T. F., and Menezes, G. (1995). Validation of a computer model of haemorrhage and transcapillary refill. *Med. Eng. Phys.* 17, 215–218.
88. Marik, P. E. (2009). Techniques for assessment of intravascular volume in critically ill patients. *J. Intensive Care Med.* 24, 329–337. doi:10.1177/0885066609340640.
89. Marik, P. E., Baram, M., and Vahid, B. (2008). Does central venous pressure predict fluid responsiveness? A systematic review of the literature and the tale of seven mares. *Chest* 134, 172–178. doi:10.1378/chest.07-2331.
90. Marquez, J., McCurry, K., Severyn, D. A., and Pinsky, M. R. (2008). Ability of pulse power, esophageal Doppler, and arterial pulse pressure to estimate rapid changes in stroke volume in humans. *Crit. Care Med.* 36, 3001–3007. doi:10.1097/CCM.0b013e31818b31f0.
91. Mathews, L., and Singh, R. K. K. (2008). Cardiac output monitoring. *Ann. Card. Anaesth.* 11, 56–68.
92. Maurer, M. S., Sackner-Bernstein, J. D., El-Khoury Rumbarger, L., Yushak, M., King, D. L., and Burkhoff, D. (2009). Mechanisms underlying improvements in

ejection fraction with carvedilol in heart failure. *Circ. Heart Fail.* 2, 189–196. doi:10.1161/CIRCHEARTFAILURE.108.806240.
93. Mazzoni, M. C., Borgström, P., Arfors, K.-E., and Intaglietta, M. (1988). Dynamic fluid redistribution in hyperosmotic resuscitation of hypovolemic hemorrhage. *Am. J. Physiol.* 255, H629-637.
94. Meier-Hellmann, A., Reinhart, K., Bredle, D. L., Specht, M., Spies, C. D., and Hannemann, L. (1997). Epinephrine impairs splanchnic perfusion in septic shock. *Crit. Care Med.* 25, 399–404.
95. Merouani, M., Guignard, B., Vincent, F., Borron, S. W., Karoubi, P., Fosse, J. P., et al. (2008). Norepinephrine weaning in septic shock patients by closed loop control based on fuzzy logic. *Crit. Care Lond. Engl.* 12, R155. doi:10.1186/cc7149.
96. Michard, F. (2005). Volume management using dynamic parameters: the good, the bad, and the ugly. *Chest* 128, 1902–1903. doi:10.1378/chest.128.4.1902.
97. Michard, F. (2013). Decision support for hemodynamic management: from graphical displays to closed loop systems. *Anesth. Analg.* 117, 876–882. doi:10.1213/ANE.0b013e31827e5002.
98. Miller, R. D. (2010). *Miller's Anesthesia*. Philadelphia, PA, USA: Elsevier Health Sciences.
99. Monnet, X., Letierce, A., Hamzaoui, O., Chemla, D., Anguel, N., Osman, D., et al. (2011). Arterial pressure allows monitoring the changes in cardiac output induced by volume expansion but not by norepinephrine. *Crit. Care Med.* 39, 1394–1399. doi:10.1097/CCM.0b013e31820edcf0.
100. Montani, J.-P., and Van Vliet, B. N. (2009). Understanding the contribution of Guyton's large circulatory model to long-term control of arterial pressure. *Exp. Physiol.* 94, 382–388. doi:10.1113/expphysiol.2008.043299.
101. Morley, D., Litwak, K., Ferber, P., Spence, P., Dowling, R., Meyns, B., et al. (2007). Hemodynamic effects of partial ventricular support in chronic heart failure: results of simulation validated with in vivo data. *J. Thorac. Cardiovasc. Surg.* 133, 21–28. doi:10.1016/j.jtcvs.2006.07.037.
102. Mukkamala, R., Reisner, A. T., Hojman, H. M., Mark, R. G., and Cohen, R. J. (2006). Continuous cardiac output monitoring by peripheral blood pressure waveform analysis. *IEEE Trans. Biomed. Eng.* 53, 459–467. doi:10.1109/TBME.2005.869780.
103. Nachar, R. A., Booth, E. A., Friedlich, P., Borzage, M., Soleymani, S., Wider, M. D., et al. (2011). Dose-dependent hemodynamic and metabolic effects of vasoactive medications in normotensive, anesthetized neonatal piglets. *Pediatr. Res.* 70, 473–479. doi:10.1203/PDR.0b013e31822e178e.
104. Nagashima, M., Hattori, Y., Akaishi, Y., Tohse, N., Sakuma, I., Kitabatake, A., et al. (1996). Alpha 1-adrenoceptor subtypes mediating inotropic and electrophysiological effects in mammalian myocardium. *Am. J. Physiol.* 271, H1423-1432.
105. Navarro, L. H. C., Bloomstone, J. A., Auler, J. O. C., Cannesson, M., Rocca, G. D., Gan, T. J., et al. (2015). Perioperative fluid therapy: a statement from the international Fluid Optimization Group. *Perioper. Med.* 4. doi:10.1186/s13741-015-0014-z.
106. Nevière, R., Mathieu, D., Chagnon, J. L., Lebleu, N., and Wattel, F. (1996). The contrasting effects of dobutamine and dopamine on gastric mucosal perfusion in septic

patients. *Am. J. Respir. Crit. Care Med.* 154, 1684–1688. doi:10.1164/ajrccm.154.6.8970355.
107. Ngan Kee, W. D., Tam, Y. H., Khaw, K. S., Ng, F. F., Critchley, L. A., and Karmakar, M. K. (2007). Closed-loop feedback computer-controlled infusion of phenylephrine for maintaining blood pressure during spinal anaesthesia for caesarean section: a preliminary descriptive study. *Anaesthesia* 62, 1251–1256. doi:10.1111/j.1365-2044.2007.05257.x.
108. Nise, N. S. (2010). *Control Systems Engineering, 6th Edition*. 6 edition. John Wiley & Sons, Inc.
109. Noori, S., and Seri, I. (2012). Neonatal blood pressure support: the use of inotropes, lusitropes, and other vasopressor agents. *Clin. Perinatol.* 39, 221–238. doi:10.1016/j.clp.2011.12.010.
110. Oren, S., Grossman, E., and Frohlich, E. D. (1996). Arterial and venous compliance in obese and nonobese subjects. *Am. J. Cardiol.* 77, 665–667.
111. Papaioannou, T. G., Vardoulis, O., and Stergiopulos, N. (2012). The "systolic volume balance" method for the noninvasive estimation of cardiac output based on pressure wave analysis. *Am. J. Physiol. Heart Circ. Physiol.* 302, H2064-2073. doi:10.1152/ajpheart.00052.2012.
112. Parkin, G., Wright, C., Bellomo, R., and Boyce, N. (1994). Use of a mean systemic filling pressure analogue during the closed-loop control of fluid replacement in continuous hemodiafiltration. *J. Crit. Care* 9, 124–133.
113. Parkin, W. G., and Leaning, M. S. (2008). Therapeutic control of the circulation. *J. Clin. Monit. Comput.* 22, 391–400. doi:10.1007/s10877-008-9147-7.
114. Parlikar, T. A., Heldt, T., Ranade, G. V., and Verghese, G. C. (2007). Model-based estimation of cardiac output and total peripheral resistance. *Comput. Cardiol.* 34, 379–382.
115. Parmer, K. R., Xiu, P. Y., Chowdhury, M. R., Patel, E., and Cohen, M. (2015). In-hospital treatment and outcomes of heart failure in specialist and non-specialist services: a retrospective cohort study in the elderly. *Open Heart* 2, e000095.
116. Peterson, D. R., and Bronzino, J. D. eds. (2007). *Biomechanics: Principles and Applications*. 2 edition. FL, USA: CRC Press.
117. Piene, H. (1984). Impedance matching between ventricle and load. *Ann. Biomed. Eng.* 12, 191–207.
118. Pirkle, J. C., and Gann, D. S. (1976). Restitution of blood volume after hemorrhage: role of the adrenal cortex. *Am. J. Physiol.* 230, 1683–1687.
119. Price, S. A., Spain, D. A., Wilson, M. A., Harris, P. D., and Garrison, R. N. (1999). Subacute sepsis impairs vascular smooth muscle contractile machinery and alters vasoconstrictor and dilator mechanisms. *J. Surg. Res.* 83, 75–80. doi:10.1006/jsre.1998.5568.
120. Pruett, W. A., Husband, L. D., Husband, G., Dakhlalla, M., Bellamy, K., Coleman, T. G., et al. (2013). A Population Model of Integrative Cardiovascular Physiology. *PLoS ONE* 8. doi:10.1371/journal.pone.0074329.
121. Pruitt, B. A. (1978). Fluid and electrolyte replacement in the burned patient. *Surg. Clin. North Am.* 58, 1291–1312.

122. Rafie, A. D., Rath, P. A., Michell, M. W., Kirschner, R. A., Deyo, D. J., Prough, D. S., et al. (2004). Hypotensive resuscitation of multiple hemorrhages using crystalloid and colloids. *Shock Augusta Ga* 22, 262–269.
123. Rech, M. A., Prasse, M., and Patel, G. (2011). Use of vasopressors in septic shock. *J. Clin. Outcomes Manag. JCOM* 18, 273–277.
124. Reil, J. C., Reil, G. H., and Böhm, M. (2009). Heart rate reduction by If-channel inhibition and its potential role in heart failure with reduced and preserved ejection fraction. *Trends Cardiovasc. Med.* 19, 152–157. doi:10.1016/j.tcm.2009.09.002.
125. Reisner, A. T., Xu, D., Ryan, K. L., Convertino, V. A., Rickards, C. A., and Mukkamala, R. (2011). Monitoring non-invasive cardiac output and stroke volume during experimental human hypovolaemia and resuscitation. *BJA Br. J. Anaesth.* 106, 23–30. doi:10.1093/bja/aeq295.
126. Rinehart, J., Alexander, B., Le Manach, Y., Hofer, C., Tavernier, B., Kain, Z. N., et al. (2011). Evaluation of a novel closed-loop fluid-administration system based on dynamic predictors of fluid responsiveness: an in silico simulation study. *Crit. Care Lond. Engl.* 15, R278. doi:10.1186/cc10562.
127. Rinehart, J., and Canales, C. (2015). Closed-loop pharmacology in anesthesia and critical care: benefits and limitations. *Int. Anesthesiol. Clin.* 53, 91–101. doi:10.1097/AIA.0000000000000051.
128. Rinehart, J., Chung, E., Canales, C., and Cannesson, M. (2012). Intraoperative stroke volume optimization using stroke volume, arterial pressure, and heart rate: closed-loop (learning intravenous resuscitator) versus anesthesiologists. *J. Cardiothorac. Vasc. Anesth.* 26, 933–939. doi:10.1053/j.jvca.2012.05.015.
129. Rinehart, J., Lee, C., Cannesson, M., and Dumont, G. (2013). Closed-loop fluid resuscitation: robustness against weight and cardiac contractility variations. *Anesth. Analg.* 117, 1110–1118. doi:10.1213/ANE.0b013e3182930050.
130. Rudis, M. I., Basha, M. A., and Zarowitz, B. J. (1996). Is it time to reposition vasopressors and inotropes in sepsis? *Crit. Care Med.* 24, 525–537.
131. Ruokonen, E., Takala, J., Kari, A., Saxén, H., Mertsola, J., and Hansen, E. J. (1993). Regional blood flow and oxygen transport in septic shock. *Crit. Care Med.* 21, 1296–1303.
132. Saeed, M., Villarroel, M., Reisner, A. T., Clifford, G., Lehman, L. W., Moody, G., et al. (2011). Multiparameter Intelligent Monitoring in Intensive Care II (MIMIC-II): A public-access intensive care unit database. *Crit. Care Med.* 39, 952–960. doi:10.1097/CCM.0b013e31820a92c6.
133. Sagawa, K., Maughan, W. L., Suga, H., and Sunagawa, K. (1988). *Cardiac Contraction and the Pressure-volume Relationship*. Oxford University Press.
134. Salinas, J., Drew, G., Gallagher, J., Cancio, L. C., Wolf, S. E., Wade, C. E., et al. (2008). Closed-loop and decision-assist resuscitation of burn patients. *J. Trauma* 64, S321-332. doi:10.1097/TA.0b013e31816bf4f7.
135. Santamore, W. P., and Burkhoff, D. (1991). Hemodynamic consequences of ventricular interaction as assessed by model analysis. *Am. J. Physiol.* 260, H146-157.
136. Shoukas, A. A., and Sagawa, K. (1971). Total systemic vascular compliance measured as incremental volume-pressure ratio. *Circ. Res.* 28, 277–289.
137. Siegal, E. M., Dressler, D. D., Dichter, J. R., Gorman, M. J., and Lipsett, P. A. (2012). Training a hospitalist workforce to address the intensivist shortage in American

hospitals: a position paper from the Society of Hospital Medicine and the Society of Critical Care Medicine. *Crit. Care Med.* 40, 1952–1956. doi:10.1097/CCM.0b013e318258eef7.
138. Simpson, S. H., Menezes, G., Mardel, S. N., Kelly, S., White, R., and Beattie, T. (1996). A computer model of major haemorrhage and resuscitation. *Med. Eng. Phys.* 18, 339–343.
139. Sng, B. L., Tan, H. S., and Sia, A. T. H. (2014). Closed-loop double-vasopressor automated system vs manual bolus vasopressor to treat hypotension during spinal anaesthesia for caesarean section: a randomised controlled trial. *Anaesthesia* 69, 37–45. doi:10.1111/anae.12460.
140. Stephens, C. T., Uwaydah, N., Kramer, G. C., Prough, D. S., Salter, M., and Kinsky, M. P. (2011). Vascular and extravascular volume expansion of dobutamine and norepinephrine in normovolemic sheep. *Shock Augusta Ga* 36, 303–311. doi:10.1097/SHK.0b013e318225b031.
141. Stergiopulos, N., Meister, J. J., and Westerhof, N. (1995). Evaluation of methods for estimation of total arterial compliance. *Am. J. Physiol.* 268, H1540-1548.
142. Storn, R., and Price, K. (1997). Differential evolution – a simple and efficient heuristic for global optimization over continuous spaces. *J Glob. Optim.* 11, 341–359. doi:10.1023/A:1008202821328.
143. Svensen, C. H., Rodhe, P. M., Olsson, J., Børsheim, E., Aarsland, A., and Hahn, R. G. (2009). Arteriovenous differences in plasma dilution and the distribution kinetics of lactated ringer's solution. *Anesth. Analg.* 108, 128–133. doi:10.1213/ane.0b013e31818c95e1.
144. Svensén, C., and Hahn, R. G. (1997). Volume kinetics of Ringer solution, dextran 70, and hypertonic saline in male volunteers. *Anesthesiology* 87, 204–212.
145. Takala, J. (2010). Should we target blood pressure in sepsis? *Crit. Care Med.* 38, S613-619. doi:10.1097/CCM.0b013e3181f2430c.
146. Tatara, T., Tsunetoh, T., and Tashiro, C. (2007). Crystalloid infusion rate during fluid resuscitation from acute haemorrhage. *Br. J. Anaesth.* 99, 212–217. doi:10.1093/bja/aem165.
147. Toutain, P. L., and Bousquet-Mélou, A. (2004). Plasma terminal half-life. *J. Vet. Pharmacol. Ther.* 27, 427–439. doi:10.1111/j.1365-2885.2004.00600.x.
148. Uemura, K., Kamiya, A., Hidaka, I., Kawada, T., Shimizu, S., Shishido, T., et al. (2006). Automated drug delivery system to control systemic arterial pressure, cardiac output, and left heart filling pressure in acute decompensated heart failure. *J. Appl. Physiol. Bethesda Md 1985* 100, 1278–1286. doi:10.1152/japplphysiol.01206.2005.
149. Uemura, K., Kawada, T., Kamiya, A., Aiba, T., Hidaka, I., Sunagawa, K., et al. (2005). Prediction of circulatory equilibrium in response to changes in stressed blood volume. *Am. J. Physiol. Heart Circ. Physiol.* 289, H301-307. doi:10.1152/ajpheart.01237.2004.
150. Ursino, M. (1998). Interaction between carotid baroregulation and the pulsating heart: a mathematical model. *Am. J. Physiol.* 275, H1733-1747.
151. Ursino, M., Antonucci, M., and Belardinelli, E. (1994). Role of active changes in venous capacity by the carotid baroreflex: analysis with a mathematical model. *Am. J. Physiol.* 267, H2531-2546.

152. Ursino, M., and Magosso, E. (2000). Acute cardiovascular response to isocapnic hypoxia. II. Model validation. *Am. J. Physiol. Heart Circ. Physiol.* 279, H166-175.
153. Ursino, M., and Magosso, E. (2003). Short-term autonomic control of cardiovascular function: a mini-review with the help of mathematical models. *J. Integr. Neurosci.* 2, 219–247.
154. Vaid, S. U., Shah, A., Michell, M. W., Rafie, A. D., Deyo, D. J., Prough, D. S., et al. (2006). Normotensive and hypotensive closed-loop resuscitation using 3.0% NaCl to treat multiple hemorrhages in sheep. *Crit. Care Med.* 34, 1185–1192. doi:10.1097/01.CCM.0000207341.78696.3A.
155. Vane, L. A., Prough, D. S., Kinsky, M. A., Williams, C. A., Grady, J. J., and Kramer, G. C. (2004). Effects of different catecholamines on the dynamics of volume expansion of crystalloid infusion. *Anesthesiology* 101, 1136–1144.
156. Varadhan, K. K., and Lobo, D. N. (2010). A meta-analysis of randomised controlled trials of intravenous fluid therapy in major elective open abdominal surgery: getting the balance right. *Proc. Nutr. Soc.* 69, 488–498. doi:10.1017/S0029665110001734.
157. Vatner, S. F. (1974). Effects of hemorrhage on regional blood flow distribution in dogs and primates. *J. Clin. Invest.* 54, 225–235. doi:10.1172/JCI107757.
158. Wassar, T., Luspay, T., Upendar, K. R., Moisi, M., Voigt, R. B., Marques, N. R., et al. (2014). Automatic control of arterial pressure for hypotensive patients using phenylephrine. *Int. J. Model. Simul.* 34. doi:10.2316/Journal.205.2014.4.205-6087.
159. Wears, R. L., and Winton, C. N. (1990). Load and go versus stay and play: analysis of prehospital i.v. fluid therapy by computer simulation. *Ann. Emerg. Med.* 19, 163–168.
160. Westerhof, N., Lankhaar, J. W., and Westerhof, B. E. (2009). The arterial Windkessel. *Med. Biol. Eng. Comput.* 47, 131–141. doi:10.1007/s11517-008-0359-2.
161. White, M., and Leenen, F. H. (1997). Effects of age on cardiovascular responses to adrenaline in man. *Br. J. Clin. Pharmacol.* 43, 407–414.
162. Wolf, S. E., Rose, J. K., Desai, M. H., Mileski, J. P., Barrow, R. E., and Herndon, D. N. (1997). Mortality determinants in massive pediatric burns. An analysis of 103 children with > or = 80% TBSA burns (> or = 70% full-thickness). *Ann. Surg.* 225, 554–569.
163. Woodruff, E. A., Martin, J. F., and Omens, M. (1997). A model for the design and evaluation of algorithms for closed-loop cardiovascular therapy. *IEEE Trans. Biomed. Eng.* 44, 694–705. doi:10.1109/10.605426.
164. Ying, H., Bonnerup, C. A., Kirschner, R. A., Deyo, D. J., Michell, M. W., and Kramer, G. C. (2002). Closed-loop fuzzy control of resuscitation of hemorrhagic shock in sheep. in *Engineering in Medicine and Biology, 2002. 24th Annual Conference and the Annual Fall Meeting of the Biomedical Engineering Society EMBS/BMES Conference, 2002. Proceedings of the Second Joint*, 1575–1576 vol.2. doi:10.1109/IEMBS.2002.1106545.
165. Ying, H., and Sheppard, L. C. (1990). Real-time expert-system-based fuzzy control of mean arterial pressure in pigs with sodium nitroprusside infusion. *Med. Prog. Technol.* 16, 69–76.

166. Young, D. B. (2010). *Control of Cardiac Output*. CA, USA: Morgan & Claypool Life Sciences.